SYNTHESIS, CHARACTERIZATION AND CHARGE TRANSPORT STUDY IN STABLE RADICAL POLYMERS

A Dissertation

Presented to the Faculty of the Graduate School

of Cornell University

In Partial Fulfillment of the Requirements for the Degree of

Doctor of Philosophy

by

Yiren Zhang

December 2019

SYNTHESIS, CHARACTERIZATION AND CHARGE TRANSPORT STUDY IN STABLE RADICAL POLYMERS

Yiren Zhang, Ph. D.

Cornell University 2019

Radical polymers, a class of polymers with robust radical pendent groups along their backbones, have demonstrated various applications as next generation energy storage materials. Among all the aliphatic radical polymers, poly(2,2,6,6-tetramethylpiperidinyloxy methacrylate) (PTMA), a poly(methacrylate) bearing the persistent 2,2,6,6-tetramethylpiperidinyloxyl (TEMPO) radical as a pendant group, has received increasing interest since its first introduction to a rechargeable battery. As the insulating nature of PTMA is straightforward and has been well-recognized among electrochemists, it is surprising that conductivity of ~ 10^{-6} S/cm was observed in neat PTMA films in 2013. The mechanism of this efficient electron transport was proposed to be charge hopping when the spacing between two adjacent radicals is less than 10 Å.

In this study, we find that PTMA is highly insulating –conductivity in the range 10^{-11} S/cm – regardless of the synthetic method of preparation. We have compared these results with variable range hopping theory and find that very few radical sites are electrically active, though the stable radical sites are closely packed. On the other hand, regioregular polythiophene backbone has also been incorporated into the stable

radical polymer structure and radical pendent group content was varied systematically. Using EPR and electrical conductivity measurements, we show that there is an exponential decrease of conductivity as we increase the percentage of pendent groups attached to repeating units, which changes the conductivity by 6 orders of magnitude between the non-radical control polythiophene material and the material with highest radical content (~80%). The conductivity of the solid films can be further improved by doping with oxidizers. These findings serve as an important guide to the future design of radical polymers on conjugated backbones with the goal of increasing conductivity for redox-active energy storage applications.

BIOGRAPHICAL SKETCH

Yiren Zhang (born September 27, 1992), was born and grew up in Shanghai, China. Intent on pursuing a career as lawyer, he attended the Law School in Shanghai Jiao Tong University in 2009. Later, he discovered his real passion in science, and graduated in 2014 with a B.S. in chemistry. He spent his undergraduate career at studying copper-catalyzed asymmetrical catalysis and pure organic luminescent materials. With hopes to know more about the mystery of polymers, Yiren pursued a graduate education in Materials Science and Engineering and is currently a fifth year PhD student in the Ober Research Group at Cornell University. In his PhD research, Yiren mainly focused on design, synthesis and characterization of functional polymers for both academic studies and engineering purposes. He is highly skilled in materials synthesis and capable of address a broad range of research topics. His currently research topic is development of chain-scissionable polymer resists for the future extreme ultraviolet lithography. Being actively involved in teaching, he also served as a teaching assistant for three semesters and have been nominated for an Excellence in Teaching Award in 2018. In his spare time, Yiren enjoys photography and is learning video editing for his future Youtube channel. After finishing his PhD degree in the summer of 2019, Yiren started his professional career in Pall Corporation as a research scientist.

Dedicated to my parents and my girlfriend

for their love and support.

ACKNOWLEDGEMENTS

First, I would like to express my deepest gratitude to my advisor Christopher Ober for his continuous support of my PhD study. He continues to influence me with his patience, motivation and immense knowledge. He also gave me strong emotional support when my girlfriend was hospitalized in 2015, the time I almost planned to quit my PhD study. I could not have imagined I can have a better advisor and mentor for my PhD study.

Besides my advisor, I would like to thank the rest of my committee members, Prof. Geoffrey Coates, Prof. Ulrich Wiesner and Prof. Emmanuel Giannelis for their insightful comments and encouragement, but also for the hard questions which incentivized me to improve my research from various perspectives.

I thank my fellow labmates for the stimulating discussions, for the sleepless nights we were working together before deadlines, and for all the fun we have had in the last four years. Although I spent most of my PhD time in Thurston 303 and Bard 359, I always feel the most warmth, fun and help come from the Duffield lab, especially during my most helpless days in my first summer in lab. I would like to thank Dr. Ziwei Liu for being a helpful friend, reliable group member and responsible roommate in the past several years. Dr. Hai Quang Tran deserves special thanks since he and his wife offered me tremendous help in both research and life, as well as my driving license. Dr. Wei-Liang Chen are like big brother who helped me to establish my early synthesis in his own fume hood and taught me various useful techniques for me to survive in the Ober group. In particular, I am grateful to Dr. Hong Xu for listening to

my complaints of my experiments and enlightening me with some useful glance of the photoresist research. His knowledge and dedication to science are great examples to me even after he started his career life in Tsing Hua University. Dr. Roselynn Cordero and Dr. Amanda Leonardi are always so kind and willing to encourage me with their warm hearts. I am glad that my limited synthesis skills can help Zhubing Han, Chengjian Shi, Jingyuan Deng, Yuming Huang and Abhaiguru Ravirajan, Alicia Cintora and Nilay Duzen. I also benefit a lot from working together with you guys.

I am grateful for having the opportunity to work with many research groups and gain a better understanding of various fields. For the stable radical polymer work, my longest ongoing project, I would like to thank all of the past and present people who made contributions. Thanks to Prof. Gregory Fuchs and Albert Park for the spin characterization, conductivity measurements and theory interpret ion. Thanks to Prof. Michael Flatté, Dr Stephen McMillan and Nicholas Harmon for the simulation work for our polymers and providing directions with great potential. I would also like to thank Prof. Jodie Lutkenhaus and Shaoyang Wang for carrying out the valuable electrochemical measurements, which is important for this dissertation. The collaboration with Prof. Julie Goddard and Dr. Zhuangsheng Lin on the metal-chelating coating are fruitful, and they also provided me with some useful background knowledge on metal chelating polymer that helped me find my current job in Pall Corp.

During the preparation of this thesis, I have benefited from interactions with many individuals and hospitality form many friends. I would like to thank particularly Dr. Yongyang Gong. My time with him taught me not only to learn the necessary skills to

survive the PhD study, but that I could pretty much develop a passion and good taste of science.

Last but not least, I would like to thank my family and to my dear high school sweetheart for supporting me spiritually throughout writing this thesis and my life in general.

TABLE OF CONTENTS

LIST OF FIGURES

LIST OF SCHEMES

LIST OF TABLES

LIST OF ABBREVIATIONS

AFM	Atomic force microscopy
ATR-FTIR	Attenuated total reflectance-Fourier transform infrared spectroscopy
ATRP	Atom-transfer radical-polymerization
CV	Cyclic Voltammetry
DB3HT	2,5-Dibromo-3-hexylthiophene
DCM	Dichloromethane
DIPEA	*N,N*-Diisopropylethylamine
DMF	*N,N*-dimethylformamide
DSC	Differential scanning calorimetry
EPR	Electron paramagnetic resonance
GPC	Gel permeation chromatography
GRIM	Grignard metathesis
^{1}H NMR	Proton nuclear magnetic resonance spctroscopy
*m*CPBA	*m*-Chloroperbenzoic acid
MPEOT	4-Methacryloyloxy-1-((10-phenylethyl)-oxy-2,2,6,6-tetramethylpiperidine)
Ni(dppp)Cl_2	[1,3-Bis(diphenylphosphino)propane]dichloronickel(II)

P3HT	Poly(3-hexylthiophene)
PEDOT	poly(3,4-ethylenedioxythiophene)
PMPEOT	Poly(4-methacryloyloxy-1-((10-phenylethyl)-oxy-2,2,6,6-tetramethylpiperidine)
PTMA	Poly(2,2,6,6-tetramethylpiperidinyloxy methacrylate)
PTMPM	Poly(2,2,6,6-tetramethyl-4-piperidyl methacrylate)
RAFT	Reversible addition-fragmentation chain transfer
TEMPO	2,2,6,6-Tetramethylpiperidine-1-oxyl
TGA	Thermogravimetric analysis
THF	Tetrahydrofuran
TMPM	2,2,6,6-Tetramethyl-4-piperidyl methacrylate
UV-vis	Ultraviolet-visible spectroscopy

CHAPTER 1: INTRODUCTION

1.1 Introduction

1.1.1 Stable radicals

Stable radical groups in organic chemistry are molecular units that contain one unpaired electron. Due to their characteristic single electron, radicals may undergo rearrangement or elimination reactions, or they may dimerize or disproportionate, leading to the annihilation of the odd electron.[1] Most simple alkyl free radicals are highly reactive, and their lifetimes are usually only of the order of milliseconds or less. Specific free radicals may be stabilized by their particular structures, which extend their lifetimes. One landmark discovery was Gomberg's introduction of three phenyl rings to form a triphenylmethyl (trityl) radical, which marked the beginning of organic free radical chemistry.[2] However, these molecules consist of a mixture of the radical form and a head-to-tail dimer in solution, which cannot be isolated as a pure species. Subsequently, heteroatoms (N, O, S) with increased steric protection and extra resonance stabilization have been found to be among the critical factors needed for radicals to survive an extended time. Radical species with such structural characteristics have been defined by Kosower as "stable" radicals in the 1960s.[3] Since then, isolable organic radicals, including nitroxides, nitronyl nitroxides, verdarzyls and phenoxy radicals, have been synthesized with surprisingly long lifetime up to years. (**Fig. 1.1**) Such excellent stability as well as their unpaired spins also make them good candidates in various applications, including spin-labels[4–7], *in vitro* and *in vivo* spin trapping agents[8–12], organic magnetic and conducting materials, initiators for polymerization[13], chemosensors

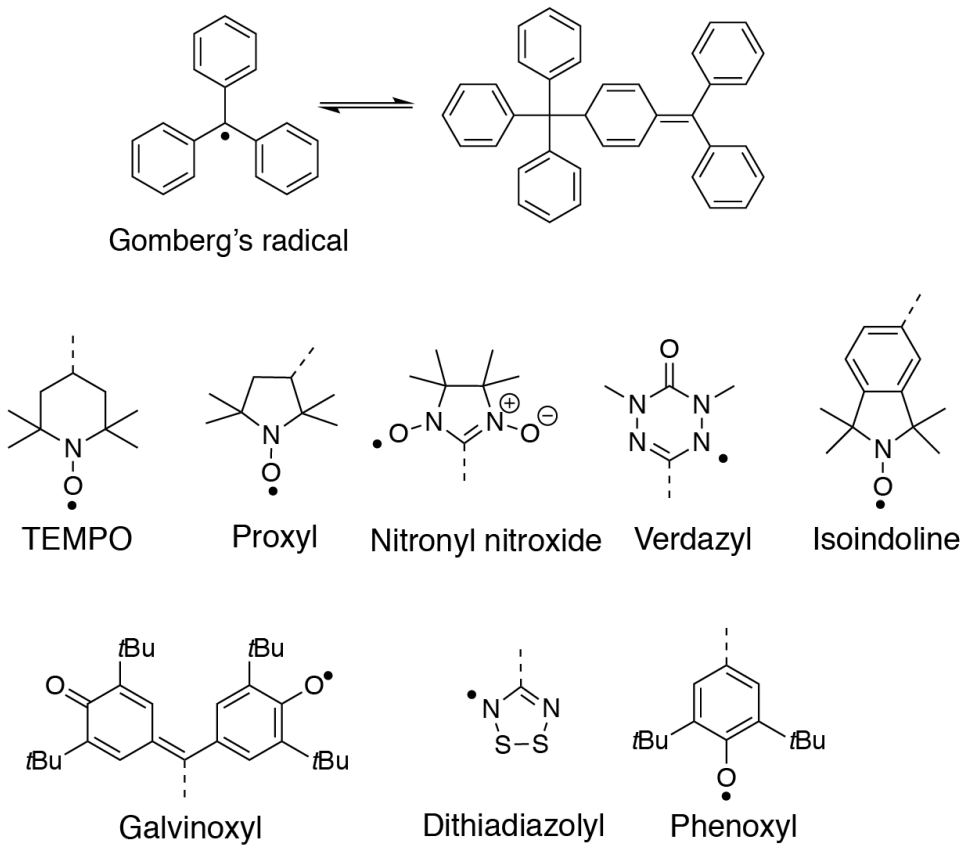

Figure 1.1. Structure of some common stable radicals.

and catalysts in organic reactions[14–16].

1.1.2 Electron transport in stable radicals

Organic stable radicals are of fundamental interest because they represent a simple neutral system with only unpaired single electrons. The idea that a neutral organic radical can conduct DC electrical current without decomposition or chemical transformation of the material always appeals to the materials scientist. However, there exists a paradox regarding the conductivity and stability of the stable radicals. If a material with crowded radical site shows high conductivity, it indicates that the single electrons are mobile and tend to pair up with each other. As the result, most attempts have led to exchange couplings and poor chemical stability at room temperature. So far, successful designs of conductive organic radicals fall into two categories: i) two planar component systems requiring a donor (D) and an acceptor (A) molecule, both in a single molecule or cocrystallized salts; ii) Neutral π-delocalized radicals as building blocks for planar stable radicals. Generally, planarity enables the closest possible packing between the adjacent molecules, while delocalization within the overlapped π structure mobilizes the electrons.

For the first category, the redox potential in the D and A molecules promotes either partial or complete intermolecular charge transfer, which can endow the charge transfer salts with remarkable magnetic exchange and conductivity. One successful example is the tetrathiafulvalene:7,7,8,8-tetracyanoquinodimethane (TTF:TCNQ) salt (**Fig. 1.2 (a)**), whose high conductivity was first reported by Ferraris *et al.* in 1973.[17] Charge transfer occurs between TTF and TCNQ molecules that are in the same plane, whereas the direction of conductivity is

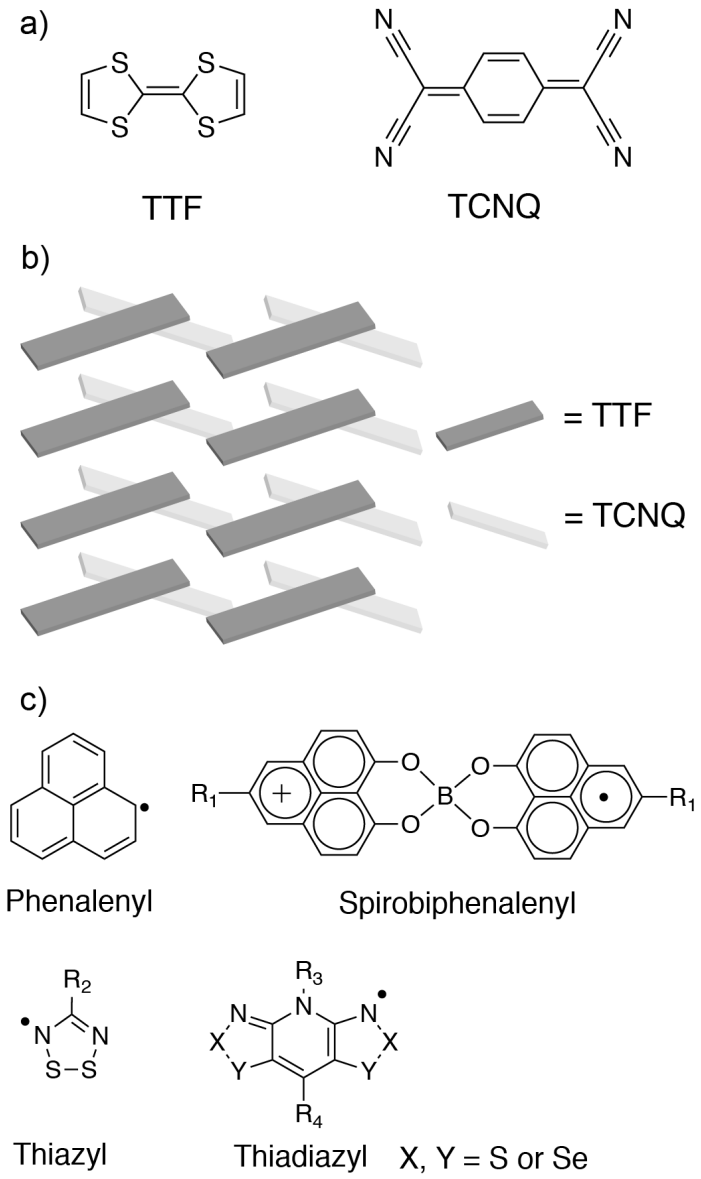

Figure 1.2. (a) Tetrathiafulvalene (TTF), 7,7,8,8-tetracyanoquinodimethane (TCNQ) and (b) sketch illustrating herringbone stacking in a 1:1 TTF:TCNQ charge transfer salt. (c) Chemical structure of some conductive neutral radicals based on phenalenyl and thiazyl cores.

parallel to the separated columns of TTF radical cations and TCNQ radical anions. (**Fig. 1.2 (b)**) For the second category, most of the reports are based on phenalenyl and thiazyl cores. (**Fig. 1.2 (c)**) Several synthesized phenalenyl radicals suffer from either σ or π dimerization in the solid state, while the perchlorinated derivative did not dimerize at the expense of increased molecular separation. It behaved as a Mott insulator with a conductivity of only 10^{-10} S/cm.[18,19] The highest conductivity achieved in the neutral phenalenyl radicals reaches 0.3 S/cm, which was from the single-crystal resistivity measurement of a cyclohexyl-substituted spiro-biphenalenyl radical.[20] On the other hand, Oakley *et al.* introduced electronegative heteroatoms into the thiadiazolyl ring to stabilize the radicals, and varied the substituents to study their effect on their radical electronic properties.[21–24] The most successful design is the "resonance stabilized bisdithiazolyl" radicals, which gives typical conductivity on the order of 10^{-6} S/cm. The highest conductivity in this family comes from the replacement of S with two or four Se atoms, which increases the room temperature conductivity to as much as 10^{-3} S/cm.[25,26]

1.1.3 Electron paramagnetic resonance (EPR) Spectroscopy

Electron paramagnetic resonance (EPR) spectroscopy has been one of the most powerful techniques to detect the local structural and dynamic behavior of paramagnetic stable radicals because the radicals absorb microwave energy in an external field upon changes of the precession of an induced macroscopic magnetization around an external static magnetic field.[27] This highly sensitive technique has been widely used for characterization of spin-containing materials in solution and in the solid state, as well as for radicals deposited on a substrate.[28] Nitroxide stable radicals have also been installed in macromolecules as spin labels,

because their EPR spectra are sensitive towards many factors, such as local polarity, viscosity and polymer segment motion. The EPR technique has been applied in the study of chain aggregation and segmental mobility in various systems, including polymer blends[29–31], block copolymers[32–35], polymer solutions[36,37], bottle brush polymers[38] and dendrimers[39-41].

The monomeric nitroxide radicals usually show a clean triplet with equal-line intensities. This is also called hyperfine splitting of the nitroxide radicals, which is the result of interactions of the unpaired electron with the nucleus ^{14}N ($I = 1$) and the number of lines is determined according to the formula $2nI + 1$ (where n is the number of N).[42] (**Fig. 1.3**) On the other hand, the EPR spectrum of the nitroxide radical polymers contains a broad featureless singlet even in diluted solutions, as a result of a locally high density and fast spin exchange process of the unpaired electrons.[43,44] For example, PTMA usually shows paramagnetic activity ($g \approx 2$), characterized by the presence of a broad central signal (linewidth around 10 G). The EPR spectra of PTMA are similar in solution or films, indicating that spin density distribution does not depend on the medium in which the polymer sample is analyzed.[45] Double integration of the peak and comparison with that of a nitroxide radical reference sample of carefully measured weight reveal the spin concentration of the polymer sample.

1.2 Stable Radical Polymers

1.2.1 Stable radicals as basic units of polymeric structures

A polymer molecule has a molecular structure consisting of a large number of similar units covalently bonded together. These repeating units are called

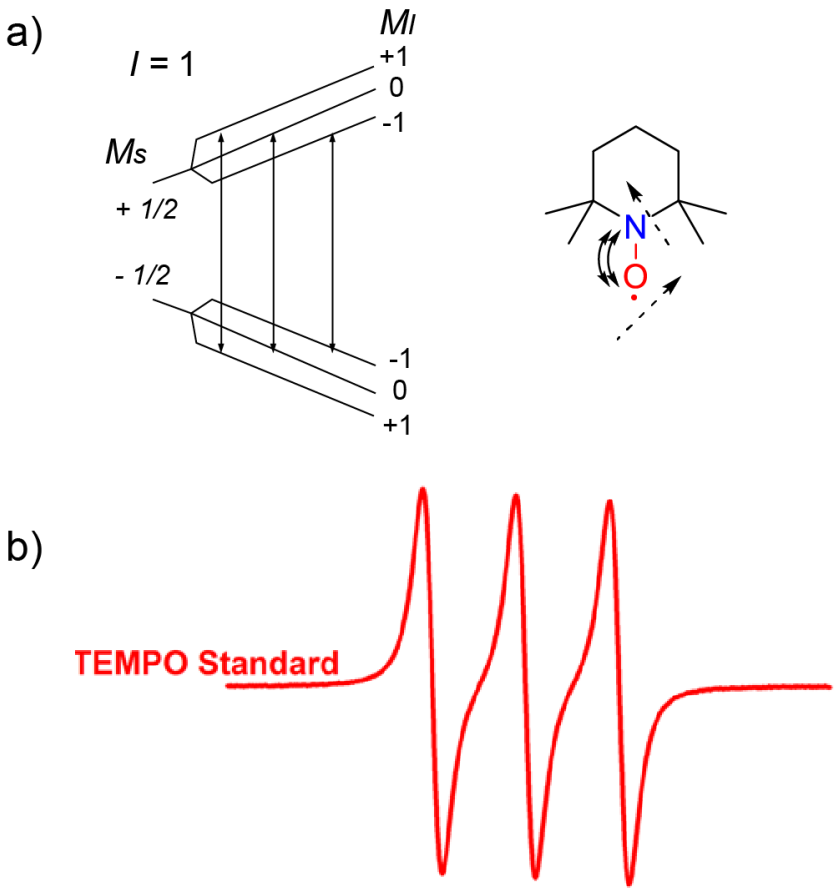

Figure 1.3. a) Hyperfine splitting of the electron-Zeeman Levels for one nucleus with $I = 1$. b) Characteristic EPR line shape of monomeric TEMPO radical, which is a clean triplet with equal-line intensities.

monomers, which usually contain a functional group for backbone construction as well as functional pendent groups. In most cases, the chemical identity of the pendent groups will be retained in the final polymers, thus endowing the final polymers with many intriguing properties for numerous applications. In addition, the ability to modify the chemical structure of the pendent groups and the composition of polymer backbone allows the preparation of functional polymers with various chemical and physical properties and provides a way to optimize their performance for certain applications.

Considering the excellent chemical stability of stable radicals, polymer chemists have made a number of attempts to incorporate multiple stable radical groups into a single polymeric structure. These polymers are usually known as stable radical polymers. Most stable radical polymers possess two major components: robust radical pendent groups and a main polymer backbone. In theory, radical polymers can have two different structures based on the locations of their spins: 1) spins on the backbone and 2) spins on the pendent groups. (**Fig. 1.4**) However, due to the difficulty of preventing the homocoupling of the spins on a single chain, the former design has been used extensively but without success. Instead, all the existing stable radical polymers are synthesized following the latter design and commonly have an aliphatic (unsaturated carbon-carbon) backbone, and the stable radicals are covalently attached to the backbone as pendent groups. Beside these two major categories, nitroxide radicals have also been covalently attached to 3-dimensional polymeric networks, including covalent organic frameworks (COFs)[46], metal-organic frameworks (MOFs)[47], nanoparticles[48], polymer brushes[49,50] and resins[51,52].

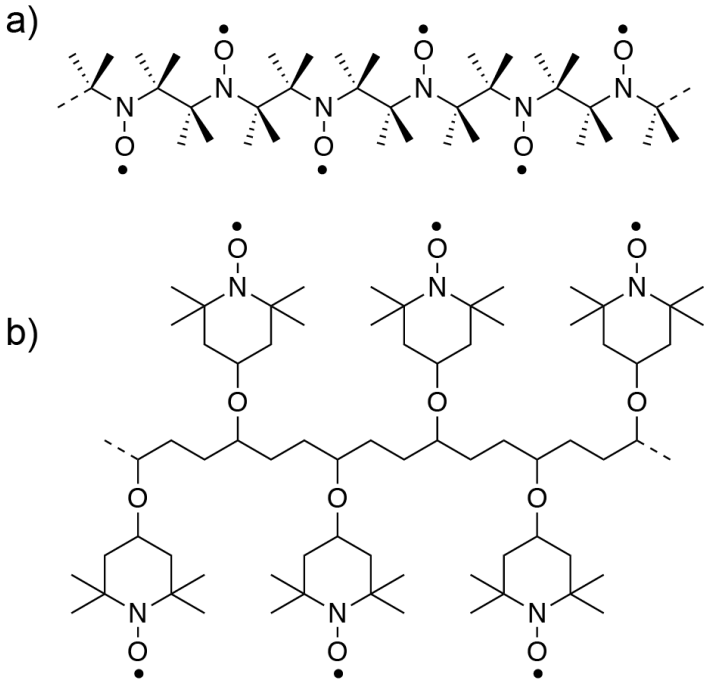

Figure 1.4. The design of stable radicals with a) spins on the backbone and b) spins on the pendent groups.

In the last century, radical polymers have been primarily used as spin carriers in organic ferromagnets due to the presence of single electrons in the chemical structure. The first report of nitroxide radical incorporation into molecule-based magnetic materials was in the 1970s from Lim and Drago, in which the TEMPO radical was coordinated by the NO group.[53] There are some previous review papers with illustration of bis-chelating nitroxide free radicals and their application in magnetic engineering.[54] Especially, π-conjugated and high-spin radical polymers have been extensively investigated as possible candidates for organic ferromagnetic materials. The magnetism of stable radical-containing materials is currently beyond the scope of this dissertation, and a more detailed description can be found in some review papers and text books.

1.2.2 Radical polymers containing TEMPO radicals

The detailed information on preparative methods of nitroxide radicals has been compiled in a number of books and reviews[55–58]. Though many radicals have been synthesized and reported, the required synthesis routes are always cumbersome and plenty of nitroxides are not sufficiently stable to isolate, which has been the main obstacle for the preparation of stable nitroxide radical polymers. Among all the stable nitroxide radicals, TEMPO radicals have been the most intensely studied species due to their excellent stability with respect to air, water, and dimerization. They have two quaternary carbon-based substituents and no α-hydrogens, which excludes the decomposition pathway to nitrones by transferring H• to another nitroxide molecule and giving hydroxylamine.[56,59] Many modification reactions can be carried out on the remote functional groups of molecules carrying a TEMPO radical group without affecting the radical site itself.

Four general strategies have been proposed for the preparation of various kinds of TEMPO-containing radical polymers. (**Fig. 1.5**) (a) A monomer containing a TEMPO free radical is directly polymerized by radical, ionic or electrochemical means. (b) A similar monomer but functionalized with a TEMPO radical precursor group is polymerized. The radical precursors can be recovered by subsequent chemical treatment. (c) A precursor polymer with reactive groups on the side chains is chemically grafted with TEMPO radicals. (d) A similar polymer with reactive groups is functionalized with TEMPO precursor groups, which are later converted to free radicals.[60,61] Usually, optimization of the radical yield in the final polymer is a major concern, and strategy (i) is preferred since it does not have the difficulty of ensuring complete conversion of the radical precursor groups. However, such polymerization methods are extremely limited in number due to the fact that radicals are incompatible with many reaction conditions and reagents. Consequently, a majority of reported stable radical polymers with TEMPO pendent groups are synthesized using strategy (ii) and (iii) as a compromise. So far, various polymer backbones have been used, such as poly(methacrylate)[45,62], polystyrene[63,64], poly(vinyl ether)[65], polyether[44,66], polynorbornene[67–69], polysiloxane[70], cellulose[71] and DNA complexes[72].

Poly(2,2,6,6-tetramethylpiperidinyloxy-4-yl methacrylate) (PTMA) is the most well-known class of stable radical polymer, which contains a conventional poly(methyl methacrylate) backbone and has a TEMPO radical in every repeating unit. It is an amorphous polymer with a glass transition temperature at ~ 170 °C, which is higher than that of common PMMA (~105 °C). This high T_g value can be ascribed to the ability of nitroxide (N-O) groups to act as acceptors of hydrogen

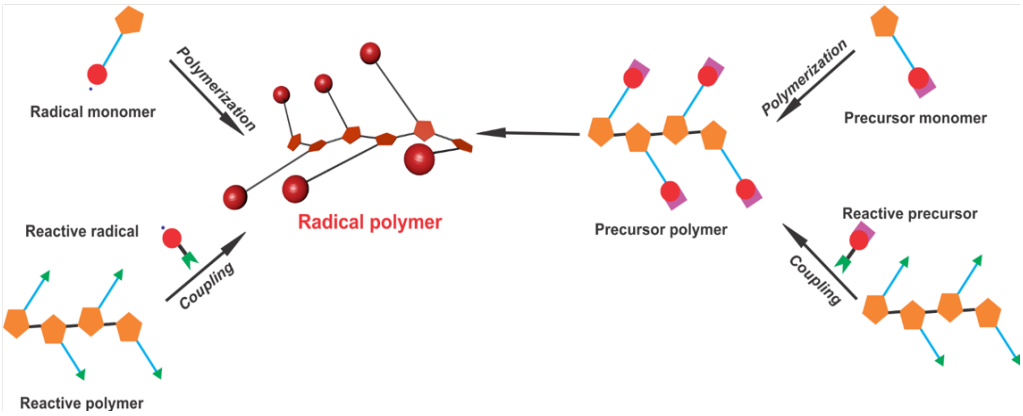

Figure 1.5. General strategies for the preparation of TEMPO radical-containing polymers.

bonds and the possibility of the formation of hydrogen-bonded networks.[73] In both solution and the solid state, PTMA usually has orange color due to the characteristic absorption of the TEMPO radical at ~463 nm. Preparation of PTMA was first reported as early as 1967 using direct polymerization of TEMPO-methacrylate monomer by Grignard initiator. Direct radical polymerization of TEMPO-methacrylate monomer is impossible because the TEMPO radical act as an efficient radical trapper. Instead, polymerization of the radical-containing monomer has been explored *via* cationic, anionic or group transfer polymerization[74]. Though most radical spins can be retained through these methods, the polymerization processes are usually not controlled. The most controlled anionic polymerization attempt of TEMPO-methacrylate was reported by Nishide *et al.* in 2014, which used methyl methacrylate-capped 1,1-diphenylhexyllithium (DPHLi/MMA) as initiator. The nucleophilicity was moderate enough to suppress side reactions between the TEMPO radical and the carbonion of DPHLi, which gave PTMA with narrow PDI (< 1.10), high yield (> 95%) and almost one radical per monomer unit.[75]

Another option would be the radical polymerization of monomers containing a TEMPO precursor, which can be converted to TEMPO radicals using subsequent chemical treatment. The major TEMPO precursors are listed as follows: 1) secondary amine, which is TMPM, a commercially available monomer that has been widely used in the preparation of PTMA. Oxidation of secondary amines in PTMPM can be done with an excess amount of *meta*-chloroperoxybenzoic acid (*m*CPBA) in the chlorinated solvent, or by oxidizing in a methanolic solution of hydrogen peroxide and sodium tungstate (Na_2WO_4/H_2O_2)[76,77]. 2) Alkoxyamines.

The alkoxyamine can reversibly decompose into a TEMPO radical and another radical. With the presence of oxygen, the pair radical will be deactivated while the air-stable TEMPO radicals will remain.

Although different synthesis methods can give satisfactory yield of TEMPO recovery (usually higher than 70%), side products are also unavoidable in the final products, and the species and content are largely dependent on the reaction conditions. Oxidation of secondary amine with *m*CPBA or Na_2WO_4/H_2O_2 both go through the aminohydroxy group then form oxoammonium. However, their reduction pathways are different: while excess H_2O_2 acts as a reducing reagent for oxoammonium in Na_2WO_4/H_2O_2 conditions, the reduction in the *m*CPBA case is solely done by the generated aminohydroxy group via reverse disproportionation. This reaction pathway has been proved in several early studies of hindered amine oxidation study with *m*CPBA, where various equivalent of an oxidant was used. On the other hand, disproportion of alkoxyamines in the presence of oxygen is a mild condition that does not generate oxoammonium cations.

Another category of radical polymers combines together conjugated polymer backbones and chemically robust radical sites, with unique magnetic[78] and electrochemical properties associated with spin-delocalization of the unpaired electrons present in free radicals with the conjugate segments. Such polymers are often difficult to synthesize because of the incompatibility of the TEMPO radicals with many reaction conditions and reagents. Early synthetic approaches involve the preparation of the TEMPO-containing thiophene[79–82] or pyrrole[83,84] monomers and subsequent electrochemical or oxidative polymerization. These synthetic routes require oxidative doping of the conjugated units, which may cause side

reactions with the radicals and have little control on the polymer structure. Traditional chemical coupling between radical-containing monomers have also been attempted as a promising method, but the relevant reports are very rare. For example, Xie *et al.* have polymerized a monomer containing a 1,6-heptadiyne and a TEMPO group through cyclopolymerization, which gave a well-defined nitroxide radical conjugated polymers with a five-membered ring-containing polyene backbone.[85] A more common strategy involves the preparation of a conjugated polymer precursor with reactive moieties, which can have highly efficient coupling reactions with functionalized nitroxide radicals.

1.2.3 Stable radical polymers as energy storage materials

A new trend in organic battery is emerging recently, focusing on the fabrication of electrodes with redox-active polymers with pendent stable radicals. For applications in organic batteries, a stable radical polymer must be insoluble in electrolyte to prevent materials loss, while the polymer must be robust in an electrochemical cell over a long period of time.[86] Among all the stable radical polymers, the nitroxide radical polymers are most widely used species because of the fact that the nitroxide radicals are among the most persistent radicals even in the presence of metal ions and can be easily synthesized in large scale. In addition to the usual advantages touted in favor of organic materials, namely structure versatility and processibility, the nitroxide radical polymers are also characterized by the small molecular weight per the active site among the redox molecules (30 for N-O, 64 for S-S and 186 for ferrocene).[45] A nitroxide radical usually has the unpaired electron centered on the oxygen atom, and can undergo single-electron reduction to form the amino hydroxyl anion or single-electron oxidation to form

the oxoammonium cation. (**Fig. 1.6 (a)**) This redox couple of a nitroxide radical is an important basis for their application in rechargeable batteries. The electron transfer rate for nitroxide radical redox is often very fast since no structural rearrangements are involved in the redox processes, which enables the high power-rate performance in organic batteries.[87] Also, the nitroxide radical polymer usually operate at a higher potentials (3.5-4.0 V vs Li), and can achieve high doping capacity and thus high theoretical capacity.[86,88] Due to these intriguing properties, polymers with pendent stable radical groups have attracted considerable attention as energy storage materials in organic radical batteries (ORB).

The structure of an ORB is similar to that of a classical secondary lithium-ion battery, while the cathode material used is replaced by a p-type nitroxide stable radical polymer. In a traditional Li-ion battery, the cathode is made up of Li-ion-containing metal oxides, such as cobalt oxides. In the charging and discharging processes, there are often intercalating diffusion of Li-ions accompanied with the lattice- and layer-structure, which sometimes produce overheat and ignition.[89] In this way, a polymer containing electrode is a possible solution to overcome the above-mentioned disadvantages of the metal-based electrodes. For a stable nitroxide radical polymer, during the charging process, the nitroxide stable radical in the cathode is oxidized to the oxoammonium form. During the discharging process, the nitroxide radical is regenerated by reduction of the oxoammonium actions. (**Fig. 1.6 (b)**) The rapid electron transfer rate for the nitroxide radical redox process is also an important feature. The electron transfer process in radical polymer electrodes are considered to have two steps: 1) the heterogeneous charge transfer from a current collector to the radical polymer; 2) the homogeneous charge

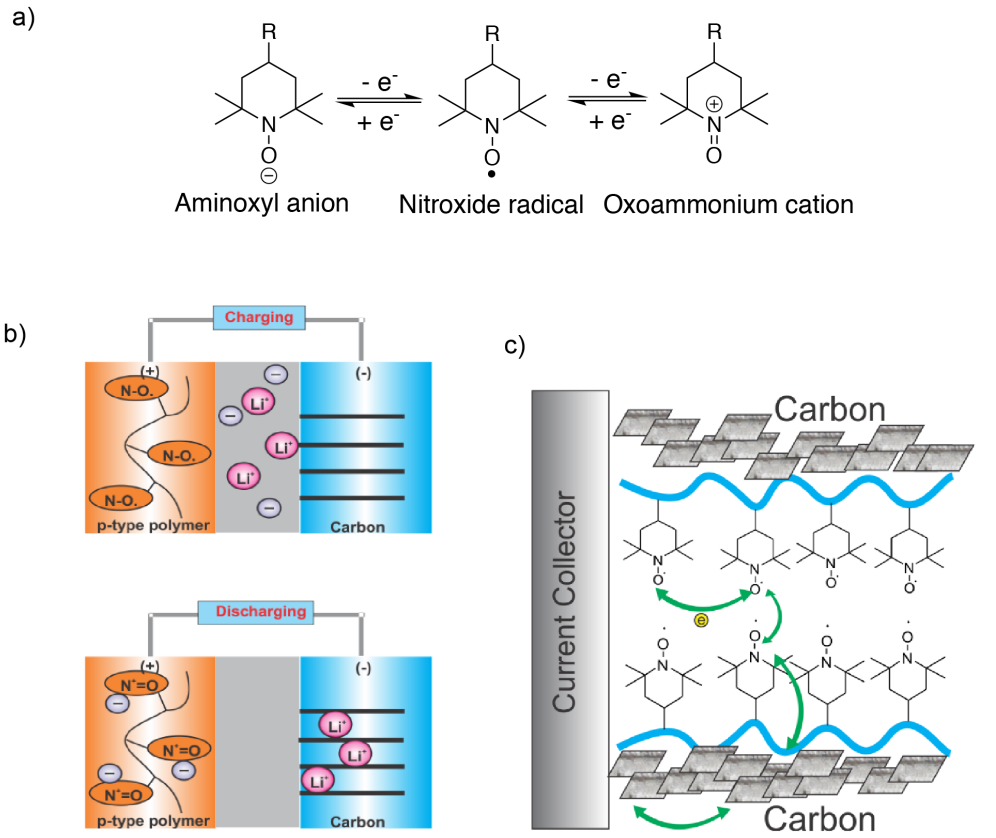

Figure 1.6. a) Redox scheme of TEMPO stable radicals. b) Schematic representation of the charging/discharging process of an organic battery containing nitroxide stable radical polymer in the cathode. c) The electron transport process in a cathode containing stable radical polymer and carbon additives.

transfer among the radical components. (**Fig. 1.6 (c)**) Nishide *et. al.* have proposed that charge can be transported through several micrometer thick layers in a battery electrode without any conducting additive.[90] However, most radical polymers do not exhibit sufficient conductivity for a pure polymer electrode, and thus must be mixed with conductive filler as a bridge between the polymer and current collector for electron transport. Also, the different redox potentials can be achieved by incorporation of different species of stable radicals, and the resultant stable radical polymers can be used as both cathode and anode to give a "pure" radical battery.[91] A well-known example has PTMA as the cathode and poly(galvinoxylstyrene) as the anode, which can be charged in less than 30 s and generate burst power at rated voltages.[92]

1.2.4 Electron transport in stable radical polymers

The electron transport studies in stable free radicals have also been extended to their polymeric radical molecules. However, the increase in molecular weight and the entanglement of the polymer backbones usually reduces the interactions and mobility of radical sites, thus decreasing the possibility of electron transport between the adjacent sites. Despite the presence of unpaired electrons which have singly-occupied orbitals in the adjacent radical center to jump to, the common organic stable radical polymers do not benefit from a crystal packing D-A structure or π delocalization in the molecular systems. As an alternative, the transport process in a radical polymer is usually related to "hopping theory". In stable radical polymer electrodes, charge can be transported via electron hopping between redox sites and/or by physical diffusion of ions through the electrode material. In this context, a liquid state or swollen state are preferred due to their

fast electrochemical reaction kinetics and thus faster charge storage.[90,93]

As major efforts were being directed toward development of stable nitroxide radical polymers as electrode-active materials in organic batteries, a critical problem surfaced: the non-conjugated stable radical polymers are usually highly insulating materials, which makes charge transport through the cathode extremely difficult. Therefore, it is not surprising that in most literature the dominant strategy to fabricate a practical stable radical electrode involves the incorporation of inorganic carbon black materials into the polymers or direct attachment of stable radical groups onto conducting substrates, even though the carbon remains inert in the redox process and impairs the total capacity. Generally, the higher the content of stable radical polymers, the higher the capacity and resistance.[94]

However, starting from 2013, the Boudouris group at Purdue University reported a series of electron transport studies based on non-conjugated stable radical polymers with pendent TEMPO groups. Their first important discovery was that they have observed conductivity of around 10^{-6} S/cm in neat PTMA solid films using a lateral two-wire device and claimed that the presence of oxidized species – oxoammonium can further increase the conductivity by 5 times. From this point on, the idea that the stable radical polymers can conduct electrons has driven not only theorists, but also many materials scientists to reinvestigate the electron transport process in these organic materials. Nonetheless, the chemical structures of stable radical polymers available for such studies are limited by the difficult synthesis, and the most exciting conductivity reports are based on previously studied species. In 2017, Boudouris *et. al.* reported conductivity as high as 10^{-4} S/cm with polynorbornene with pendent TEMPO radicals[95], which was first

studied by Nishide in last decade. So far, no reports of comparable conductivity of PTMA have been published by other research groups. In 2018, Boudouris *et al.* reported that they found the conductivity in poly(ethylene oxide) with pendent cyclic nitroxide radicals can be as high as 20 S/m,[96] while similar structure have been investigated by Nishide *et al.* in 2008 and no substantial electrical conductivity was found.[66]

From a series of reports from Boudouris group, several conclusions can be drawn for the conducting polymer with nitroxide stable radicals. i) Enough nitroxide radical sites and proximity between the radicals are prerequisites for efficient electron hopping.[95,97] ii) The electrical conductivity of the solid-state radical polymer films is independent of the testing environment, including presence of water and air. iii) Their electron transport behavior is independent of the temperature or the radical content inside the thin film, which is totally different from the charge hopping models proposed for conjugated polymers.

Despite the series of exciting reports from the Boudouris group, so far there are few reported comparable conductivity values from other groups. One possible explanation of the contradictory results from the different groups could be the switchable conductor-insulator transitions in the stable radical polymer thin films. Nishide *et al.* have observed an ON-OFF transition in a battery-inspired device with an ITO/PTMA/PVDF/PGSt/Al (PVDF = poly(vinylidene difluoride)) configuration. When an increasing voltage of 0 to -5 V was applied, the state of the device switched to low resistance (ON state) at -4.5 V, which was maintained during the reverse sweep of the voltage from -5 to 1.4 V. However, using a bias at +1.5V can switch the device sharply to the high-resistance or OFF state again.[98] Gilroy *et. al.* have synthesized redox-active 6-oxoverdazyl polymers *via* ring-

opening metathesis polymerization (ROMP) and investigated the electrical properties of thin films, from approximately 10 nm to 50 nm in thickness, by using a sandwich structure device. They observed non-ohmic conductivity and thickness-dependent resistivity in ultra-thin polymeric films. While the high-conductivity state can be explained by extended-state transport *via* free electrons, the low-conductivity, Poole-Frenkel-like transport mechanism was attributed to hopping between localized states situated at specific charged monomers along a polymer filament. Also, the hopping may strongly depend on the alignment of the polymer.[99] In Boudouris's report, though sandwich architecture and thin films were intensively used for reports after 2016, very often these conductor-insulator transitions and related measurement conditions are not mentioned or observed when such mechanisms are suggested to describe their higher conductivity values. As a result, the thin film properties of the stable radical polymers in sandwich devices cannot be assumed active for the bulk polymer, since these intriguing high conductivity values could be misleading for research on energy storage devices and other related fields.

1.3 Polythiophenes

1.3.1 Kumada Catalyst-Transfer Polymerization (KCTP)

Synthesis of polythiophenes were dominated by oxidative or electrochemical polymerization before the chemical preparation of soluble 3-alkylpolythiophene (P3AT) *via* transition metal-catalyzed cross-coupling polymerizations. Later, synthesis of regioregular P3HT (**Fig. 1.7 (a)**) with narrow dispersity were reported in 2004 by two groups, McCullough and Yokozawa. Both

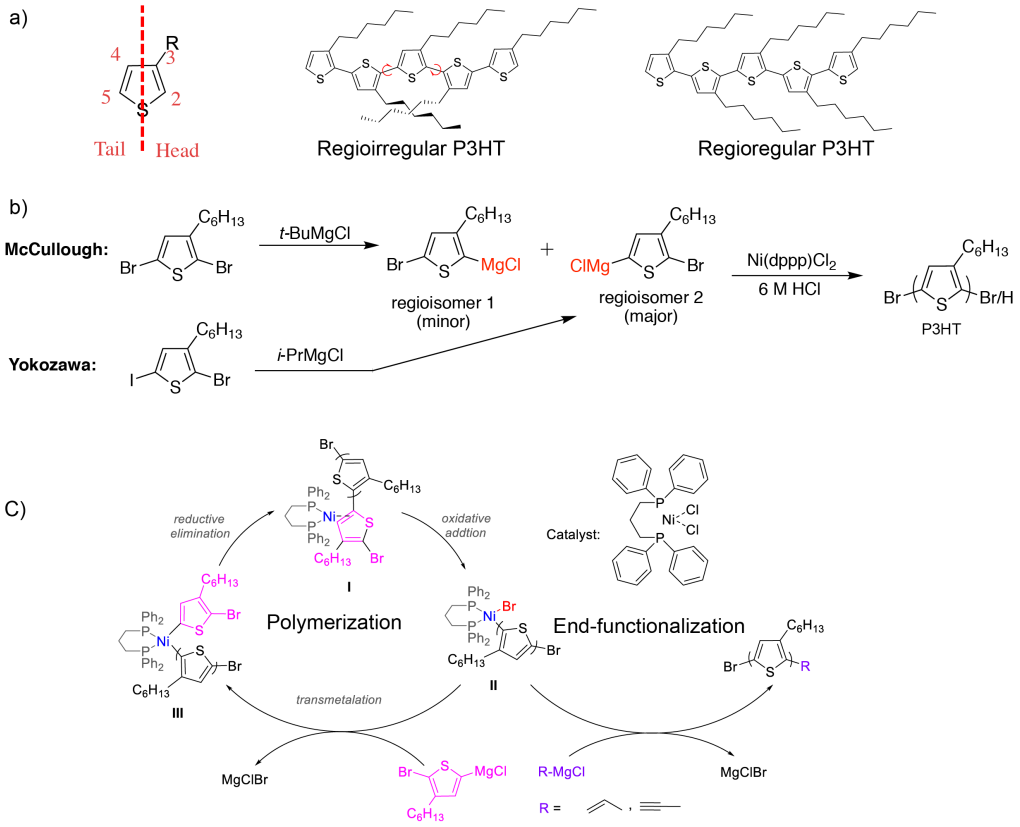

Figure 1.7. a) Schematic presentation of regioirregular and regioregular poly(3-hexylthiophene) (P3HT). b) Synthesis of regioregular P3HT *via* McCullough and Yokozawa methods. c) Mechanism of chain propagation and chain end-functionalization *via* Kumada Catalyst-Transfer Polymerization (KCTP).

methods are based on the Ni-catalyzed cross-coupling reactions of a bifunctional thiophene Grignard monomer with halogen substituent, but the preparation of the Grignard monomers differs. (**Fig. 1.7 (b)**) Briefly, the McCullough method (also known as Grignard Metathesis (GRIM) Polymerization) involves the magnesium-halogen exchange between 2,5-dibromo-3-alkylthiophene and *tert*-butyl magnesium chloride, which gives a preferred generation of regioisomer 2 (85%) due to the steric hindrance.[100] During the polymerization, the regioisomer 2 is incorporated into the polymer chain, while the more sterically hindered regioisomer 1 is not consumed. On the other hand, Yokozawa method starts from a different monomer, 2-bromo-5-iodo-3-alkylthiophene, which undergoes magnesium-halogen exchange with *iso*-propylmagnesium chloride exclusively on the iodo group rather than on the bromo group. For this reason, the Yokozawa method has the advantage of higher monomer efficiency and better molecular weight control, since the efficiency of Grignard methathesis in McCullough's method is susceptible to many factors, such as concentration, temperature and Grignard structure. However, the synthesis and purification of the monomers for Yokozawa method are often cumbersome, which makes McCullough method the most frequently used option for the material research groups.

Later, many reports demonstrated that both McCullough and Yokozawa methods follow the same chain-growth mechanism, which is termed as Kumada Catalyst-Transfer Polymerization (KCTP). The KCTP has the potential to control the conjugated segment length, sequence, and functionality at the chain end, which make it an advantageous polymerization method for electron rich monomers, especially 3-substituted thiophenes.[101] In KCTP, controlled chain propagation

proceeds through a M(0)/M(II) catalytic cycle, including oxidative addition, transmetallation and reductive elimination. (**Fig. 1.7 (c)**) Although palladium catalysts have been used[102], the Ni catalysts usually have a better control over the polymerization process[103,104]. The most crucial difference between KCTP and traditional step-growth polymerization is ring-walking, wherein the catalyst has complexes with the conjugated π-system of the growing polymer chain and migrates to the terminal C-Br for oxidative addition.[105] This mechanism enables the catalyst to remain on a single chain to add monomers sequentially, so that well-defined structures and low dispersities can be achieved through the quasi-living process. On the other hand, poor association between catalyst and the polymer backbone results in termination due to disproportionation[106] or chain transfer of reactive Ni(0)[107]. Later, more studies have revealed the details of the KCTP, including the effect of changing the initiator structure[108,109], ligand effects[110], monomer species[111,112], additives[113], halogen and the organometallic function[114].

Besides the excellent control of the conjugated polymer backbone, the quasi-living KCTP is also capable of introducing various moieties for preparation of end-functionalized polymers.[115] The functional groups can be easily introduced by either deploying a functional initiator in the beginning of each polymer chain[116] or appropriate quencher at the end of polymerization. Generally, KCTP has two kinds of initiation processes: i) internal initiation by a precatalyst having an L_nMX_2 structure, such as Ni(dppp)Cl_2 (dppp = 1,3-bis(diphenylphosphino)propane), and ii) external initiation by $L_nM(Ar)X$ counterparts. For internal initiation, catalyst first reacts with the monomer to form a tail-to-tail (T-T) bithiophene initiator, and the Đ of the synthesized polymer is controlled by this catalyst activation with

respect to the subsequent chain propagation.[117] However, if an aromatic ring to the Ni is functionalized with an end group, then the polythiophene chain can be end-functionalized.

The KCTP methodology has also been extended towards the preparation of surface-bound conjugated polymer brushes in surface-initiated KCTP (SI-KCTP).[118,119] Due to the steric constraints at the interface, the traditional method using the coupling between solution synthesized conjugated polymers and reactive groups on the substrate ("grafting to" method) usually suffer from low grafting density and brush thickness.[120,121] Alternatively, polymerization of the AB-type Grignard monomer from a surface-bound layer containing an aryl halide with Ni(II) complex ("grafting from") gives polythiophene films of up to 200 nm.[122] Currently, most of the Ni(II) initiator layers are prepared by oxidative addition of a highly reactive Ni(0) species (such as $Ni(COD)_2$) to the surface-bound aryl halide layer followed by ligand exchange with a bidentate phosphine ligand (such as dppp). However, inherent limitations exist, including the low grafting densities due to incomplete exchange reactions and side reactions of a highly reactive Ni(0).[123] As an alternative, a direct method was proposed by Nesterov *et al.* by synthesizing an active Ni(II) catalyst in a separate step before surface immobilization, which can exclude the incomplete conversion of aryl halide precursor and therefore improve the surface density of initiator (**Fig. 1.8**).[124] The air-stable $L_nM(Ar)X$ initiators can be prepared from air-stable Ni(II) precatalysts rather than the reactive Ni(0) species[125], which makes the direct method a promising strategy for the synthesis of homogeneous thick conjugated polymer brushes.

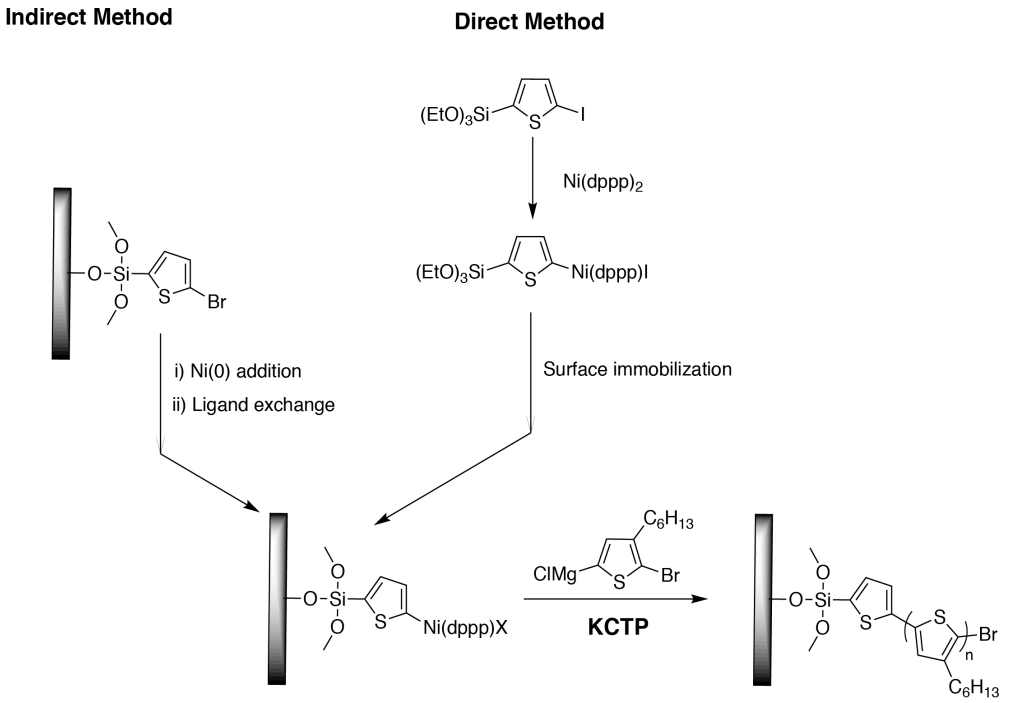

Figure 1.8. Two different methods for the preparation of surfaced-confined Ni(II) initiator of surface-initiated Kumada catalyst-transfer polymerization (KCTP). In the indirect method, the surface-immobilized initiator is prepared by oxidative addition of Ni(0) precatalyst to a surface immobilized initiator, followed by a subsequent ligand exchange with dppp. On the other hand, the direct method relies on the preparation of a Ni(II) initiator in solution and a subsequent surface immobilization, which can improve the grafting density of Ni.

1.3.2 Structure-property relationships in P3HT

Polythiophenes have been intensively studied as a prototypical semiconducting polymer due to their fascinating properties, such as high conductivity, and solution processability. These excellent properties usually originate from the polymer conformations and the morphologies of the conjugated polymers. There are numerous studies based on the structure-property relationship in polythiophene based polymers, and P3HT has been the most popular one and there are several review papers and books[126] regarding their synthesis and characterization and properties.

From a morphological perspective, the most important structure parameter for P3HT is the degree of order, which requires a structural descriptor that can quantifiably describe the linking between the 3-substituted thiophene monomers. In the asymmetrical 3-substituted thiophene, the 2-position is labeled as the “head” position (H) and the 5-position is labeled as the “tail” position (T). Three different regioisomers can be generated during dimer formation, which are head-head (H-H), head-tail (H-T) and tail-tail (T-T). The regioregularity of polythiophene is denoted at the percentage of the arranged H-T units in the backbone. In the perfect poly(3-alkylthiophene) polymer chain synthesized *via* KTCP, all the coupling between the thiophene rings are H-T couplings, which gives the polymer backbone a planar conformation for better π-stacking with adjacent chains. However, the oxidative and electrochemical polymerization often give a mixture of three connection, which is called regioirregular polythiophenes.

Optical spectroscopy is a good tool to give information about the structure as well as the aggregation state of P3HT. In the solution state, P3HT usually exhibits

a single broad absorption peak in UV-vis spectrum without any structural features, indicating that the individual P3HT chain takes a coiled conformation without any interchain packing effects.[127] Incorporation of H-H or T-T defects in the P3HT chain results in a wider distribution of conformation due to the unfavorable side chain interactions, which results in the changes of absorbance and fluorescence. When dissolved in good solvents, regioregular P3HT has absorption and fluorescence spectra maxima at 454 and 577 nm, respectively. However, for the regioirregular P3HT, the peak maxima shift to 420 nm and 577 nm, suggesting the larger dihedral twist of polythiophene backbone and thus a decreased conjugation length.[128–130] In thin films, the P3HT can have efficient packing and form an ordered crystalline structure due to its rigid and planar chain conformation. Depending on its regioregularity, molecular weight, side chain length and processing, P3HT can exhibit colors from orange to dark purple when cast from solution. For well-packed P3HT films, the absorption maxima significantly red-shift compared with that of P3HT solution, and the well-defined vibronic features can often be observed. This can be explained by chain planarization and conjugation extension during film formation, which enhances the π-π interaction between the adjacent polythiophene backbones.

Regarding charge transport, there are two factors, intrachain and interchain transport, that need to be considered for P3HT homopolymer. Firstly, the interchain charge transport occurs along the backbone axis (c-axis) and is a fast process. However, due to the limited chain length of individual polythiophene backbones, the conductivity of the P3HT film is mainly determined by the interchain charge transport rather than intrachain transport. It is generally believed that the interchain transport occurs along the π-stacking direction (c-axis) is a fast process, whereas

the insulating side chains (a-axis) act as charge barriers and leads to low mobility. In this context, the overall conductivity of P3HT film is mainly determined by the twisted chains in the amorphous matrix because the charges become trapped at grain boundaries between the crystalline regions. In this context, the high molecular weight P3HT usually exhibits higher conductivity because the longer chains can bridge the crystalline domains, which enhance the macroscopic electron transport process.[131]

1.3.3 P3HT-containing block copolymers

Owing to its semicrystalline nature, the performance of P3HT is closely related to the crystallization behavior, which is determined by factors such as molecular weight, regioregularity and processing method.[126] The crystalline domains in low molecular weight P3HT always exist as randomly oriented short fibers embedded in an amorphous matrix, and such lack of long range order often impedes the further enhancement of charge transport since the amorphous component acts as charge traps. Although increasing the molecular weight of P3HT can be a facile solution, the mobilization of the chains also becomes more difficult as the chains get longer, thus excluding the possibility of treatments like simple annealing.

Another option to tune the crystallinity and long-range order is fabrication of block copolymers which contain a P3HT segment and a non-conjugated segments.[132] Due to their different persistence lengths, the conjugated block is always referred to as a “rod” component while the non-conjugated block is called a “coil” segment. By connecting the coil segment to the end of “rod”-like P3HT by a fcovalent bond, additional mobility can be provided to the conjugated segments

and microphase separation between the “rod” and “coil” domains can be achieved, thus providing a better chance to manipulate the crystalline behavior of the conjugated domain and control the film architecture at the nanoscale.[133] Many reports have studied the self-assembly of conjugated rod-coil block copolymers and found they are promising to stack highly ordered structures to improve the charge transport and the resulting device performance.[134–137]

In general, two methods have been widely used in the preparation of rod-coil P3HT-containing block copolymers. The first method is synthetically more challenging, which requires the preparation of end-functionalized polythiophene block, from which a second polymerization can be initiated. Such method is called as “grafting from”, and various P3HT macro-initiator have been developed for different polymerization techniques, including reversible addition-fragmentation chain transfer polymerization (RAFT)[138], atom transfer radical polymerization (ATRP)[139–141], nitroxide-mediated living radical polymerization (NMP)[142], ring-opening[143] and anionic polymerization[144]. In the second approach, the end-functionalized rod segment is first prepared and then subsequently reacted with an end-modified, non-conjugated coil block. Due to the lower number of reactive sites, highly efficient reaction conditions, such as anionic coupling and click reactions, are often used.[137,145–147]

1.4 Summary

In a broader context, polymers with pendent stable radicals can be viewed as a new class of spin-containing materials in which many competing effects generate experimental interest, characterization potential and theoretical difficulty. In this

thesis, research studies will focus on synthesis of these stable radical containing polymers and several important fundamental questions on electron transport in the solid-state radical polymers: 1) What are the fundamental mechanisms of electronic transport involving stable radical polymers? 2) How do stable radicals influence conductivity and charge storage in solid polymer films? 3) Can we control the conductivity of stable radical polymers by introducing conjugation to the polymer backbone? 4) Can we use confinement and orientation imposed through block copolymer self-assembly to influence the conductivity and charge storage?

With these questions in mind, the purpose of **Chapter 2** is to prepare PTMA, a nitroxide radical-containing polymers with aliphatic backbone, by utilizing a combination of controlled polymerization techniques and appropriate chemical oxidations. Different synthetic methods and their impact on PTMA conductivity will be discussed in **Chapter 2**, which mainly focus on the redox pair consisting of neutral radicals and the oxoammonium cations. Using both solution-state and solid-state EPR measurements, the content of spins in the synthesized PTMA samples can be known. By careful electrical measurements using a four-point geometry, the highly insulating nature of PTMA has been revealed, and theoretical understanding was also included to interpret these results.

In **Chapter 3**, we developed a facile preparation method to replace the aliphatic backbone of PTMA with conjugated polythiophene backbone. By using a combination of Grignard metathesis (GRIM) polymerization and subsequent "click" reaction, the resultant conjugated radical polymer can be obtained with both high regioregularity and tunable contents of nitroxide radical pendent groups.

Optical spectroscopy combined with atomic force microscopy (AFM) indicate that the introduction of bulky TEMPO radical groups twists the conjugated polymer backbone as well as impede the intermolecular packing between the adjacent polythiophene chains. As a result, the crystallinity of the synthesized P3HT-TEMPO films decreases with the TEMPO content, and the conductivities n the neutral polymer films show an exponential decrease as TEMPO content increases.

In **Chapter 4**, we continued to study the doping behavior of the conjugated radical polymers due to the presence of two distinct redox components in these materials. Using electrochemical doping, we found that there exist a two-step doping process in the P3HT-TEMPO, including the oxidation of nitroxide radical at the first stage (~ 3.6 V vs. Li^+/Li), followed by the oxidation of polythiophene backbone at a higher voltage. The capacity of P3HT-TEMPO was also found to be much lower compared with both P3HT and PTMA homopolymer, which can be explained by the proposed internal charge transfer mechanism. Finally, two chemical dopants, iodine and F4-TCNQ, were used to dope the neutral P3HT-TEMPO polymer films, and the conductivity of the doped samples were improved by up to 5 orders of magnitude. However, due to the steric hindrance of TEMPO radicals, the decreasing trend in conductivity still exists as the TEMPO content increases.

In **Chapter 5**, the major aim is to synthesize a "rod-coil" P3HT-*b*-PTMA diblock copolymer consisting of a conjugated segment and an aliphatic stable radical polymer segment. By connecting the stable radical polymer segment to conjugated polythiophene, we hope that it can increase the mobility of P3HT segment as well as have microphase separation. Two methods, "grafting from" and

“grafting to” have been explored, and “grafting to” turned out to be a better method since it showed more control over the molecular structure as well as the elimination of unwanted oxidation on the conjugated blocks. By using single-electron transfer living radical polymerization, shorter PTMA chains can be prepared, which enables better tunability of the resultant diblock copolymer structure.

1.5 References

1 D. I. Davies and M. J. Parrott, *Free Radicals in Organic Synthesis*, Springer Berlin Heidelberg, Berlin, Heidelberg, 1978, vol. 7.

2 M. Gomberg, *Journal of the American Chemical Society*, 1900, **22**, 757–771.

3 E. M. Kosower and E. J. Poziomek, *Journal of the American Chemical Society*, 1964, **86**, 5515–5523.

4 L. J. Berliner and J. Reuben, *Spin Labeling: Theory and Applications*, Springer US, Boston, MA, 1989.

5 W. L. Hubbell, D. S. Cafiso and C. Altenbach, *Nat. Struct Biol.*, 2000, **7**, 735–739.

6 P. A. Kosen, in *Methods in Enzymology*, Elsevier, 1989, vol. 177, pp. 86–121.

7 S. Pou, H. J. Halpern, P. Tsai and G. M. Rosen, *Accounts of Chemical Research*, 1999, **32**, 155–161.

8 E. G. Janzen, *Accounts of Chemical Research*, 1971, **4**, 31–40.

9 D. Rehorek, *Chemical Society Reviews*, 1991, **20**, 341.

10 G. R. Buettner, *Free Radical Biology and Medicine*, 1987, **3**, 259–303.

11 A. L. J. Beckwith, V. W. Bowry and K. U. Ingold, *Journal of the American Chemical Society*, 1992, **114**, 4983–4992.

12 V. W. Bowry and K. U. Ingold, *Journal of the American Chemical Society*, 1992, **114**, 4992–4996.

13 A. Studer and T. Schulte, *The Chemical Record*, 2005, **5**, 27–35.

14 Q. Cao, L. M. Dornan, L. Rogan, N. L. Hughes and M. J. Muldoon, *Chem. Commun.*, 2014, **50**, 4524–4543.

15 R. A. Sheldon, I. W. C. E. Arends, G.-J. ten Brink and A. Dijksman, *Accounts*

of Chemical Research, 2002, **35**, 774–781.

16 A. Studer, *Chemistry*, 2001, **7**, 1159–1164.

17 John. Ferraris, D. O. Cowan, V. Walatka and J. H. Perlstein, *Journal of the American Chemical Society*, 1973, **95**, 948–949.

18 R. C. Haddon, S. V. Chichester, S. M. Stein, J. H. Marshall and A. M. Mujsce, *The Journal of Organic Chemistry*, 1987, **52**, 711–712.

19 P. A. Koutentis, Y. Chen, Y. Cao, T. P. Best, M. E. Itkis, L. Beer, R. T. Oakley, A. W. Cordes, C. P. Brock and R. C. Haddon, *Journal of the American Chemical Society*, 2001, **123**, 3864–3871.

20 J. Huang and M. Kertesz, *Journal of the American Chemical Society*, 2006, **128**, 1418–1419.

21 L. Beer, J. F. Britten, J. L. Brusso, A. W. Cordes, R. C. Haddon, M. E. Itkis, D. S. MacGregor, R. T. Oakley, R. W. Reed and C. M. Robertson, *Journal of the American Chemical Society*, 2003, **125**, 14394–14403.

22 L. Beer, J. L. Brusso, A. W. Cordes, E. Godde, R. C. Haddon, M. E. Itkis, R. T. Oakley and R. W. Reed, *Chem. Commun.*, 2002, 2562–2563.

23 L. Beer, J. L. Brusso, A. W. Cordes, R. C. Haddon, M. E. Itkis, K. Kirschbaum, D. S. MacGregor, R. T. Oakley, A. A. Pinkerton and R. W. Reed, *Journal of the American Chemical Society*, 2002, **124**, 9498–9509.

24 L. Beer, J. F. Britten, O. P. Clements, R. C. Haddon, M. E. Itkis, K. M. Matkovich, R. T. Oakley and R. W. Reed, *Chemistry of Materials*, 2004, **16**, 1564–1572.

25 J. L. Brusso, S. Derakhshan, M. E. Itkis, H. Kleinke, R. C. Haddon, R. T. Oakley, R. W. Reed, J. F. Richardson, C. M. Robertson and L. K. Thompson, *Inorganic Chemistry*, 2006, **45**, 10958–10966.

26 J. L. Brusso, K. Cvrkalj, A. A. Leitch, R. T. Oakley, R. W. Reed and C. M. Robertson, *Journal of the American Chemical Society*, 2006, **128**, 15080–15081.

27 F. Gerson and W. Huber, *Electron spin resonance spectroscopy of organic radicals*, Wiley-VCH, Weinheim, 2003.

28 M. Mas-Torrent, N. Crivillers, C. Rovira and J. Veciana, *Chemical Reviews*, 2012, **112**, 2506–2527.

29 P. L. Kumler and R. F. Boyer, *Macromolecules*, 1976, **9**, 903–910.

30 G. G. Cameron, D. Stewart, R. Buscall and J. Nemcek, *Polymer*, 1994, **35**, 3384–3388.

31 G. G. Cameron and D. Stewart, *Polymer*, 1996, **37**, 5329–5334.

32 M. Pannier, V. Schädler, M. Schöps, U. Wiesner, G. Jeschke and H. W. Spiess, *Macromolecules*, 2000, **33**, 7812–7818.

33 M. Pannier, M. Schöps, V. Schädler, U. Wiesner, G. Jeschke and H. W. Spiess, *Macromolecules*, 2001, **34**, 5555–5560.

34 Y. Miwa, K. Tanida, K. Yamamoto, S. Okamoto, M. Sakaguchi, M. Sakai, S. Makita, S. Sakurai and S. Shimada, *Macromolecules*, 2004, **37**, 3707–3716.

35 Y. Miwa, K. Yamamoto, M. Sakaguchi, M. Sakai, K. Tanida, S. Hara, S. Okamoto and S. Shimada, *Macromolecules*, 2004, **37**, 831–839.

36 A. Maliakal, M. Weber, N. J. Turro, M. M. Green, S. Y. Yang, S. Pearsall and M.-J. Lee, *Macromolecules*, 2002, **35**, 9151–9155.

37 M. J. N. Junk, W. Li, A. D. Schlüter, G. Wegner, H. W. Spiess, A. Zhang and D. Hinderberger, *Angewandte Chemie International Edition*, 2010, **49**, 5683–5687.

38 Y. Xia, Y. Li, A. O. Burts, M. F. Ottaviani, D. A. Tirrell, J. A. Johnson, N. J.

Turro and R. H. Grubbs, *Journal of the American Chemical Society*, 2011, **133**, 19953–19959.

39 M. F. Ottaviani, S. Bossmann, N. J. Turro and D. A. Tomalia, *Journal of the American Chemical Society*, 1994, **116**, 661–671.

40 A. W. Bosman, R. A. J. Janssen and E. W. Meijer, *Macromolecules*, 1997, **30**, 3606–3611.

41 A. J. Maliakal, N. J. Turro, A. W. Bosman, J. Cornel and E. W. Meijer, *The Journal of Physical Chemistry A*, 2003, **107**, 8467–8475.

42 G. M. Coppinger and J. D. Swalen, *Journal of the American Chemical Society*, 1961, **83**, 4900–4902.

43 J. A. Weil and J. R. Bolton, *Electron paramagnetic resonance: elementary theory and practical applications*, Wiley-Interscience, Hoboken, N.J, 2nd ed., 2007.

44 K. Oyaizu, T. Kawamoto, T. Suga and H. Nishide, *Macromolecules*, 2010, **43**, 10382–10389.

45 H. Nishide, S. Iwasa, Y.-J. Pu, T. Suga, K. Nakahara and M. Satoh, *Electrochimica Acta*, 2004, **50**, 827–831.

46 B. K. Hughes, W. A. Braunecker, D. C. Bobela, S. U. Nanayakkara, O. G. Reid and J. C. Johnson, *The Journal of Physical Chemistry Letters*, 2016, **7**, 3660–3665.

47 K. M. Zwoliński and M. J. Chmielewski, *ACS Applied Materials & Interfaces*, 2017, **9**, 33956–33967.

48 H.-C. Lin, C.-C. Li and J.-T. Lee, *Journal of Power Sources*, 2011, **196**, 8098–8103.

49 Y.-H. Wang, M.-K. Hung, C.-H. Lin, H.-C. Lin and J.-T. Lee, *Chem.*

Commun., 2011, **47**, 1249–1251.

50 C.-H. Lin, W.-J. Chou and J.-T. Lee, *Macromolecular Rapid Communications*, 2012, **33**, 107–113.

51 A. Gheorghe, A. Matsuno and O. Reiser, *Advanced Synthesis & Catalysis*, 2006, **348**, 1016–1020.

52 J. Luo, C. Pardin, W. D. Lubell and X. X. Zhu, *Chemical Communications*, 2007, 2136.

53 Y. Y. Lim and R. S. Drago, *Inorganic Chemistry*, 1972, **11**, 1334–1338.

54 D. Luneau and P. Rey, *Coordination Chemistry Reviews*, 2005, **249**, 2591–2611.

55 J. F. W. Keana, *Chemical Reviews*, 1978, **78**, 37–64.

56 A. Nilsen and R. Braslau, *Journal of Polymer Science Part A: Polymer Chemistry*, 2006, **44**, 697–717.

57 C. Prescott and S. E. Bottle, *Cell Biochemistry and Biophysics*, 2017, **75**, 227–240.

58 K.-A. Hansen and J. P. Blinco, *Polymer Chemistry*, 2018, **9**, 1479–1516.

59 R. G. Hicks, *Organic & Biomolecular Chemistry*, 2007, **5**, 1321.

60 J. A. Crayston, A. Iraqi and J. C. Walton, *Chemical Society Reviews*, 1994, **23**, 147.

61 A. J. Wingate and B. W. Boudouris, *Journal of Polymer Science Part A: Polymer Chemistry*, 2016, **54**, 1875–1894.

62 K. Nakahara, S. Iwasa, M. Satoh, Y. Morioka, J. Iriyama, M. Suguro and E. Hasegawa, *Chemical Physics Letters*, 2002, **359**, 351–354.

63 T. Suga, Y.-J. Pu, S. Kasatori and H. Nishide, *Macromolecules*, 2007, **40**, 3167–3173.

64 T. Suga, S. Sugita, H. Ohshiro, K. Oyaizu and H. Nishide, *Advanced Materials*, 2011, **23**, 751–754.

65 M. Suguro, S. Iwasa, Y. Kusachi, Y. Morioka and K. Nakahara, *Macromolecular Rapid Communications*, 2007, **28**, 1929–1933.

66 K. Oyaizu, T. Suga, K. Yoshimura and H. Nishide, *Macromolecules*, 2008, **41**, 6646–6652.

67 T. Katsumata, M. Satoh, J. Wada, M. Shiotsuki, F. Sanda and T. Masuda, *Macromolecular Rapid Communications*, 2006, **27**, 1206–1211.

68 J. Qu, T. Katsumata, M. Satoh, J. Wada and T. Masuda, *Macromolecules*, 2007, **40**, 3136–3144.

69 K. Oyaizu, Y. Ando, H. Konishi and H. Nishide, *Journal of the American Chemical Society*, 2008, **130**, 14459–14461.

70 M. Suguro, A. Mori, S. Iwasa, K. Nakahara and K. Nakano, *Macromolecular Chemistry and Physics*, 2009, **210**, 1402–1407.

71 J. Qu, F. Z. Khan, M. Satoh, J. Wada, H. Hayashi, K. Mizoguchi and T. Masuda, *Polymer*, 2008, **49**, 1490–1496.

72 J. Qu, R. Morita, M. Satoh, J. Wada, F. Terakura, K. Mizoguchi, N. Ogata and T. Masuda, *Chemistry - A European Journal*, 2008, **14**, 3250–3259.

73 H. A. López-Peña, L. S. Hernández-Muñoz, B. A. Frontana-Uribe, F. J. González, I. González, C. Frontana and J. Cardoso, *The Journal of Physical Chemistry B*, 2012, **116**, 5542–5550.

74 L. Bugnon, C. J. H. Morton, P. Novak, J. Vetter and P. Nesvadba, *Chemistry of Materials*, 2007, **19**, 2910–2914.

75 T. Sukegawa, H. Omata, I. Masuko, K. Oyaizu and H. Nishide, *ACS Macro Letters*, 2014, **3**, 240–243.

76 T. Kurosaki, K. W. Lee and M. Okawara, *Journal of Polymer Science Part A-1: Polymer Chemistry*, 1972, **10**, 3295–3310.

77 T. Janoschka, A. Teichler, A. Krieg, M. D. Hager and U. S. Schubert, *Journal of Polymer Science Part A: Polymer Chemistry*, 2012, **50**, 1394–1407.

78 J. H. Osiecki and E. F. Ullman, *Journal of the American Chemical Society*, 1968, **90**, 1078–1079.

79 M. Aydın, B. Esat, Ç. Kılıç, M. E. Köse, A. Ata and F. Yılmaz, *European Polymer Journal*, 2011, **47**, 2283–2294.

80 M. Aydin and B. Esat, *Journal of Solid State Electrochemistry*, 2015, **19**, 2275–2281.

81 F. Li, Y. Zhang, S. R. Kwon and J. L. Lutkenhaus, *ACS Macro Letters*, 2016, **5**, 337–341.

82 N. Casado, G. Hernández, A. Veloso, S. Devaraj, D. Mecerreyes and M. Armand, *ACS Macro Letters*, 2016, **5**, 59–64.

83 J. Lu, J. Ma, J. Yi, Z. Shen, Y. Zhong, C. Ma and M. Li, *Electrochimica Acta*, 2014, **130**, 412–417.

84 L. Xu, F. Yang, C. Su, L. Ji and C. Zhang, *Electrochimica Acta*, 2014, **130**, 148–155.

85 Y. Xie, K. Zhang, M. J. Monteiro and Z. Jia, *ACS Applied Materials & Interfaces*, 2019, **11**, 7096–7103.

86 K. Nakahara, K. Oyaizu and H. Nishide, *Chemistry Letters*, 2011, **40**, 222–227.

87 T. Suga, Y.-J. Pu, K. Oyaizu and H. Nishide, *Bulletin of the Chemical Society of Japan*, 2004, **77**, 2203–2204.

88 Y. Liang, Z. Tao and J. Chen, *Advanced Energy Materials*, 2012, **2**, 742–769.

89 H. Nishide, K. Koshika and K. Oyaizu, *Pure and Applied Chemistry*, 2009, **81**, 1961–1970.

90 C. Karlsson, T. Suga and H. Nishide, *ACS Applied Materials & Interfaces*, 2017, **9**, 10692–10698.

91 T. Suga, H. Ohshiro, S. Sugita, K. Oyaizu and H. Nishide, *Advanced Materials*, 2009, **21**, 1627–1630.

92 H. Nishide and K. Oyaizu, *Science*, 2008, **319**, 737–738.

93 E. Mourad, L. Coustan, P. Lannelongue, D. Zigah, A. Mehdi, A. Vioux, S. A. Freunberger, F. Favier and O. Fontaine, *Nature Materials*, 2017, **16**, 446–453.

94 J.-K. Kim, G. Cheruvally, J.-H. Ahn, Y.-G. Seo, D. S. Choi, S.-H. Lee and C. E. Song, *Journal of Industrial and Engineering Chemistry*, 2008, **14**, 371–376.

95 M. E. Hay, S. Hui Wong, S. Mukherjee and B. W. Boudouris, *Journal of Polymer Science Part B: Polymer Physics*, 2017, **55**, 1516–1525.

96 Y. Joo, V. Agarkar, S. H. Sung, B. M. Savoie and B. W. Boudouris, *Science*, 2018, **359**, 1391–1395.

97 T. W. Kemper, R. E. Larsen and T. Gennett, *The Journal of Physical Chemistry C*, 2014, **118**, 17213–17220.

98 Y. Yonekuta, K. Susuki, K. Oyaizu and K. Honda, *Journal of the American Chemical Society*, 2007, **129**, 14128–14129.

99 J. A. Paquette, S. Ezugwu, V. Yadav, G. Fanchini and J. B. Gilroy, *Journal of Polymer Science Part A: Polymer Chemistry*, 2016, **54**, 1803–1813.

100 M. C. Iovu, E. E. Sheina, R. R. Gil and R. D. McCullough, *Macromolecules*, 2005, **38**, 8649–8656.

101 A. K. Leone, E. A. Mueller and A. J. McNeil, *Journal of the American Chemical Society*, 2018, **140**, 15126–15139.

102 Y. Zhao, A. J. Nett, A. J. McNeil and P. M. Zimmerman, *Macromolecules*, 2016, **49**, 7632–7641.

103 X. Shi, A. Sui, Y. Wang, Y. Li, Y. Geng and F. Wang, *Chemical Communications*, 2015, **51**, 2138–2140.

104 M. P. Bhatt, H. D. Magurudeniya, P. Sista, E. E. Sheina, M. Jeffries-EL, B. G. Janesko, R. D. McCullough and M. C. Stefan, *Journal of Materials Chemistry A*, 2013, **1**, 12841.

105 K. Mikami, M. Nojima, Y. Masumoto, Y. Mizukoshi, R. Takita, T. Yokozawa and M. Uchiyama, *Polymer Chemistry*, 2017, **8**, 1708–1713.

106 J. A. Bilbrey, S. K. Sontag, N. E. Huddleston, W. D. Allen and J. Locklin, *ACS Macro Letters*, 2012, **1**, 995–1000.

107 B. C. Achord and J. W. Rawlins, *Macromolecules*, 2009, **42**, 8634–8639.

108 N. Doubina, A. Ho, A. K.-Y. Jen and C. K. Luscombe, *Macromolecules*, 2009, **42**, 7670–7677.

109 N. Doubina, S. A. Paniagua, A. V. Soldatova, A. K. Y. Jen, S. R. Marder and C. K. Luscombe, *Macromolecules*, 2011, **44**, 512–520.

110 N. Doubina, M. Stoddard, H. A. Bronstein, A. K.-Y. Jen and C. K. Luscombe, *Macromolecular Chemistry and Physics*, 2009, **210**, 1966–1972.

111 C. R. Bridges, H. Yan, A. A. Pollit and D. S. Seferos, *ACS Macro Letters*, 2014, **3**, 671–674.

112 T. Hardeman and G. Koeckelberghs, *Macromolecules*, 2015, **48**, 6987–6993.

113 S. Wu, L. Huang, H. Tian, Y. Geng and F. Wang, *Macromolecules*, 2011, **44**, 7558–7567.

114 T. Hardeman, J. De Becker and G. Koeckelberghs, *Journal of Polymer Science Part A: Polymer Chemistry*, 2016, **54**, 3701–3706.

115 N. V. Handa, A. V. Serrano, M. J. Robb and C. J. Hawker, *Journal of Polymer Science Part A: Polymer Chemistry*, 2015, **53**, 831–841.

116 A. Smeets, P. Willot, J. De Winter, P. Gerbaux, T. Verbiest and G. Koeckelberghs, *Macromolecules*, 2011, **44**, 6017–6025.

117 R. Grisorio and G. P. Suranna, *Polymer Chemistry*, 2015, **6**, 7781–7795.

118 N. Marshall, S. K. Sontag and J. Locklin, *Macromolecules*, 2010, **43**, 2137–2144.

119 R. Tkachov, V. Senkovskyy, U. Oertel, A. Synytska, M. Horecha and A. Kiriy, *Macromolecular Rapid Communications*, 2010, **31**, 2146–2150.

120 N. Ayres, *Polym. Chem.*, 2010, **1**, 769–777.

121 W.-L. Chen, R. Cordero, H. Tran and C. K. Ober, *Macromolecules*, 2017, **50**, 4089–4113.

122 A. Roy, J. Gao, J. A. Bilbrey, N. E. Huddleston and J. Locklin, *Langmuir*, 2014, **30**, 10465–10470.

123 S. K. Sontag, G. R. Sheppard, N. M. Usselman, N. Marshall and J. Locklin, *Langmuir*, 2011, **27**, 12033–12041.

124 S. G. Youm, E. Hwang, C. A. Chavez, X. Li, S. Chatterjee, K. L. Lusker, L. Lu, J. Strzalka, J. F. Ankner, Y. Losovyj, J. C. Garno and E. E. Nesterov, *Chemistry of Materials*, 2016, **28**, 4787–4804.

125 E. A. Standley, S. J. Smith, P. Müller and T. F. Jamison, *Organometallics*, 2014, **33**, 2012–2018.

126 S. Ludwigs and D. Andrienko, Eds., *P3HT revisited - from molecular scale to solar cell devices*, Springer, Berlin, 2014.

127 G. W. Heffner and D. S. Pearson, *Macromolecules*, 1991, **24**, 6295–6299.

128 T.-A. Chen, X. Wu and R. D. Rieke, *Journal of the American Chemical*

Society, 1995, **117**, 233–244.

129 H. Mao, B. Xu and S. Holdcroft, *Macromolecules*, 1993, **26**, 1163–1169.

130 B. Xu and S. Holdcroft, *Macromolecules*, 1993, **26**, 4457–4460.

131 R. Noriega, J. Rivnay, K. Vandewal, F. P. V. Koch, N. Stingelin, P. Smith, M. F. Toney and A. Salleo, *Nature Materials*, 2013, **12**, 1038–1044.

132 A. Yassar, L. Miozzo, R. Gironda and G. Horowitz, *Progress in Polymer Science*, 2013, **38**, 791–844.

133 H. Lim, C.-Y. Chao and W.-F. Su, *Macromolecules*, 2015, **48**, 3269–3281.

134 M. Lee, B.-K. Cho and W.-C. Zin, *Chemical Reviews*, 2001, **101**, 3869–3892.

135 F. J. M. Hoeben, P. Jonkheijm, E. W. Meijer and A. P. H. J. Schenning, *Chemical Reviews*, 2005, **105**, 1491–1546.

136 B. Olsen and R. Segalman, *Materials Science and Engineering: R: Reports*, 2008, **62**, 37–66.

137 J.-Y. Lee, C.-J. Lin, C.-T. Lo, J.-C. Tsai and W.-C. Chen, *Macromolecules*, 2013, **46**, 3005–3014.

138 M. R. Kern and S. G. Boyes, *Journal of Polymer Science Part A: Polymer Chemistry*, 2014, n/a-n/a.

139 C. R. Craley, R. Zhang, T. Kowalewski, R. D. McCullough and M. C. Stefan, *Macromolecular Rapid Communications*, 2009, **30**, 11–16.

140 M. Surin, O. Coulembier, K. Tran, J. D. Winter, P. Leclère, P. Gerbaux, R. Lazzaroni and P. Dubois, *Organic Electronics*, 2010, **11**, 767–774.

141 J. B. Gilroy, D. J. Lunn, S. K. Patra, G. R. Whittell, M. A. Winnik and I. Manners, *Macromolecules*, 2012, **45**, 5806–5815.

142 E. Kaul, V. Senkovskyy, R. Tkachov, V. Bocharova, H. Komber, M. Stamm and A. Kiriy, *Macromolecules*, 2010, **43**, 77–81.

143 V. Ho, B. W. Boudouris, B. L. McCulloch, C. G. Shuttle, M. Burkhardt, M. L. Chabinyc and R. A. Segalman, *Journal of the American Chemical Society*, 2011, **133**, 9270–9273.

144 C.-A. Dai, W.-C. Yen, Y.-H. Lee, C.-C. Ho and W.-F. Su, *Journal of the American Chemical Society*, 2007, **129**, 11036–11038.

145 T. Higashihara, K. Ohshimizu, A. Hirao and M. Ueda, *Macromolecules*, 2008, **41**, 9505–9507.

146 T. Higashihara and M. Ueda, *Macromolecules*, 2009, **42**, 8794–8800.

147 S.-H. Lin, S.-J. Wu, C.-C. Ho and W.-F. Su, *Macromolecules*, 2013, **46**, 2725–2732.

CHAPTER 2: IMPACT OF SYNTHESIS METHOD ON THE SOLID-STATE CHARGE TRANSPORT OF RADICAL POLYMERS

2.1 Contributors

This chapter describes a collaboration between the Ober group, the Fuchs group in Applied Engineering Physics of Cornell and the Flatté group in the Department of Physics and Astronomy of University of Iowa. Albert Park (a graduate student in the Fuchs group) and Yiren Zhang (author) contributed equally to the experimental work and are co-first-authors on the manuscript. Zhang synthesized monomers and PTMA samples for the four different routes proposed, carried out GPC, UV-vis and ATR-FTIR and part of the solution EPR measurements. Park performed the four-wire device fabrication, electrical measurements and majority of the spin-characterizations. The synthesis of PTMA homopolymer via anionic polymerization was carried out by Alicia Cintora (a graduate student in the Ober group). Stephen R. McMillan and Nicholas J. Harmon (postdocs in the Flatté group) contributed tremendously to the simulation work and interpretation of the spin transport process in the reported homopolymers.

2.2 Overview

Poly(2,2,6,6-tetramethylpiperidinyloxy methacrylate) (PTMA), a redox active polymer with radical groups pendent to an insulating backbone, has been considered to be an electrically insulating material in organic radical batteries. Recently, however, it has been reported that thin films of PTMA show conductivity in the magnitude of 10^{-6} S/cm, which is comparable to undoped conjugated polymers.

Given the disagreement on the conductivity, direct comparison of PTMA prepared by different synthesis methods is a crucial test of robustness of charge transport phenomena. We prepared PTMA using three living methods – anionic, ATRP and RAFT polymerization. The synthesized PTMA samples all have radical yields of 70 – 80%, controlled molecular weight, and low dispersity. Additionally, we used on-chip EPR to probe the robustness of radical content in solid films under ambient air and light, which is indicated by the slight changes in the radical content over time. Electrically, we find that PTMA is highly insulating – conductivity in the magnitude of 10^{-11} S/cm – regardless of the synthetic method of preparation. We have compared these results with variable range hopping theory and find that very few radical sites are electrically active, although the stable radical sites are closely packed.

2.3 Introduction

Radical polymers, a class of polymers with robust radical pendent moieties along their backbone, have demonstrated suitable performance to meet the requirements for energy storage applications such as organic radical batteries (ORBs).[1–6] Poly(2,2,6,6-tetramethylpiperidinyloxy methacrylate) (PTMA) remains the most popular stable radical polymer for ORBs due to its facile preparation and fast redox kinetics of the 2,2,6,6-tetramethyl pipiridine-1-oxyl (TEMPO) stable radical moiety side group. The incorporation of TEMPO moieties in polymers also has a rich history in the study of such diverse applications as organic magnets[7] and is currently being explored in antifouling coatings as a component to inhibit curing of biological adhesives[8]. Such structures are also associated with certain types of stable radical polymerization.[9]

Pristine PTMA has been largely considered to be an electrically insulating material in ORBs, which has been synthesized primarily via radical polymerization and subsequent oxidation.[10–13] As a result, many attempts have been made to improve its charge transport capabilities in battery electrodes, such as by incorporating carbon black-based additives to the active cathode material.[14–16] Recently, however, it has been reported that thin films of PTMA synthesized via reversible addition-fragmentation chain transfer (RAFT) can be considered as a novel class of highly-transparent polymers with a conductivity of $\sim 1\times10^{-6}$ S/cm, comparable to π-conjugated semiconducting polymers such as undoped poly(3-hexylthiophene) (P3HT).[17–19] Motivated by the lack of agreement over the intrinsic conductivity of PTMA, we have set out to understand the impact of different synthetic preparation routes on charge transport.

Despite the versatility of synthetic techniques, the only prior reported preparation of conductive PTMA homopolymer follows a two-step process which involves the preparation of a precursor polymer, poly(2,2,6,6-tetramethyl-4-piperidyl methacrylate) (PTMPM) by RAFT and subsequent oxidation by peracid.[19,20] Limited by the specific chemistry of polymerization or chemical treatment, the resulting PTMA is often accompanied by unwanted functionalities due to incomplete conversion or side reactions. These additional functionalities were found to have an effect on the measured solid state conductivity of PTMA thin films.[20] Efforts to understand the charge transport in these systems found that the intrinsic conductivity of PTMA can be increased by a factor of two by incorporating the oxoammonium cation, which can be introduced either by chemical oxidation of PTMPM or as an external dopant. The conductivity enhancement was attributed to

the oxoammonium cations serving as additional hopping sites for the nitroxide radical.[20,21]

In support of these results, charge transport in electrochemical systems has also been considered in the literature.[22] TEMPO stable radicals pendent to an insulating, hydrocarbon backbone can effectively transport charge with the aid of an electrolyte solution. It has been suggested that in these systems, charge carriers travel from TEMPO group to TEMPO group via a variable range hopping mechanism enabled by chain motion.[5,23,24] This model suggests that there can be a series of electron hops in the polymer from pendent site to pendent site with the aid of delocalized electrons. As such, elucidating the nature of the electron transport process in non-conjugated macromolecules with pendent stable radical groups could aid in opening new pathways to the designs of organic electronic materials.

Given the disagreement on the conductivity of non-conjugated stable radical polymers, direct comparison of PTMA prepared by different synthesis techniques is a crucial test of the robustness of charge transport phenomena that can reveal the role of structure and impurities in conductivity.

In this work, we have created a set of PTMA polymers synthesized via three different synthetic methods to understand how the variation of resulting pendent groups can affect the intrinsic conductivity of PTMA thin films. We used two living radical polymerization methods, RAFT and atom transfer radical polymerization (ATRP), for the preparation of two precursor polymers of PTMPM, which were then transformed to PTMA polymers (PTMA-RAFT, PTMA-H_2O_2, PTMA-*m*CPBA) by oxidation reactions. ATRP of 4-methacryloyloxy-1-((1'-phenylethyl)oxy-2,2,6,6-tetramethylpiperidine (MPEOT) resulted in the precursor polymer PMPEOT, which

was transformed to PTMA-O_2 by oxidative C-O bond cleavage of the polyalkoxyamines[25] (**Scheme 2.1**). For comparison, we also produced PTMA (PTMA-Anionic) with both low molecular weight distribution and high TEMPO stable radical yield via anionic polymerization. Considering that this method can directly polymerize the TEMPO-bearing methacrylate monomer with few side reactions, PTMA-Anionic can act as a suitable model polymer for physical characterization.

To characterize conductivity, we used equipment designed for measuring high-resistance PTMA samples in a 4-wire geometry. This both avoids the effect of contact resistance and eliminates artifacts that can occur when the sample resistance is higher than the meter input impedance. In the following sections, we describe our studies on this comprehensive measurement of PTMA conductivity, which is a key step to the understanding of charge transport in a neat PTMA film. Finally, we analyze the results in the context of a variable range hopping theoretical analysis.

2.4 Experimental section

2.4.1 Materials

All chemicals were purchased from Sigma-Aldrich and used as received unless otherwise noted. *m*-Chloroperbenzoic acid (*m*CPBA) was washed with DI water from diethyl ether and dried under vacuum. 2,2,6,6-Tetramethyl-4-piperidyl methacrylate (TMPM) and dibenzo-18-crown-6 were purchased from TCI America. Dibenzo-18-crown-6 was recrystallized from acetonitrile and dried under vacuum overnight. CuBr was stirred in acetic acid overnight, washed repeatedly with anhydrous ethanol and diethyl ether and dried under vacuum before use. The

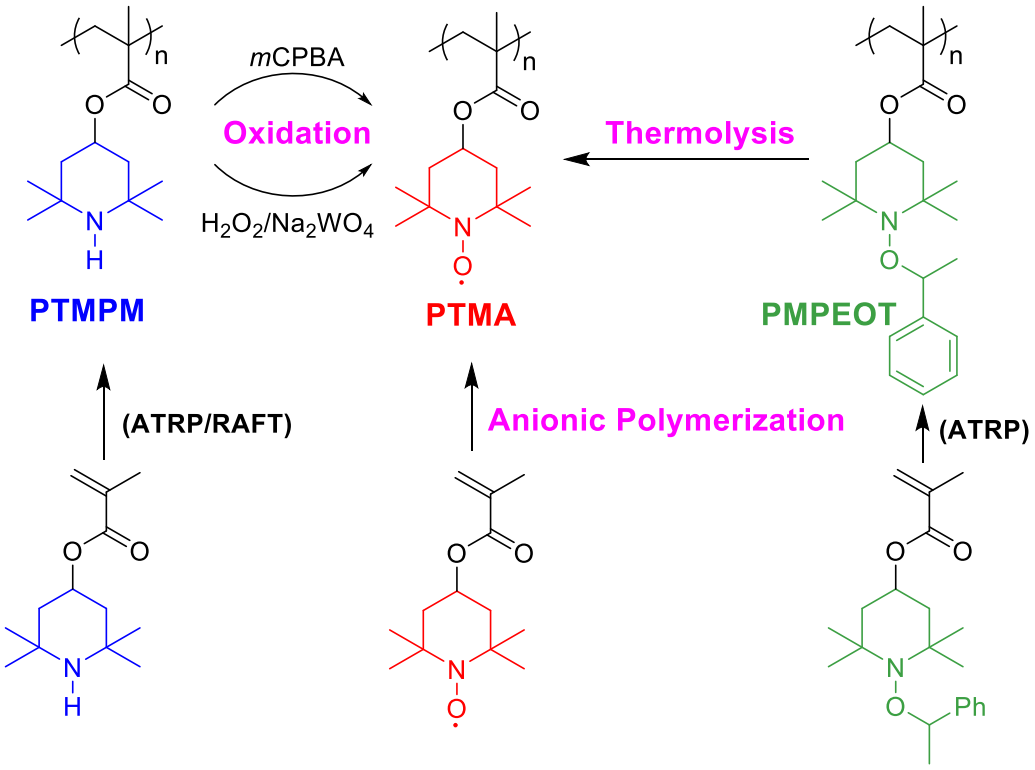

Scheme 2. 1. Synthesis of PTMA and precursor polymers via living polymerization and subsequent oxidation.

TEMPO methacrylate monomer and 2-phenyl-2-propylbenzodithioate[26] were synthesized according to literature procedures.

2.4.2 Characterization

Molecular weights (M_n) and polydispersities (M_w/M_n) of the PTMA samples and precursor polymers were dertermined by gel permeation chromatography (GPC). The GPC was performed on Waters Ambient Temperature GPC equipped with a Waters 410 differential refractive index detector. GPC columns were eluted at 1.0 mL/min with tetrahydrofuran (THF) at 40 °C. Polymer samples were dissolved in THF at 1 mg/mL. Polystyrene standards with narrow molecular weight distribution were used for calibration. ^{1}H-NMR spectra were recorded on a Varian INOVA 400 (^{1}H, 400 MHz) spectrometer. Spectra were referenced to the residual chloroform (7.26 ppm) signal. The ATR-FTIR spectra ranging between wavenumbers 4000 and 400 cm^{-1} were recorded under vacuum with Bruker Vertex V80V Vacuum FTIR system. Spectra resolution was set at 4 cm^{-1}.

2.4.3 Polymer synthesis

2.4.3.1 PTMA-anionic synthesis

Dibenzo-18-crown-6 (0.126 g, 0.35 mmol) and a stir bar were placed in a hot Schlenk flask with a Rotaflo stopcock and was taken into a nitrogen filled glovebox, where 50 mL of THF were added. The flask was sealed with a septum and transferred to an acetone/dry ice bath at -78 °C where the flask was purged with argon for 20 min. All consecutive additions were measured in the nitrogen glovebox and added via syringe. Approximately 1 mL of a 1.4 M solution of sec-butyllithium solution in cyclohexane was added to the flask in order to react with any additional impurities.

The flask was then allowed to warm up to room temperature for 1 h. After cooling to -78 °C for an additional 20 min, 25 µL (0.035 mmol) of sec-butyllithium and 25 µL (0.14 mmol) of diphenylethylene (DPE) were added and the mixture turned bright red, indicating a successful reaction. After stirring for 30 min, 87.5 µL (0.175 mmol) of a 2.0 M sodium *tert*-butoxide solution in THF were added, and there was no color change. After stirring for 45 min, a TEMPO methacrylate solution in THF was slowly added, and allowed to react for 5 h. The reaction was quenched with 1 mL of degassed methanol and allowed to cool to room temperature. The THF was removed by rotavap, and the polymer residue was re-dissolved in chloroform. Once re-dissolved, 3 consecutive water washes were done to remove the excess sodium in the solution. The washed polymer/chloroform solution was precipitated in cold hexanes, and dried under vacuum overnight.

2.4.3.2 PMPEOT synthesis

MPEOT (345 mg, 1.00 mmol, 1.00 equiv.) was placed in a Schlenk tube under nitrogen. Then 1 mL of a solution of ethyl 2-bromo-2-methylpropionate (2-EBiB) (15 mL, 100 mol) and 1,1,4,7,7-pentamethyldiethylenetriamine (PMDETA) (21 mL, 100 mmol) in anisole (10 mL) was added. The tube was subjected to three freeze–pump–thaw cycles, and the mixture was transferred via a cannula to a Schlenk tube with CuBr (1.4 mg, 10 mmol, 1.0 mol%) added. The mixture was stirred at 50 °C for 9 h. The crude product was precipitated in 25 mL of cold methanol. The precipitate was collected and washed with methanol. It was dissolved in a small amount of dichloromethane (DCM), and filtered through an aluminum oxide column. The filtered solution was concentrated under vacuum and precipitated in cold methanol. The polymer was collected and dried under vacuum at 40 °C

overnight.

2.4.3.3 PTMPM oxidation with *m*CPBA

A solution of *m*CPBA (480 mg, 2.78 mmol, 2.6 eq.) in 4.8 mL of anhydrous DCM was made. PTMPM (0.24 g, 1.07 mmol of amine functions, 1 eq.) was dissolved in 4.8 mL of anhydrous DCM at 0 °C. The *m*CPBA solution was added dropwise to the polymer solution and allowed to stir at room temperature for 3 h. After completion, the mixture was extracted with DCM and washed repeatedly with sodium carbonate solution. The organic phase was dried with anhydrous $MgSO_4$, concentrated under vacuum and precipitated in hexane. The polymer was collected and dried under vacuum at 40 °C overnight.

2.4.3.4 PTMPM oxidation with Na_2WO_4/Na_2EDTA/H_2O_2.

PTMPM (232 mg, 1.03 mmol of amine functions, 1 eq.), $Na_2WO_4.2H_2O$ (85 mg, 0.26 mmol, 0.25 eq.), $Na_2EDTA.2H_2O$ (45 mg, 0.15 mmol, 0.15 eq.) and methanol (12 mL) was added to a three-neck round-bottom flask with a condenser. The solution was stirred at 60 °C for 5 min and H_2O_2 (1.17 mL, 10.3 mmol, 10 eq.) was added dropwise over 60 min. The mixture was further stirred at 60 °C for 24 h. The polymer was extracted with DCM, washed repeatedly with water and dried with anhydrous $MgSO_4$. After filtration, the solution was concentrated and precipitated in cold hexane, filtered and dried under vacuum at 40 °C overnight.

2.4.3.5 PMPEOT oxidation

100 mg PMPEOT was dissolved in 10 mL of tert-butylbenzene (c = 10 mg/mL), and the mixture was heated at 135 °C for 5 h with a reflux condenser. During the reaction dry oxygen (produced by MnO_2 catalyzed H_2O_2 decomposition, dried over

anhydrous $CaCl_2$) was bubbled through the solution. After completion, tert-butylbenzene was removed under vacuum, and the solid was dissolved in a minimum amount of DCM. The polymer was collected from precipitation in cold hexane and dried under vacuum at 40 °C overnight.

2.4.4 Solution-state spin characterization

Solution-state measurements were performed in a Bruker X-band EPR spectrometer at room temperature. PTMA solutions for EPR measurements (1 mM of repeating unit concentration) were prepared by dilution of 384.6 μL of PTMA stock solutions to 4.00 mL of total volume with toluene. Stock solution was prepared by dissolving 10.0 mg of each polymer in 4.00 mL toluene overnight. The resulting EPR spectra were double-integrated and compared with the TEMPO standard (1 mM solution in toluene) to calculate radical yields. Error bars were generated by calculating the standard deviation of average radical yield from three parallel quantitative EPR tests in which the same PTMA stock solution was used to prepare independent test solutions.

2.4.5 Solid-state spin characterization using a coplanar waveguide

Samples were prepared either by drop casting or spin coating a 10 mg/mL solution of PTMA directly onto the microfabricated coplanar waveguide meander.[27] The waveguide was then wire-bonded into the microwave chip carrier, and the 6 GHz transmitted microwave power was monitored as a function of magnetic field with a microwave diode and a lock-in amplifier. Error bars were calculated by propagating errors including the uncertainties from the fitting and the noise in the lock-in voltage.

2.4.6 Electrical characterization

Micro-fabricated 4-wire lateral templates consisting of 100-nm-thick, 2.5-mm-long gold electrodes were patterned on insulating, thermally oxidized Si substrates. The four electrodes are equally spaced at a distance of either 2, 5, 10, or 20 μm (**Fig. 2.1**). We used more than one electrode spacing for each PTMA type to validate that the results are not an artifact of the geometry. PTMA films were prepared by drop-casting PTMA solution (25 mg/mL in toluene) on a template and heated at 70 °C for 15 min to remove the residual toluene. PTMA film thickness was measured using both an ellipsometer and Tencor AlphaStep 500 profilometer. After wire-bonding the template into a chip carrier, each sample was placed within a continuously pumped vacuum box to eliminate resistive shunting through a surface water layer. Current was applied to the outer electrodes and measure voltage between the inner electrodes. To eliminate a systematic error that can arise when measuring samples with very large resistance (a typical resistance is between 60 to 200 GΩ in our experiment) relative to the input impedance of a standard voltmeter, a Keithley 6514 electrometer that has an input impedance of 210 TΩ was used. Current was sourced using a Keithley 6610 precision current source enabling current with sub-1 pA accuracy. The set-up was calibrated against standard Ohmite MOX resistors in the range 100 GΩ to 1 TΩ. (for the details of calibration please refer to the supplemental information) As a control, the resistance of a 4-wire template in our set-up without a PTMA film under the same conditions was measured and found that the resistance was above 10 TΩ which exceeds the reasonable range for calibration. All measurements were done in a Faraday cage to prevent electrostatic artifacts.

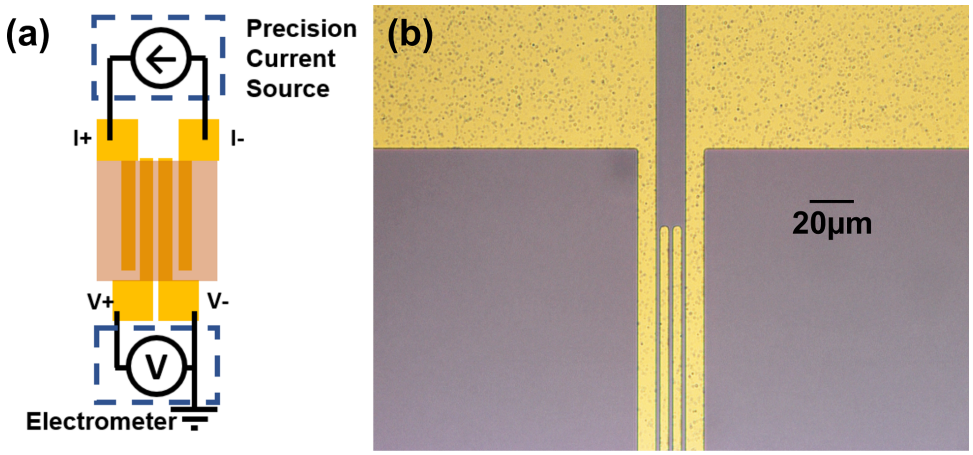

Figure 2.1. **(a)** Schematics of circuits for conductivity measurement. **(b)** Optical image of fabricated template with 2 μm spacing between electrodes.

2.5 Results and Discussions

2.5.1 Polymerization

Scheme 2.1 summarizes our synthetic strategy of PTMA synthesis in this study. In previous reports, PTMA synthetic routes mainly fall into two categories: (i) direct polymerization of TEMPO-containing methacrylate monomer using reactions that are compatible with stable radicals, such as anionic polymerization[28] and group-transfer polymerization[29]; and (ii) synthesis of precursor polymers via radical polymerization, which can be terminated by nitroxide radical, and subsequent radical regeneration via chemical treatment. To overcome the intrinsic drawback of traditional radical polymerizations, including lack of control over the molar mass and the dispersity, reversible-deactivation polymerizations allow the creation of well controlled PTMA precursor polymer due to their fast initiation rates and consistent concentration of active sites. To minimize the influence of dispersity, here we used only living polymerization, including anionic polymerization, ATRP and RAFT.

Table 2.1 summarizes the corresponding polymerization methods, chemical oxidation, molecular weights and dispersity index (PDI) of synthesized PTMA samples. All of the PTMA products show low PDI of 1.15 – 1.28, which is in agreement with previous reports. Among them, PTMA-anionic show a narrow dispersity, indicating that the TEMPO bearing methacrylate monomers can be polymerized with high suppression of side reactions on nitroxide radical via sodium-mediated anionic polymerization. Such controlled polymer structures are desired in exploration of the effects of different existing pendent groups due to minimization of molecular weight and distribution effect.

Table 2.1. Preparation methods and GPC data of PTMA

Sample	Polymerization	Oxidation	M_n (kg/mol)	Đ
PTMA-anionic	Anionic	—	19.9	1.22
PTMA-*m*CPBA	ATRP	*m*CPBA	24.7	1.15
PTMA-H_2O_2	ATRP	Na_2WO_4/H_2O_2	24.4	1.16
PTMA-O_2	ATRP	O_2	14.2	1.17
PTMA-RAFT	RAFT	*m*CPBA	17.8	1.28

2.5.2 Oxidation

Due to the fact that modern synthetic chemistry of stable nitroxides developed historically from piperidine derivatives, the oxidation of sterically hindered secondary amines by peroxides and peracids has been the most popular preparative method for the synthesis of PTMA. Though various reaction conditions have been used, including H_2O_2/EDTA/Na_2WO_4 combination and *m*CPBA, the oxidation of amine actually occurs by a similar mechanism.[30] In the first stage, the hydroxylamino derivative (N-OH) is generated as a major product, which is converted into an oxoammonium moiety ($^+$N=O) via subsequent oxidation. The consumption of $^+$N=O, the intermediate product, is realized by reaction with reducing species, which is hydroxylamino derivative (N-OH) for *m*CPBA system and H_2O_2 derivative for H_2O_2/EDTA/Na_2WO_4 system.

Meanwhile, thermolysis of alkoxyamine under aerated conditions can also be a reliable method for efficient TEMPO recovery, considering its simpler mechanism and less intermediate species compared with the oxidation of amines. Here, optimized oxidation conditions using either H_2O_2/Na_2EDTA/Na_2WO_4 combination and *m*CPBA were adopted for our PTMPM samples, while PMPEOT polymer were deprotected in tert-butylbenzene at 135 °C under oxygen atmosphere. After oxidation, all the PTMA samples were pale orange solid, while corresponding polymer solutions exhibited the characteristic absorption of TEMPO moiety at 463 nm, suggesting the successful generation of TEMPO radical in all the PTMA samples.

Prevention of unintentional oxoammonium ($^+$N=O) production is important to our study, since we want to establish the base conductivity of pristine PTMA, and

oxoammonium has been reported previously as a conductivity enhancing dopant.[21,22,31,32] We used attenuated total internal reflectance-Fourier transform infrared (ATR-FTIR) spectroscopy to study the existence of $^{+}$N=O species in our PTMA samples as shown in **Fig. 2.2**. Compared with their precursor polymers, all the PTMA samples exhibit the characteristic peak of N-O• at 1365 cm^{-1}, while only PTMA oxidized by *m*CPBA show an observable single peak at 1540 cm^{-1}, which corresponds to the $^{+}$N=O. Beside the disproportionation and over-oxidation by *m*CPBA, this can also be explained by the inefficient reduction of intermediate $^{+}$N=O formed in amine oxidation by polymer-bounded N-OH, while reduction by excess H_2O_2 in PTMA-H_2O_2 is enough for complete $^{+}$N=O reduction. The unavoidable presence of $^{+}$N=O is consistent with lower radical conversion in PTMA oxidized by *m*CPBA as compared with other methods. In the samples not oxidized with *m*CPBA, we conclude that the pendent groups consist only of TEMPO stable radicals and a small fraction of corresponding precursor groups. These materials with their high purity and range of synthetic strategies appear to be suitable systems for the subsequent conductivity tests.

2.5.3 Spin characterization

We measured radical yields using quantitative solution-state electron paramagnetic resonance (EPR). **Fig. 2.3 (b)** shows that the radical yield of PTMA, regardless of synthesis approach, varied by only 10 percent within the range 70 to 80%. PTMA-Anionic had the highest average yield of 77%, while PTMA-ATRP showed lowest yield of 70%. Although we prepared PTMA using different polymerization and oxidation methods, we found no significant variation in radical content among all PTMA samples (**Fig. 2.3 (b)**). The absence of a triplet signal,

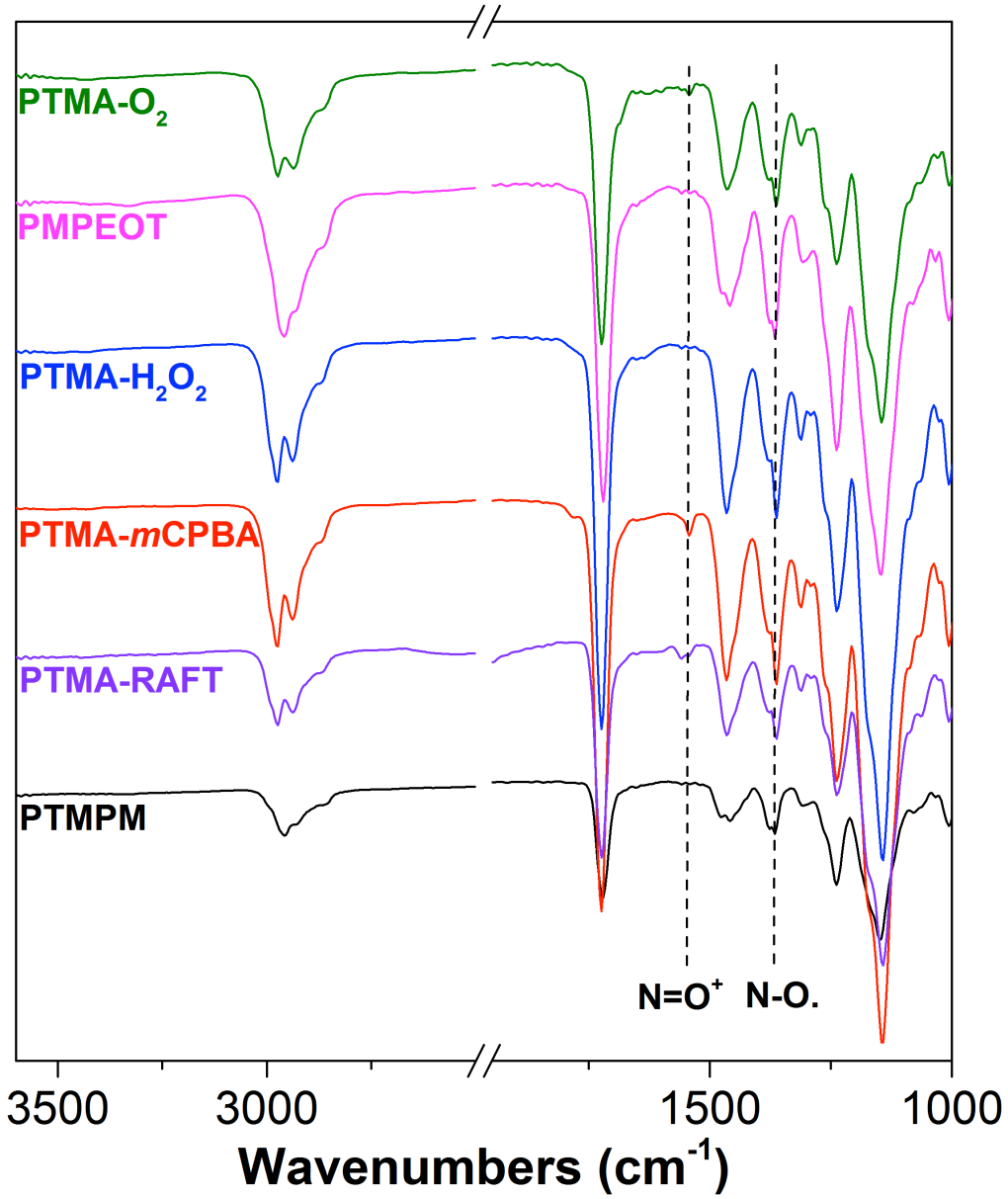

Figure 2.2. FTIR of PTMA samples and the precursor polymers. The peak at 1365 cm^{-1} is associated with N-O•, while the peak at 1540 cm^{-1} is associated with $^{+}$N=O. The $^{+}$N=O peak is only observable in *m*CPBA-oxidized PTMA (PTMA-RAFT, PTMA-*m*CPBA)

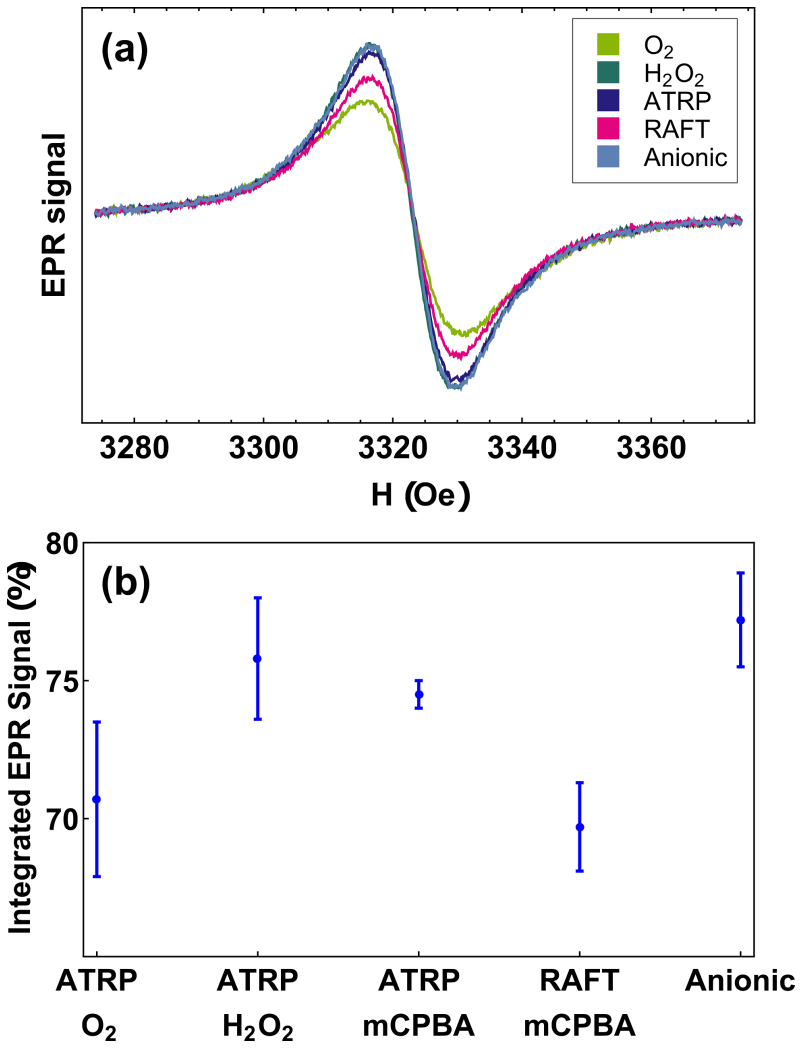

Figure 2.3. (a) EPR line shapes of PTMA samples. (b) Radical yield of PTMA samples determined by liquid-state EPR.

which originates either from free-floating TEMPO molecules or isolated radical groups along the polymer chain, further confirms high radical contents and good purity in our PTMA samples. Consistent with FTIR results and with our understanding of the synthetic methods, we expect that most of side-groups that are not converted to radicals are not electrically active oxoammonium.

Motivated to understand the stability of the radical spins in solid films, which is relevant for applications, we also performed room temperature EPR of solid PTMA films using a broadband, on-chip coplanar waveguide set-up shown in **Fig. 2.4 (a-b).** The transmitted microwave power, P, that passes through a meandering coplanar waveguide is demodulated with respect to a 6 G, 587 Hz magnetic field, H, modulation. This is a measurement of dP/dH which rejects H independent microwave power transmission. As the static component of H is swept through the spin resonance, we expect a single, derivative-of-Lorentzian line-shape because of the high radical yield in our materials and because of the decreased radical inter-chain spacing within a solid film. We verified that the signal scales with film thickness as expected for thin films, and that spin-coating and drop-casting give similar amplitudes once normalized for film thickness.

The robustness of radical spins in PTMA exposed to ambient light and air is a particular concern for many applications, including for conductive polymer materials.[33–36] Although the radical spins in PTMA films are generally believed to be stable, there has been no prior quantitative test in solid films, which is the relevant form of the material for applications. **Fig. 2.4(c)** shows our measurement of waveguide EPR, which is representative of all of our measurements of PTMA materials in this study. Because we measure the solid-state form of PTMA,

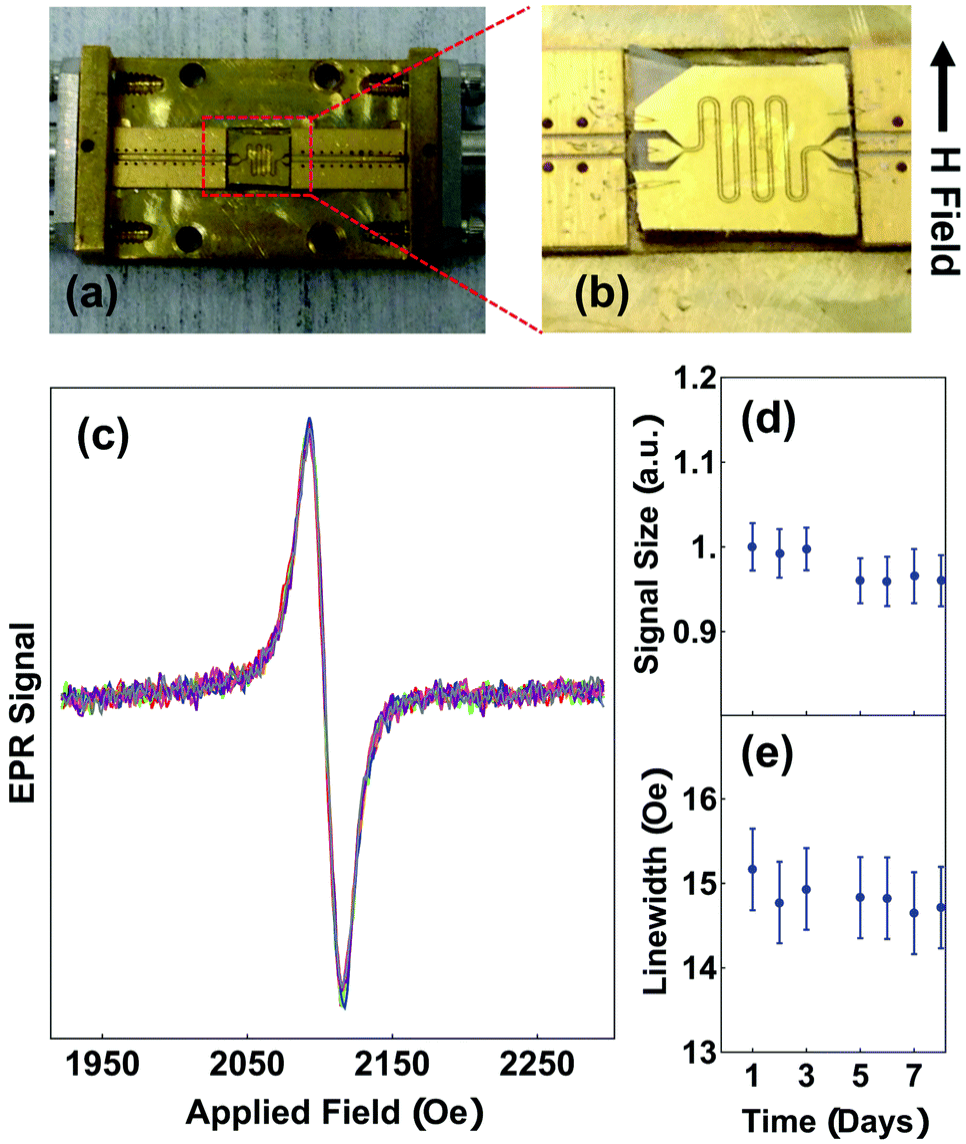

Figure 2.4. EPR (a) Brass box with coplanar waveguide for microwave experiments (b) RF waveguide wire bonded to a box with sample drop-casted on top. (c) Overlay of on-chip EPR curves taken for 8 days (d and e) change in size of the signal and linewidth over the course of 8 days.

singlet linewidth is larger than that measured in solution state due to a closer spacing between radical groups, which enhances exchange narrowing.[37,38] Without breaking any microwave contacts, we repeated our measurement of the solid-state EPR over a period of eight days **(Fig. 2.4 (d-e))**, over which the sample was exposed to ambient fluorescent lighting and air. We found a negligible decrease in the EPR signal amplitude over that period. We also re-measured PTMA samples after 5 months without a significant change to the EPR amplitude. However, we note that there are small variations in signal amplitudes that originate from breaking and re-making microwave contacts that adds uncertainty to quantitative comparisons. From these measurements, we conclude that radical groups in PTMA solid films are robust to ambient conditions.

2.5.4 Conductivity measurement

We performed electrical measurements of solid PTMA films to understand how different synthetic methods influence the steady-state electrical conductivity of this material. We chose a lateral, 4-wire geometry in this measurement for two reasons: first, it eliminates contact resistance, which may vary significantly depending on the contact electrode materials and surface preparation. Second, it eliminates the potential for unintentional parallel conductance pathways that could occur in a vertically stacked sandwich structure[18–21,32] (e.g. bottom electrode, PTMA film, top electrode deposited on top via evaporation). For example, these structures are susceptible to pin-holes and uncontrolled diffusion of the top electrode into the polymer film, which provide a shunt resistive path. Furthermore, because the polymer film is not over-coated in metal, residual solvent could persist in the polymer if it is not fully baked out after PTMA film deposition. Finally, we note

that unintentional conductivity is difficult to check for in vertically-stacked structures. Thus, we choose to eliminate these uncertainties by working in a lateral measurement geometry, consistent with some prior studies.[17]

Table 2.2 summarizes our findings for PTMA-Anionic, PTMA-H_2O_2 and PTMA-RAFT. Note that of the three ATRP-synthesized PTMA materials, we studied only PTMA-H_2O_2 electrically because it had the largest radical yield of that group. We found that while the conductivity of PTMA prepared using different synthetic methods varies by a factor of ~5, all samples were highly insulating, independent of synthetic approach. The conductivity values that we report, between $1.09 \pm 0.76 \times 10^{-11}$ and $5.59 \pm 0.78 \times 10^{-11}$ S/cm, are orders of magnitude smaller than some prior reports[18–21] but in agreement with others[32]. This could indicate that while ionic transport between TEMPO moieties can lead to much higher conductivity as compared to PMMA, which has conductivity in range of 10^{-14}~10^{-15} S/cm, it is far below the conductivity of organic semiconductors with a π-conjugated backbone. For confirmation of this statement, we also measured the resistance of an undoped regioregular P3HT film, which is a common conjugated polymer. We found a conductivity of 4.5×10^{-8} S/cm, which is 2 orders of magnitude smaller than typically reported[39] but which is consistent with the lack of crystallinity from drop casting and with normal sample aging.[40] Nonetheless, we found that the P3HT film is 3 orders of magnitude more conductive than PTMA films, regardless of synthetic preparation.

To understand these results in the context of radical-mediated electronic transport mechanisms, here we theoretically estimate the number of radical sites involved in electronic transport. We consider charge transport due to phonon-

Table 2.2. Conductivity of PTMA prepared by different polymerization and oxidation methods.

Sample	Polymerization	Oxidation	Conductivity (S/cm)
PTMA-anionic	Anionic	—	$1.09 \pm 0.76 \times 10^{-11}$
PTMA-H_2O_2	ATRP	H_2O_2	$5.59 \pm 0.78 \times 10^{-11}$
PTMA-RAFT	RAFT	*m*CPBA	$2.54 \pm 0.31 \times 10^{-11}$
P3HT	—	—	$4.46 \pm 2.03 \times 10^{-8}$

assisted tunneling between sites with Mott variable range hopping[41], which assigns hopping rates depending on both the wave function overlap and also any thermal activation required to hop. An increase in site separation, or a difference in site energy, both lead to lower hopping rates[42] by reducing the density of states *g(μ)*, near the Fermi level μ. The concentration of conducting sites correspond to $N_c = 2\mathrm{g}(\mu)\varepsilon_0^{opt}$, where the optimal bandwidth

$$\varepsilon_0^{opt} = \left(\frac{k_B T}{a}\right)^{3/4} \left(\frac{1}{\mathrm{g}(\mu)}\right)^{1/4} \tag{1}$$

where *a* is the carrier's wave function localization length. From these assumptions, the resistivity in an amorphous semiconducting material is expressed as

$$\rho = \rho_0 \exp\left[\left(\frac{T_0}{T}\right)^{\frac{1}{4}}\right] \tag{2}$$

where $T_0 = \beta/[a^3 k_B \mathrm{g}(\mu)]$ with β a percolative constant,[41] and ρ_0 a material dependent constant describing the minimum resistivity based on carrier-phonon interactions,[41]

$$\rho_0 = \frac{9\pi}{4} \frac{a^3 d s^5 h^4 \kappa^2}{{E_1}^2 e^6 {k_c}^2} \left(\frac{\beta}{a^3 \mathrm{g}(\mu) k_B T}\right)^{\frac{\nu+2}{4}} \tag{3}$$

In the above expression *d* is the mass density of the dielectric, *s* is the speed of sound in the dielectric,[43] κ is the dielectric constant,[44] E_1 is the deformation potential,[45] *e* is the electronic charge, k_c is the Coulomb constant, and *v* is a numerical constant determined through percolation simulations.[41] An estimate of the density of states is made by equating **Eq (2)** with measured values of the resistivity. For the anionic PTMA sample with $\rho = 9.19 \times 10^{10}$ Ω cm, $\mathrm{g}(\mu) = 2.5 \times 10^{20}$ $\mathrm{eV^{-1}\,cm^{-3}}$,

and from **Eq (1)**, $\varepsilon_0^{\mathrm{opt}} = 0.52$ eV. It is assumed that each monomer of PTMA contains one side chain and given a mass density of $\mu_s = 1.018$ g/cm^3 and the molecular weight of a monomer $w = 240.32$ Da, the average spacing between sites is $r = 4.5$ Å. The concentration of conducting sites is $N_c = 2.5 \times 10^{20}$ cm^{-3} and so the ratio of conducting sites to insulating sites, *f*, is

$$f = N_c \frac{4\pi}{3} r^3 \tag{4}$$

For the parameters outlined above, $f = 0.10$ suggesting that about 10% of sites within the sample contribute to charge transport, with on average half of these sites occupied and half empty of carriers - a statement of single occupancy. This corresponds to approximately 5% of sites being unoccupied and able to host a carrier, which is consistent with our FTIR measurements and our expectation that nearly all side groups that are not converted to radical sites are not electrically active.

2.6 Conclusions

In this study, we have prepared a series of PTMA materials of controlled molecular weight and dispersity using a range of living polymerization methods. We have used both controlled radical and anionic polymerizations to make the target polymers. Anionic polymerization enables formation of narrow dispersity polymer directly from the stable radical monomer. Controlled radical methods require that we polymerize from a precursor amine to make a polymer and then oxidize the polymer to form the stable radical. Using solution EPR methods to evaluate the stable radical content in each polymer, we find that all synthetic methods result in a TEMPO content per repeat of between 70 and 80 percent. Only in the case of peracid

oxidation can we observe by IR spectroscopy an overoxidation to form an oxoammonium species. We also used an on-chip EPR technique to probe the stability of solid PTMA films, finding no appreciable change in the radical content for more than a week. Having established the high-quality synthesis of stable radical polymers, we then investigate the electrical conductivity in these materials using lateral template devices that enable a four-point measurement. We find that independent of synthetic method, these polymers are highly insulating, with conductivities ranging from 1.1×10^{-11} to 5.6×10^{-11} S/cm. We have compared these results with variable range hopping theory and find that very few radical sites are electrically active. These results have implications for the production of energy storage systems and motivate future research seeking to increase conductivity in stable radical containing materials.

2.7 Acknowledgements

This work was supported the Department of Energy Office of Basic Energy Science (Grant DE-SC0014336). We acknowledge use of the facilities of the Cornell NanoScale Facility, a member of the National Nanotechnology Coordinated Infrastructure (NNCI), supported by the National Science Foundation (NSF) (Grant ECCS-1542081). This material is based upon work supported by the National Science Foundation Graduate Research Fellowship under Grant No. DGE-1650441. We also acknowledge the use of shared facilities of the Cornell Center for Materials Research which is supported through the NSF MRSEC program (Grant DMR-1719875) and the shared facilities of the National Biomedical Center for Advanced Electron Spin Resonance Technology, which is supported by the National Institute

of General Medical Sciences, a part of the National Institutes of Health (Grant P41GM103521).

2.8 References

1 T. Suga, H. Ohshiro, S. Sugita, K. Oyaizu and H. Nishide, *Advanced Materials*, 2009, **21**, 1627–1630.

2 H. Nishide, S. Iwasa, Y.-J. Pu, T. Suga, K. Nakahara and M. Satoh, *Electrochimica Acta*, 2004, **50**, 827–831.

3 H. Nishide and K. Oyaizu, *Science*, 2008, **319**, 737–738.

4 H. Nishide and T. Suga, *Electrochem. Soc. Interface*, 2005, **14**, 32–36.

5 K. Nakahara, K. Oyaizu and H. Nishide, *Chemistry Letters*, 2011, **40**, 222–227.

6 T. Janoschka, M. D. Hager and U. S. Schubert, *Advanced Materials*, 2012, **24**, 6397–6409.

7 H. Nishide, *Advanced Materials*, 1995, **7**, 937–941.

8 Brandon Wenning, Cornell University, 2016.

9 C. J. Hawker, A. W. Bosman and E. Harth, *Chemical Reviews*, 2001, **101**, 3661–3688.

10 J.-K. Kim, G. Cheruvally, J.-W. Choi, J.-H. Ahn, D. S. Choi and C. E. Song, *Journal of The Electrochemical Society*, 2007, **154**, A839.

11 K. Nakahara, S. Iwasa, M. Satoh, Y. Morioka, J. Iriyama, M. Suguro and E. Hasegawa, *Chemical Physics Letters*, 2002, **359**, 351–354.

12 J.-K. Kim, Y. Kim, S. Park, H. Ko and Y. Kim, *Energy & Environmental Science*, 2016, **9**, 1264–1269.

13 J.-K. Kim, J. Scheers, J.-H. Ahn, P. Johansson, A. Matic and P. Jacobsson, *J. Mater. Chem. A*, 2013, **1**, 2426–2430.

14 C. M. Liu, J. Chen, F. Q. Wang and B. L. Yi, *Russian Journal of Electrochemistry*, 2012, **48**, 1052–1057.

15 Y. Kim, C. Jo, J. Lee, C. W. Lee and S. Yoon, *J. Mater. Chem.*, 2012, **22**, 1453–1458.

16 W. Guo, Y.-X. Yin, S. Xin, Y.-G. Guo and L.-J. Wan, *Energy Environ. Sci.*, 2012, **5**, 5221–5225.

17 L. Rostro, A. G. Baradwaj and B. W. Boudouris, *ACS Applied Materials & Interfaces*, 2013, **5**, 9896–9901.

18 A. G. Baradwaj, L. Rostro and B. W. Boudouris, *Macromolecular Chemistry and Physics*, 2016, **217**, 477–484.

19 A. G. Baradwaj, L. Rostro, M. A. Alam and B. W. Boudouris, *Applied Physics Letters*, 2014, **104**, 213306.

20 L. Rostro, S. H. Wong and B. W. Boudouris, *Macromolecules*, 2014, **47**, 3713–3719.

21 A. G. Baradwaj, S. H. Wong, J. S. Laster, A. J. Wingate, M. E. Hay and B. W. Boudouris, *Macromolecules*, 2016, **49**, 4784–4791.

22 C. Karlsson, T. Suga and H. Nishide, *ACS Applied Materials & Interfaces*, 2017, **9**, 10692–10698.

23 K. Oyaizu, Y. Ando, H. Konishi and H. Nishide, *Journal of the American Chemical Society*, 2008, **130**, 14459–14461.

24 K. Oyaizu and H. Nishide, *Advanced Materials*, 2009, **21**, 2339–2344.

25 F. Behrends, H. Wagner, A. Studer, O. Niehaus, R. Pöttgen and H. Eckert, *Macromolecules*, 2013, **46**, 2553–2561.

26 S. Perrier, C. Barner-Kowollik, J. F. Quinn, P. Vana and T. P. Davis, *Macromolecules*, 2002, **35**, 8300–8306.

27 Y. Wiemann, J. Simmendinger, C. Clauss, L. Bogani, D. Bothner, D. Koelle, R. Kleiner, M. Dressel and M. Scheffler, *Applied Physics Letters*, 2015, **106**, 193505.

28 T. Sukegawa, H. Omata, I. Masuko, K. Oyaizu and H. Nishide, *ACS Macro Letters*, 2014, **3**, 240–243.

29 L. Bugnon, C. J. H. Morton, P. Novak, J. Vetter and P. Nesvadba, *Chemistry of Materials*, 2007, **19**, 2910–2914.

30 L. B. Volodarsky, V. A. Reznikov and V. I. Ovcharenko, *Synthetic Chemistry of Stable Nitroxides*, CRC Press, 1st edn., 2017.

31 T. W. Kemper, R. E. Larsen and T. Gennett, *The Journal of Physical Chemistry C*, 2014, **118**, 17213–17220.

32 T. Suga, S. Takeuchi, T. Ozaki, M. Sakata, K. Oyaizu and H. Nishide, *Chemistry Letters*, 2009, **38**, 1160–1161.

33 K. Lee, J. Y. Kim, S. H. Park, S. H. Kim, S. Cho and A. J. Heeger, *Advanced Materials*, 2007, **19**, 2445–2449.

34 A. P. Monkman, H. D. Burrows, M. da G. Miguel, I. Hamblett and S. Navaratnam, *Chemical Physics Letters*, 1999, **307**, 303–309.

35 K. Z. Xing, N. Johansson, G. Beamson, D. T. Clark, J.-L. Brédas and W. R. Salaneck, *Advanced Materials*, 1997, **9**, 1027–1031.

36 R. D. Scurlock, B. Wang, P. R. Ogilby, J. R. Sheats and R. L. Clough, *Journal of the American Chemical Society*, 1995, **117**, 10194–10202.

37 M. S. Davis, C. Mao and R. W. Kreilick, *Molecular Physics*, 1975, **29**, 665–672.

38 C. R. Mao and R. W. Kreilick, *Chemical Physics Letters*, 1975, **34**, 447–450.

39 I. R. Gearba, C.-Y. Nam, R. Pindak and C. T. Black, *Applied Physics Letters*, 2009, **95**, 173307.

40 Y. Wang and M. F. Rubner, *Synthetic Metals*, 1990, **39**, 153–175.

41 B. I. Shklovskii and A. L. Ėfros, *Electronic properties of doped semiconductors*, Springer-Verlag Berlin Heidelberg GmbH, Berlin Heidelberg, Softcover reprint of the original 1st edition 1984., 2013.

42 A. Miller and E. Abrahams, *Physical Review*, 1960, **120**, 745–755.

43 J. E. Mark, Ed., *Physical properties of polymers handbook*, Springer, New York, NY, 2. ed., 2007.

44 T. W. Kemper, R. E. Larsen and T. Gennett, *The Journal of Physical Chemistry C*, 2015, **119**, 21369–21375.

45 J. E. Northrup, *Applied Physics Letters*, 2011, **99**, 062111.

2.8 Supporting Information

Materials Synthesis and Characterization

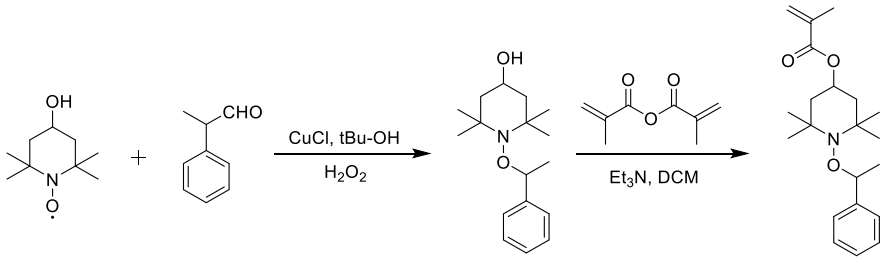

Scheme 2.2. Synthesis route of monomer MPEOT.

1-(1-Phenyl-ethoxy)-2,2,6,6-tetramethylpiperidin-4-ol (PEOT).[17] To a solution of 10.0 g (58 mmol) 4-hydroxy-TEMPO in 40 mL *tert*-butanol was added CuCl (200 mg, 3.5 mol%) and 2-phenylpropionaldehyde (16.0 g, 116 mmol). 13.0 g (116 mmol) 30% H_2O_2 was added slowly over a period of 2 h (using a water bath if necessary), after which time the mixture was stirred at room temperature overnight. After completion, the mixture was extracted with methyl *tert*-butyl ether (MTBE) three times. The combined organic layer was washed with 10% ascorbic acid solution, 1 N NaOH solution, DI water and brine. After drying with anhydrous $MgSO_4$, the excess 2-phenylpropionaldehyde was removed under vacuum to give viscous liquid. The crude product was purified by subsequent recrystallization from hexane as a white solid. The crystals were separated by filtration, dried under vacuum to give the target product.

^{1}H-NMR (400 MHz, $CDCl_3$): δ = 7.45-7.24 (*m*, 5H, Ph-H), 4.80 (*q*, 1H, C*H*ON), 3.81 (*m*, 1H); 1.88-1.50 (*m*, 4H, CH_2); 1.48 (*d*, 3H, CH_3CHON); 1.33 (*s*, 3H, CH_3); 1.27 (*s*, 3H, CH_3); 1.13 (*s*, 3H, CH_3); 0.66 (*s*, 3H, CH_3) ppm.

4-Methacryloyloxy-1-((1'-phenylethyl)oxy-2,2,6,6-tetramethylpiperidine (MPEOT). To a solution of PEOT (10.0 g, 36.05 mmol, 1 eq.) in 100 mL of CH_2Cl_2, triethylamine (15.1 mL, 108.14 mmol, 3 eq.) and DMAP (73 mg, 1.7 mol%) was added. Methacrylic anhydride (10.7 mL, 72.10 mmol) was added dropwise and the resulting mixture was stirred at room temperature overnight. After completion, the $NaHCO_3$ (60 mL, saturated solution) was added to quench the reaction. After separation of an organic layer, the aqueous layer was extracted with CH_2Cl_2 (30 mL × 3) and the combined organic phases were dried over anhydrous $MgSO_4$. The solvent was removed by rotavap, and purification by flash chromatography (eluent: hexane) gave the target product as a viscous colorless liquid, which solidified after a while.

^{1}H-NMR (400 MHz, $CDCl_3$): δ = 7.34–7.18 (*m*, 5H, Ph-*H*); 6.04 (*s*, 1H, *H*HC=C); 5.51 (*s*, 1H, H*H*C=C); 5.11-4.98 (*m*, 1H, C*H*OC(O)); 4.77 (*q*, 1H, C*H*ON); 1.90 (*s*, 3H, CH_3); 1.88-1.50 (*m*, 4H, CH_2); 1.48 (*d*, 3H, CH_3CHON); 1.33 (*s*, 3H, CH_3); 1.27 (*s*, 3H, CH_3); 1.13 (*s*, 3H, CH_3); 0.66 (s, 3H, CH_3) ppm.

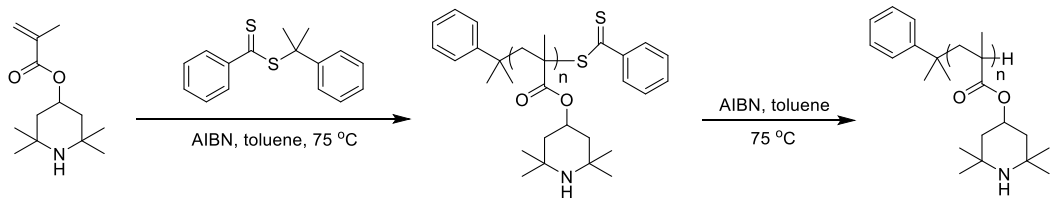

Scheme 2.3. Synthesis route of PTMPM using RAFT polymerization.

PTMPM-RAFT. To a 100 mL Schlenk flask containing a Teflon-coated magnetic stir bar, 20 mL of anhydrous toluene were added. 10.0 g (0.04 mol) of TMPM, 18.3 mg (0.1 mmol) of 2,2'-azobis(2-methylpropionitrile) (AIBN), and 0.135 mL (0.5 mmol) 2-phenyl-2-propylbenzodithioate were then added to the flask. After the

TMPM solid was dissolved, three freeze-pump-thaw cycles were performed on the mixture prior to backfilling with nitrogen. The reaction flask was heated to 75 ˚C and stirred overnight. After completion, the solution was cooled to room temperature and exposed to air to terminate the reaction. Most of the solvent was removed under vacuum, and the concentrated solution was precipitated in cold hexane to obtain the target polymer. The PTMPM-RAFT was then dried overnight under vacuum at 40 ˚C.

PTMPM (RAFT). To a 100 mL Schlenk flask containing a Teflon-coated magnetic stir bar, 17 mL of anhydrous toluene was added. Next, 1 g of PTMPM-RAFT and 0.34 g of AIBN (2.05 mmol) were added to the reaction flask. Then three freeze-pump-thaw cycles were performed to the mixture prior to backfilling with nitrogen. The reaction was heated to 75 ˚C and stirred overnight. After completion, the solution was cooled to room temperature and exposed to air to terminate the reaction. The solution was then precipitated in hexane to obtain the target polymer. The PTMPM was then dried overnight under vacuum at 40 ˚C.

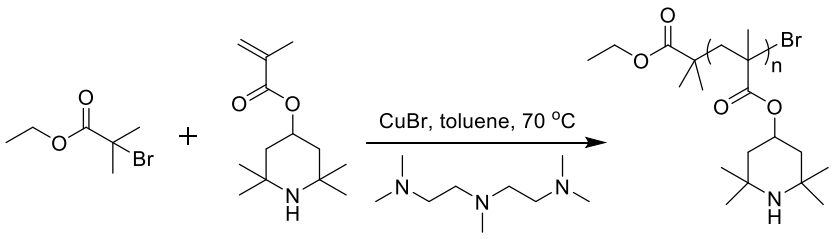

Scheme 2.4. Synthesis of PTMPM using ATRP.

PTMPM (ATRP). TMPM (7.89 g, 35.00 mmol, 70.0 equiv) was placed in a 100 mL Schlenk flask containing a Teflon-coated magnetic stir bar. Then ethyl 2-bromo-2-methylpropionate (2-EBiB) (73.4 µL, 0.5 mmol, 1.0 eq) and 1,1,4,7,7-

pentamethyldiethylenetriamine (PMDETA) (208.8 μL, 1.00 mmol, 2.0 eq) in 16 mL of anhydrous toluene was added. The flask was subjected to three freeze-pump-thaw cycles, and the mixture was transferred via a cannula to a Schlenk tube with CuBr (35.86 mg, 0.25 mmol, 0.5 eq) under nitrogen. The mixture was stirred at 70 °C for 4 h. The reaction was terminated by cooling to room temperature and exposure to air. The mixture was diluted in a small amount of CH_2Cl_2 and filtered through an aluminum oxide column. The filtered solution was concentrated under vacuum and precipitated in cold hexane. The polymer was collected and dried overnight under vacuum at 40 °C.

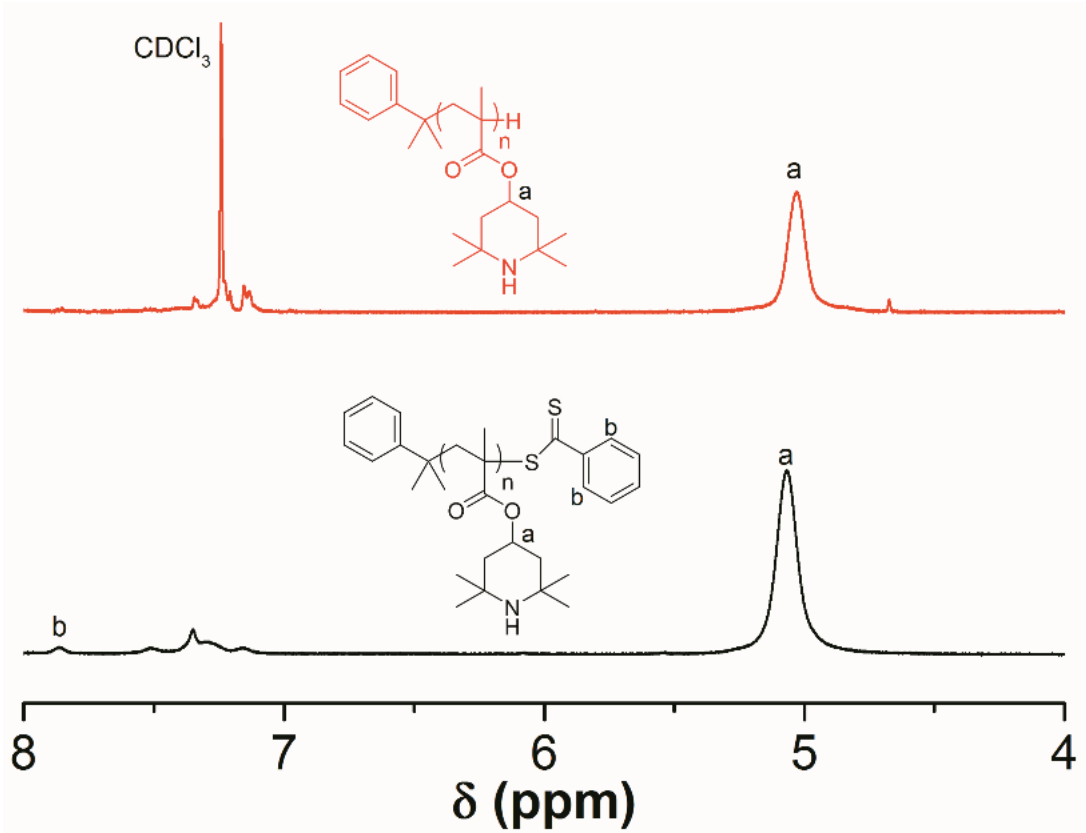

Figure 2.5. ^{1}H NMR spectra for PTMPM synthesized by RAFT polymerization with chain transfer reagent (lower) and without chain transfer reagent (upper). The end group is indicated by peak (b).

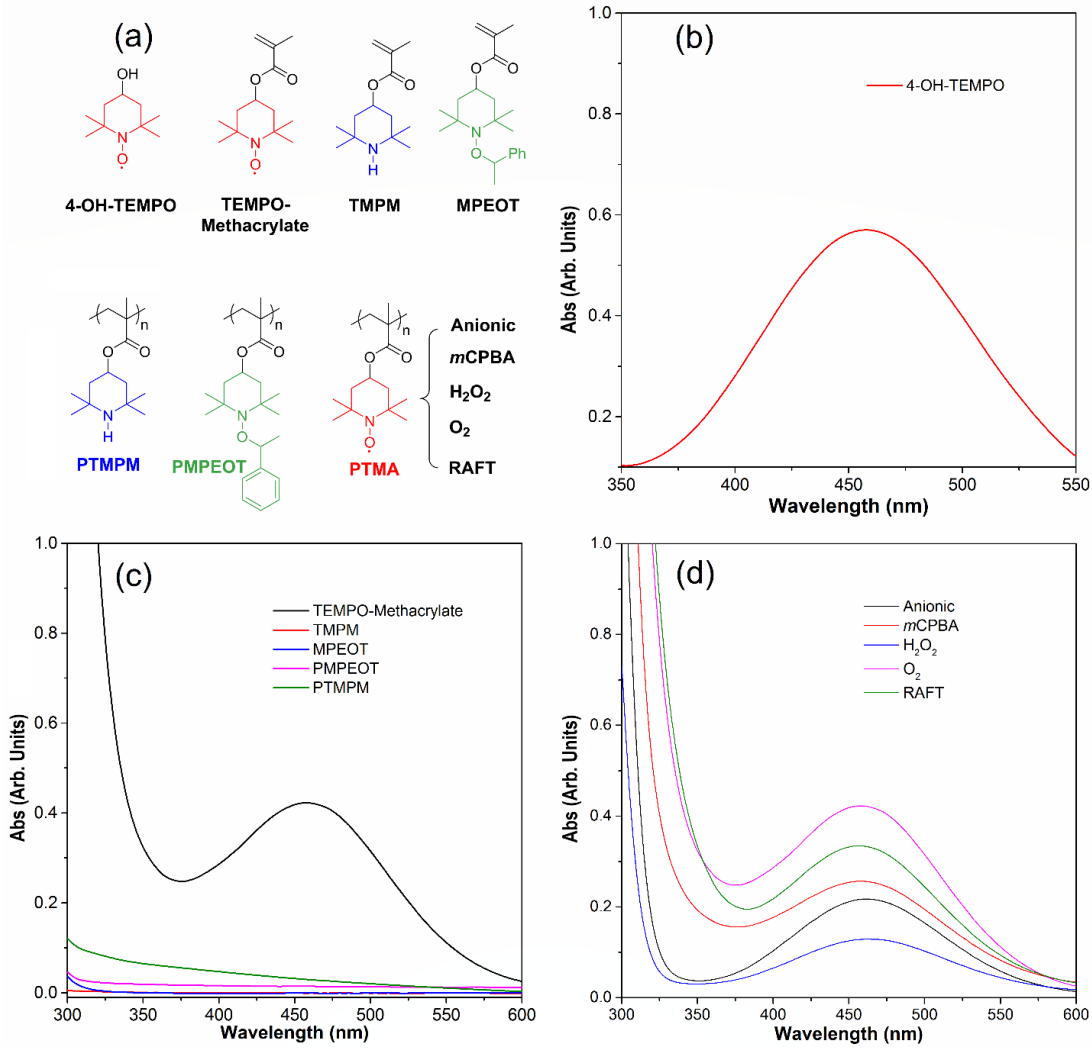

Figure 2.6. (a) Chemical structures of the monomers and polymers (b) monomeric TEMPO (4-hydroxy-TEMPO) (c) TEMPO-methacrylate and precursor monomers (TMPM, MPEOT) and precursor polymers (PTMPM, PMPEOT) (d) Oxidized PTMA (Anionic, *m*CPBA, H_2O_2, O_2, RAFT). While the amine-bearing and alkoxyamine-bearing molecules do not show any obvious absorption, all the TEMPO-containing molecules/polymers show a broad characteristic absorption peak at ~ 463 nm, which is consistent with the absorption peak of 4-hydroxy-TEMPO.

CHAPTER 3: CHARGE TRANSPORT IN CONJUGATED POLYMERS WITH PENDENT STABLE RADICAL GROUPS

3.1 Contributors

This chapter describes an extended collaborative effort between the Ober group, the Fuchs group in Applied Engineering Physics of Cornell and the Flatté group in the Department of Physics and Astronomy of University of Iowa. Yiren Zhang (author) synthesized all the conjugated radical polymer samples, carried out GPC, ATR-FTIR, UV-vis, Raman, AFM and part of the solution EPR measurements. Park performed electrical measurements using the same device described for PTMA measurements and found the exponential relationship between solid-state conductivities and stable radical content. Stephen R. McMillan and Nicholas J. Harmon (postdocs in the Flatté group) contributed tremendously to quantify the intramolecular and intermolecular effects and understand in the context of a disordered network hopping theory.

3.2 Overview

For charge storage applications that take advantage of the redox-active nature of stable radical polymers, enhanced conductivity would improve performance. The substitution of insulating backbone of PTMA for conducting polymer backbone can be a strategy to improve the poor electron transport in solid PTMA film. To address this issue, we prepare and study soluble polythiophene with high regioregularity and vary the concentration of pendent radical groups to systematically examine the variation of conductivity with radical incorporation. Using EPR and electrical conductivity measurements, we show that there is an

exponential decrease of conductivity as we increase the percentage of pendent groups attached to repeating units, which changes the conductivity by 6 orders of magnitude between the non-radical control polythiophene material and the material with highest radical content (~80%). The conductivity of the solid films can be further improved by doping with oxidizers. These findings serve as an important guide to the future design of radical polymers on conjugated backbones with the goal of increasing conductivity for redox-active energy storage applications.

3.3 Introduction

Polymers bearing pendent stable organic radicals have demonstrated excellent properties ranging from tunable electrochemical properties[1], rapid electron self-exchange[2] to reversible redox behavior in the electrode layer[2,3] and facile solution processing[4]. As a result, radical polymers have been investigated as energy storage materials in batteries, and their critical property for charge collection – conductivity – has been studied extensively.[5-8] To date, most investigations focus on non-conjugated stable radical polymers with the existence of electrolytes, whose conductivity can be explained by "diffusive hopping" conduction.[9] However, the charge transport mechanism in solid-state stable radical polymers remains unclear, and the reported conductivity varies dramatically from study to study even for a single model polymer, poly(2,2,6,6-tetramethylpiperidinyloxy methacrylate) (PTMA).

The stable radical group present in PTMA, (2,2,6,6-tetramethylpiperidin-1-yl)oxyl (TEMPO), is a common nitroxide radical and is thought to be by many

insulating in the molecular state.[10] It has also been reported that PTMA has a conductivity near 10^{-10} S/cm.[5,11–13] In a previous study, we have tested the conductivity of PTMA films made by a series of different polymerization methods, and found the conductivity of all samples is 10^{-11} S/cm over distances ranging from 2 - 10 μm.[14] It has been theorized that a series of redox reactions, in which electrons hop between redox sites with the aid of delocalized electrons, can result in efficient charge transport in the pure radical solid[3,15], and some recent reports have appeared describing conductivity close to 10^{-6} S/cm in neat PTMA films over a 100 μm path.[16] In a more recent study, a related polymer with TEMPO side groups and a poly(ethylene oxide) backbone, poly(4-glycidyloxy-2,2,6,6-tetramethylpiperidine-1-oxyl), showed unexpectedly high conductivity when measured in thin (sub-100 nm) films. It was proposed that formation of conducting TEMPO domains explained the transport behavior.[17]

Considering its generally insulating nature, achieving long-range electron transport in a single stable radical polymer requires a system with alternate conducting pathways besides the presence of organic radical sites. In stable radical polymer batteries, the most common way to provide conductivity is by introduction of a conducting species, like carbon black or carbon nanotubes at the expense of energy density.[5,6,18,19] Attempts on a single-component polymer system have also been made in the past two decades, mostly based on conjugated backbones as extra redox sites, such as polypyrrole and polythiophene, as potential cathode materials.[20–24] Recently, for conjugated polythiophenes bearing pendent TEMPO stable radicals (PT-TEMPO), the low capacity and modest conductivity have been explained on the basis of interactions between the radical unit and the

conjugated backbone.[25] Since most reported studies of conjugated polymers with pendent stable radical units focused on electrochemical properties, a detailed study of electron transport in the solid-state films remains important to understand this system.

Synthesis of an effective conjugated stable radical polymer requires that enough stable radical is covalently attached to the conjugated backbone. Meeting this criterion alone is challenging given that the unpaired electrons on stable radicals usually interfere with the transition metal-catalyzed coupling reactions. As a result, many reported cases are homopolymers based on a thiophene with TEMPO radical groups, which are polymerized via either oxidative reactions or electropolymerization. However, the oxidative nature of the above-mentioned methods usually lacks control in final polymer structures or inevitably introduces some oxidative impurities as dopants.

In the first report of PT-TEMPO, conductivity was reported to be 10^{-5} S/cm with the presence of the $FeCl_4^-$ dopant anions.[20] In more recent reports of electropolymerized undoped PT-TEMPO, conductivity values fall between the 10^{-7}-10^{-13} S/cm range,[21,23] which is almost comparable with that of non-conjugated PTMA.[21,23] To date, the highest conductivity of such polymers was found to be near 10^{-2} S/cm in poly(3,4-ethylenedioxythiophene) (PEDOT) with pendent TEMPO radicals, but still 5 orders lower than that of pristine PEDOT.[22] Because the design of conjugated polymers with stable radical pendent groups can act as a replacement of two ingredients in an organic radical battery: carbon black and polymeric binders, understanding the effect of TEMPO radical functionalization on conjugated backbone is important to the future electrode materials and organic

electronics fabrication.

Unlike their non-conjugated counterparts, the local organization of their nanoscale crystallized regions is usually important in determining structure-property behaviors in conjugated polymers. Besides the processing conditions, regioregularity, i.e. head-tail linkages in poly(3-hexylthiophene) (P3HT) can influence self-organization, and hence greatly influence the resulting charge carrier transport and device performance.[26,27] However, such systematic studies on the structure effects have rarely been carried out on conjugated stable radical polymers. In this study, we have adopted a regioregular P3HT backbone to minimize defects in the resultant radical polymers, and systematically varied the loadings of the stable radicals on each repeating unit for the first time. Compared with simple blends of conjugated polymer and stable radicals, the construction of a single molecular species will enhance mixing and also simplify study of charge transport in these stable radical polymers.

Here we report the synthesis of a series of conjugated polythiophenes with pendent TEMPO radical groups using Grignard metathesis polymerization (GRIM) and azide-click reaction, affording the resultant polymer with a regioregular backbone, controlled molecular weight, and low dispersity. Additionally, the synthesized polymers show good solubility without the limitations on molecular weight reported in the literature when polymers are made by other means.[21–23] It should be emphasized that this study uses soluble and narrow dispersity conjugated polymers in contrast to most of the reports in the literature. This enables detailed structural characterization and physical tests from well-controlled materials in both solution and the solid state. We use EPR spectroscopy to study the lineshape of

these materials and to quantitatively assess the TEMPO radical content. To address the intrinsic charge transport in all-conjugated radical polymers, we measure the conductivity of drop-cast films, in the pristine state without polaron doping, for the set of synthesized polymers. We find that as the TEMPO radical content increases linearly, the overall conductivity decreases exponentially. This is consistent with radical sites introducing steric distortions of the conjugated structure, which modifies both inter- and intrachain hopping conductivity. These results and the associated insights provide valuable guidance for the design of conjugated radical-containing polymers with controlled conductivity for energy storage applications.

3.4 Experimental section

3.4.1 Chemicals

All commercial chemicals were purchased from Sigma-Aldrich, VWR, and A&K Scientific and used as received unless otherwise noted. 2,5-dibromo-3-hexylthiophene was purchased from Ark Pharm. Anhydrous THF was distilled from sodium/benzophenone mixture prior to synthesis of monomer and polymerizations. Synthesis of monomers used in the polymer synthesis are shown in **Schemes 3.2** to **3.3**. All reactions were conducted in oven-dried glassware under nitrogen atmosphere.

3.4.2 Characterization

^{1}H-NMR studies of the synthesized monomers and polymers were performed in $CDCl_3$ using a Varian INOVA 400 (^{1}H, 400 MHz) spectrometer. Fourier transform infrared (FTIR) spectra of polymers were recorded under vacuum on a Bruker Vertex V80V Vacuum FTIR spectrometer with an attenuated total

reflection (ATR) mode at a resolution of 4 cm^{-1}. Molecular weights (M_n) and dispersities (Đ) of the polymers were determined by gel permeation chromatography (GPC). The GPC was performed on Waters Ambient Temperature GPC equipped with a Waters 410 differential refractive index detector. GPC columns were eluted at 1.0 mL/min with tetrahydrofuran (THF) at 40 °C. Spectroscopic measurements of diluted solutions were obtained on a Shimadzu UV-vis-NIR spectrophotometer. The samples were closed from the ambient air atmosphere and temperature control was set to 25 °C. Raman spectra of polymer films were obtained on a Renishaw InVia Confocal Raman microscope using an excitation wavelength of 785 nm with a spectral resolution of ~1 cm^{-1}. Polymer thin films were characterized by Asylum MFP-3D atomic force microscope (AFM) using the tapping mode (AC mode) and silicon cantilevers (model: ACCESS-NC).

3.4.3 Grignard metathesis (GRIM) polymerization

Homopolymers (P3HT, P3BrHT) and copolymer P3HT-ran-P3BrHT were synthesized following the same GRIM procedure but using various starting thiophene monomer ratios. Detailed synthesis of P3BrHT is listed here as an example. In a 100 mL round bottom flask, 2,5-dibromo-3-(6-bromohexyl)thiophene (1.30 g, 4.0 mmol, 1.0 eq.) was dissolved in 4.0 mL of anhydrous THF. 4.00 mL of *t*-BuMgCl solution (1.0 M in THF, 4.0 mmol, 1.0 eq.) was added, and the mixture was stirred at 25 °C for 20 h. Then the mixture was diluted with 32.0 mL of THF, and Ni(dppp)Cl_2 ([Ni]:[M] = 1:80) was added in one portion to start the polymerization. After 2 h, the reaction was quenched with 1 M HCl aqueous solution and poured into methanol to precipitate the polymer. The crude polythiophene was collected by filtration, and purified by sequential Soxhlet

extraction with methanol, hexane and chloroform. The target polymer was recovered from chloroform fraction and dried in vacuum at 40 °C. The ^{1}H-NMR spectra of the precursor homopolymer and copolymers are shown in **Figs. 3.8** and **3.9**, respectively.

3.4.4 Azide substitution

P3BrHT (100 mg, 0.40 mmol of Br, 1.0 eq.) was dissolved in 4 mL of anhydrous THF. Sodium azide (210.4 mg, 3.24 mmol, 8.0 eq.) and 18-crown-6 (855.42 mg, 3.24 mmol, 8.0 eq.) were dissolved in 1.0 mL N,N-Dimethylformamide (DMF) and thorough mixing was applied to obtain a homogenous solution. The DMF solution was then added to P3BrHT solution and the resultant mixture was stirred at 60 °C for 15 h. After completion, the mixture was poured into methanol and the precipitate was collected. The crude polymer P3HT-azide was purified by repeated Soxhlet extraction with methanol and dried in vaccum at 40 °C.

3.4.5 Synthesis of P3HT-TEMPO-X via azide-click reaction

The azide-click reaction was conducted under nitrogen in a Schlenck tube. P3HT-azide (71.5 mg, 341.6 μmol of azide, 1.0 eq.), alkyne-TEMPO (86.2 mg, 1.2 eq.), copper(I) iodide (CuI) (5% eq.) was dissolved in THF/DIPEA mixture (V:V = 9:1, 4.0 mL). Then the mixture was degassed with nitrogen for 30 minutes and stirred at 50 °C for 24 h. After completion, the mixture was diluted with THF and filtered through a short alumina column to remove copper. The subsequent precipitation and filtration gave the crude polymer P3HT-TEMPO-X, which was further purified by repeated Soxhlet extraction with methanol (**Scheme 3.1**).

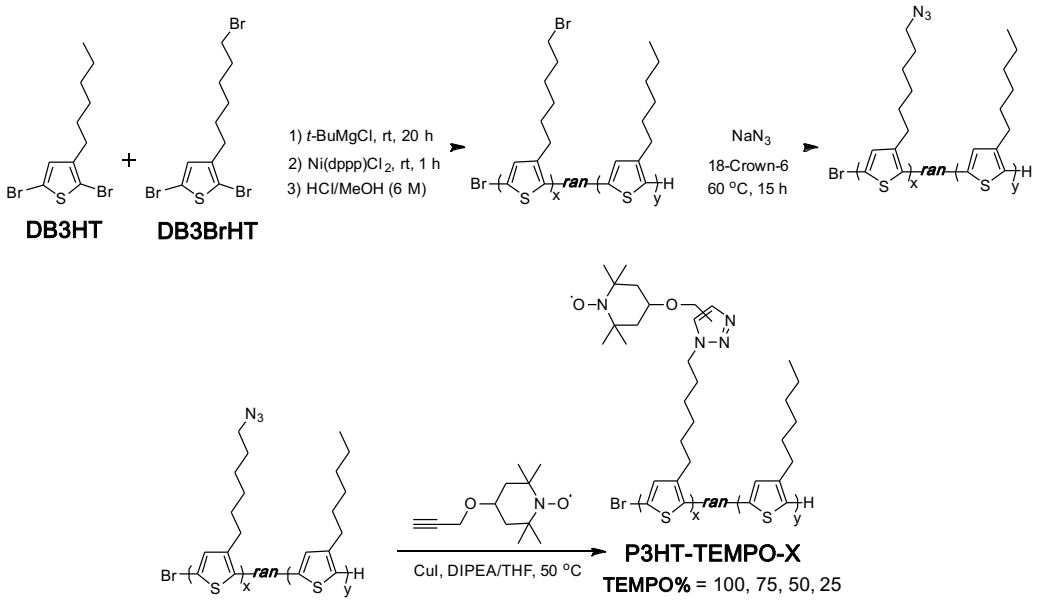

Scheme 3.1. Synthesis route of P3HT-TEMPO-X.

3.4.6 Magnetic Resonance and Conductivity Measurements

Solutions for EPR were prepared in THF such that they contain the equivalent of 1mM concentration of the clicked TEMPO group. To ensure there is no other source of EPR signal, solutions of the precursor P3HT-*ran*-P3BrHT were also prepared in THF as a control with the same concentration of repeating unit. Measurements were repeated three times for each of the clicked species using independently prepared solutions. The solution concentration of P3HT-TEMPO-X samples were prepared to target a constant overall TEMPO concentration. The EPR data were normalized with respect to a reference solution with the same nominal concentration of TEMPO spins. We report the average and standard error of the three measurements, which primarily originates from uncertainty in solution preparation. All measurements were made using Bruker X-band EPR spectrometer at room temperature. EPR spectra of TEMPO and the TEMPO-free precursor polymer are shown in **Figs. 3.6** and **3.7**, respectively.

3.4.7 Conductivity Measurement

Microfabricated 4-wire lateral templates with 2.5 mm length and 10 or 20 μm separation were patterned using photolithography. 100 nm thick, gold contact electrodes were prepared by sputtering and lift-off on a thermally oxidized silicon substrate. Polymer films were prepared by dropcasting 10 mg/mL sample stock solutions on templates. The typical film thickness varies from 250 nm to 2.2 μm for the drop-cast films. The P3HT-TEMPO-X samples were dissolved in chlorobenzene, except for P3HT-TEMPO-100, which was dissolved in 1,4-dioxane due to its limited solubility in chlorobenzene. To obtain the conductivity without contribution from parasitic contact resistance, all four electrodes were used for

measurement, applying current to the outer electrodes with a Keithley 6610 precision current sourcemeter and reading voltages from the inner electrodes with a Keithley 6514 electrometer. Film thickness measured using a Tencor Alphastep profilometer. As a control sample, P3HT without TEMPO groups was prepared in toluene and measured in a similar fashion using the 4-wire template. All measurements were done in a dark, vacuum-sealed and continuously pumped chamber.

3.5 Results and Discussion

Since the commonly used and effective methods for direct polymerization of radical-bearing thiophene monomer, such as oxidative polymerization or electropolymerization, usually produce materials with poor control of molecular weight and backbone regioregularity, it is necessary to employ alternative synthetic strategies to provide a sample with good solubility and low PDI. Our approach relies on Grignard metathesis (GRIM) polymerization, which affords highly regioregular polythiophene backbones based on Ni-catalyzed transfer reaction.[28–30] To avoid the deactivation of TEMPO radical by the Grignard reagent, we initially started with direct polymerization of a novel thiophene monomer bearing 2,2,6,6-tetramethylpiperidine, a TEMPO-precursor moiety used in our previous work. Unfortunately, this amine precursor of TEMPO can deprotonate the thiophene ring with the presence of a Grignard reagent.[31] Instead, alkoxyamine-containing thiophene was synthesized due to its stability towards the Grignard reagent.[32] However, the subsequent polymerization after Grignard metathesis only produced oligomers, which may be ascribed to interference of the large

alkoxyamine structure with polymerization process.

As an alternative, a post-functionalization method was developed for this study. Poly(3-(6-bromohexyl)thiophene) (P3BrHT) was chosen as the precursor polymer due to its high regioregularity, similar to P3HT, while the bromine at the side chain terminus acts as a handle for chemical modifications. In order to covalently attach the TEMPO radical, etherification in THF using the 4-hydroxy-TEMPO/sodium hydride combination (40 eq. to Br) was attempted. For higher conversion, the reaction mixture was heated at 72 °C for 72 h. However, solution EPR showed low radical content in the product, which indicates the deactivation of the TEMPO radical under extended strong basic conditions.

To achieve a high level of TEMPO attachment, the azide-click reaction was used for the preparation of the target polymer due to its compatibility with the TEMPO stable radical.[33] P3HT-azide was prepared by reacting P3BrHT with sodium azide, and complete substitution was demonstrated by the shift of the proton peak. (**Fig. 3.8**) The subsequent click reaction with alkyne-TEMPO was carried out at 50 °C for 24 h in THF/DIPEA (V:V = 9:1) with CuI as catalyst. After completion, a red fiber-like precipitate formed, which can be easily filtered and purified by subsequent Soxhlet extraction. However, like previous reports, the resultant P3HT-TEMPO-100 (target MW = 22 kDa) was insoluble in many solvents, including THF, chloroform, toluene, chlorobenzene, DMSO and dichlorobenzene, even when heated. Successful modification of the azide group is indicated by the absence of a strong azide peak at 2083 cm^{-1}, while the removal of excess alkyne-TEMPO is suggested by the absence of alkyne peak at 3230 cm^{-1}. (**Fig. 3.1**)

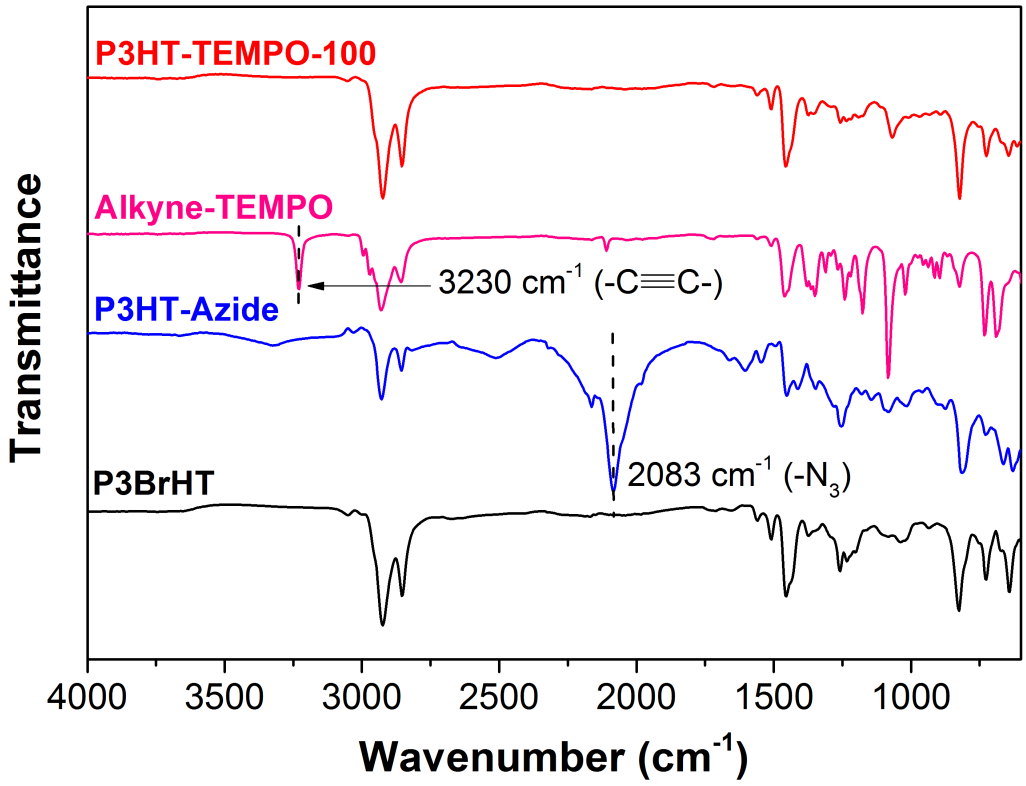

Figure 3.1. ATR-FTIR spectra of precursor polymer P3BrHT, P3HT-azide, reactant alkyne-TEMPO, and target polymer P3HT-TEMPO-100.

Due to the insoluble nature of the model polymer P3HT-TEMPO-100 with target molecular weight 22 kDa, we attempted to increase solubility by decreasing the degree ofpolymerization of the polythiophene backbone. Finally, P3HT-TEMPO-100 with molecular weight ~10 kDa was synthesized, which can be easily dissolved in hot THF or 1,4-dioxane, but not in hot toluene or chlorobenzene. After dissolution in hot THF and aging for several days at room temperature, a red P3HT-TEMPO-100 precipitate started to form. Upon reduction of TEMPO radical by addition of hydrazine hydrate, the precipitate dissolved immediately, which indicates that the poor solubility may originate from the interactions between pendent TEMPO radicals. To further improve solubility, 2,5-dibromo-3-hexylthiophene was introduced as comonomer in the precursor polymer synthesis, and a series of statistical polymers of P3HT-ran-P3BrHT were made (Br% = 25, 50, 75%). Due to the similar structure and reactivity, copolymerization of two thiophene monomers produced a copolymer with similar M_n and low dispersity, but without large composition deviations from the starting monomer ratio. (**Table 3.1**) Finally, P3HT-TEMPO-X (TEMPO-X % = 25, 50, 75 %) was prepared using the same azide-click reaction, and is soluble in many solvents, including toluene and chlorobenzene.

We characterized the radical yield of TEMPO clicked on the P3HT backbone using EPR in the solution state. As shown in **Fig. 3.2 (a)**, the quantitative EPR signal increases as the intended percentage of monomers with a pendent TEMPO group (X value) increases. We find that for X=100, the quantitative yield of TEMPO groups containing a radical electron is 81 ± 13 %, and that other X values show a similar conversion rate. This indicates that our method of click reaction is

Table 3.1. Synthesis and characterization of P3HT-*ran*-P3BrHT and P3HT-TEMPO-X

Sample	[HT]:[BrHT][a]	HT:BrHT[b]	Regioregularity (%)	M_n (kDa)	Đ
P3HT-TEMPO-25	75:25	76.1:23.9	89	5.9	1.10
P3HT-TEMPO-50	50:50	50.5:49.5	92	7.3	1.07
P3HT-TEMPO-75	25:75	23.7:76.3	92	6.5	1.09
P3HT-TEMPO-100	0:100	0:100	93	9.2	1.09

[a]Starting monomer ratio of 2,5-dibromo-3-hexylthiophene ([HT] and 2,5-dibromo-3-(6-bromohexyl)thiophene ([BrHT]). [b]Percentage of repeating units 3-hexylthiophene in P3HT-*ran*-P3BrHT, determined by ^{1}HNMR. [c]Determined by ratio of the ^{1}H NMR signal of P3HT-*ran*-P3BrHT at 2.81 and 2.58 ppm (Figure S4).

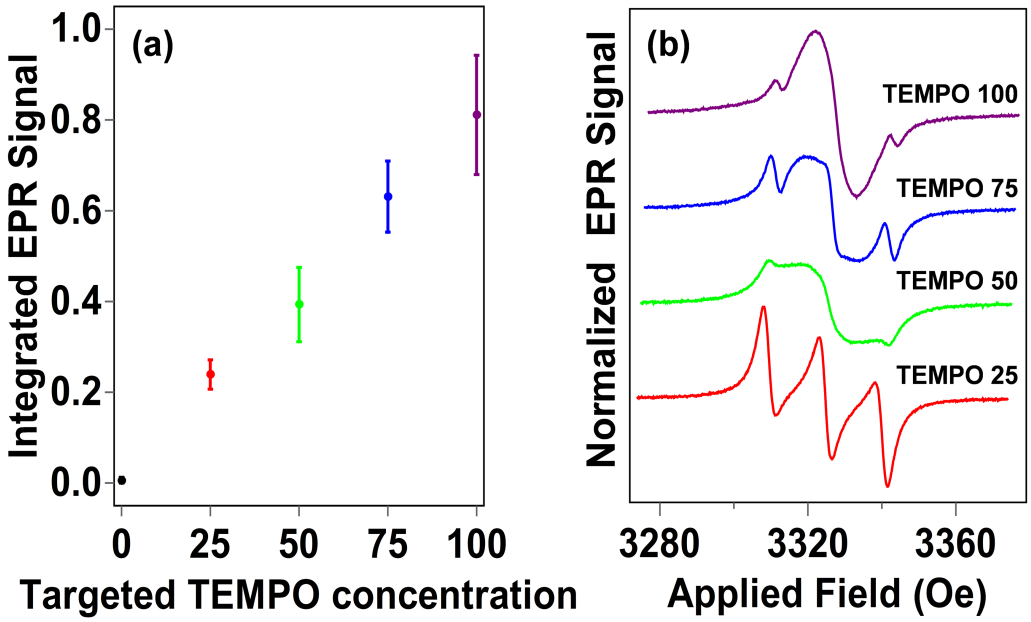

Figure 3.2. (a) Integrated EPR signal of solution-state P3HT-TEMPO as a function of target TEMPO concentration. The signal is normalized to a TEMPO standard with a radical concentration of fully functionalized P3HT-TEMPO. For a target TEMPO concentration of 0, we used a precursor polymer that does not have attached TEMPO groups. Error bars show the standard error or three independently prepared samples. (b) individual line shapes of P3HT-TEMPO-X.

capable of reliably controlling the fraction of TEMPO groups pendent to the P3HT backbone. From the absence of EPR signal of the precursor polymer we can again confirm that the polymer is in the undoped state.

Analysis of the EPR line shape is an indicator of the relative amount of radical electrons in the synthesized polymer. For samples with a high concentration of unpaired electrons, the exchange interaction between closely spaced radicals quenches the hyperfine-induced triplet lineshape of small-molecule TEMPO in solution **(Fig. 3.6)**[34], and we observe instead broad Lorentzian singlets. In lower concentration samples, however, many of the radical electron spins are comparably isolated, and thus they have narrow triplet lineshapes. From the lineshapes of P3HT-TEMPO-X (**Fig. 3.2 (b)**), we see that increasing the concentration of radical electrons follows this trend. The P3HT-TEMPO-25 is dominated by a triplet lineshape whereas the P3HT-TEMPO-100 has little triplet contribution and is dominated by a broad singlet. We also confirm there is no distinguishable EPR signal from P3HT precursor polymer that does not have attached TEMPO **(Fig. 3.7**).

Next, we measured the conductivity of the polymer series in the pristine state to study the correlation between TEMPO concentration and electrical conductivity. Details of the electrical measurement procedure are given in **Ref. 16**. **Fig. 3.3** shows that the film conductivity decreases monotonically from 7×10^{-5} S/cm to 3.8×10^{-11} S/cm as the normalized TEMPO content per monomer increases from 0 for the control sample to 0.81 for TEMPO% X=100. The high conductivity at low radical concentration and the decaying trend of conductivity with increasing radical content suggests that the main mechanism of conductivity in this material is

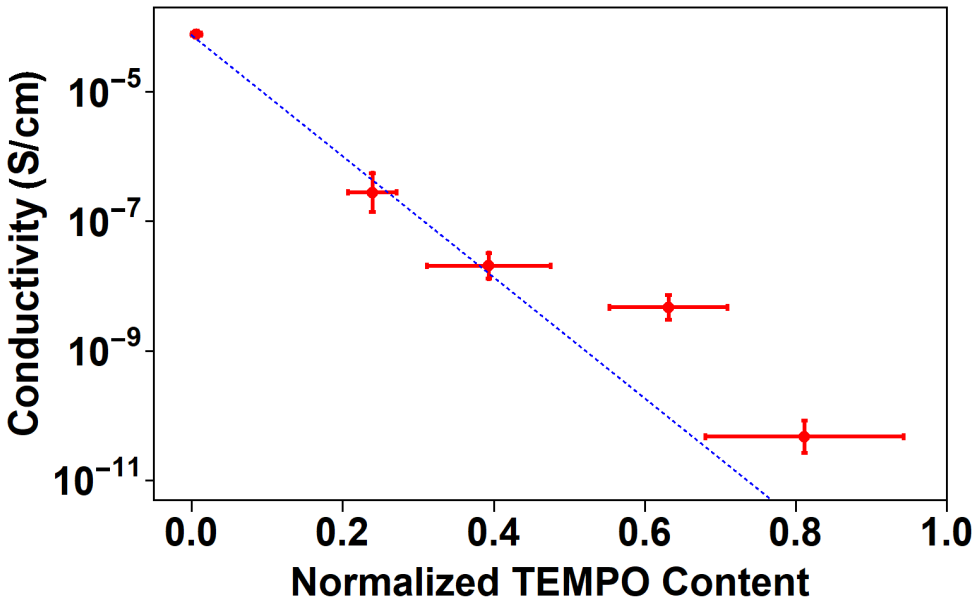

Figure 3.3. Semilog plot of the conductivity of P3HT-TEMPO-X as a function of calibrated TEMPO content. The dashed line is a fit to the simple model described by **eq 3.4**.

via charge transport along on the conjugated backbone rather than variable range hopping (VRH) between radical pendent sites.

In the P3HT-TEMPO system, when the concentration of clicked TEMPO is low, the conjugated backbone can be organized to form crystalline regions, which leads to higher conductivity. However, as more TEMPO groups are introduced, the ordered packing of the polythiophene backbone decreases due to the steric hindrance from the TEMPO side-chains. This mechanism also agrees with previous results that showed that differences in crystalline ordering of domains in conjugated polymers can lead to orders of magnitude differences in conductivity.[35]

Considering the bulky methyl substituents of a TEMPO radical, we used ultraviolet-visible (UV-vis) spectroscopy to assess the extent of conjugation and its effect on conductivity given the possible steric interactions upon introduction of TEMPO groups. UV-vis absorption spectra were recorded for all four polymers studied in solution (THF) and as-cast films on glass substrates. In THF solution, all the polymers showed an absorption maximum around 444 nm (**Fig. 3.4 (a)**), which is red-shifted by around 20 nm as compared to previous reports of regiorandom analogs.[23] This result suggests extended conjugation caused by a regioregular polythiophene backbone in the solution state. No further absorption features can be observed upon variation of TEMPO content, indicating that the attachment of the bulky TEMPO structure to the polythiophene backbone did not change its electronic structure significantly in the solution state. This result is also consistent with an earlier report that the TEMPO radical has no doping effect on neutral polythiophenes. The results in **Ref. 25** should be distinguished from our findings because, while we study conductivity in the solid state where radicals are all in the

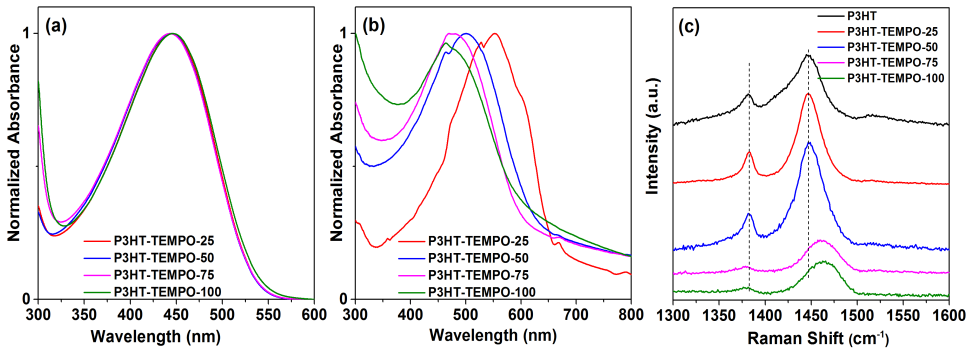

Figure 3.4. (a) Ultraviolet-visible (UV-vis) absorption of P3HT-TEMPO-X in a THF solution. (b) UV-vis absorption of a drop-casted P3HT-TEMPO-X film on a glass substrate. (c) Raman spectra of drop-cast P3HT and P3HT-TEMPO-X films on a Si substrate.

neutral state, **Ref. 25** included electrochemical measurements that involve oxidation of the radical, redox-active sites leading to doping and charged species.[25]

In the as-cast films, the absorption maxima of four TEMPO-containing polymers were red-shifted with respect to the solution absorption maxima, with P3HT-TEMPO-25 showing the largest red-shift and P3HT-TEMPO-100 showing the smallest. Such phenomena can be ascribed to planarization of the conjugated segments or enhanced interchain interactions between adjacent polythiophene backbones in solid films. (**Fig. 3.4 (b)**) As the TEMPO radical loading increases, the vibronic features usually observed in P3HT films disappeared, suggesting the interchain packing of the conjugated backbones has been reduced. This can be explained if the bulky TEMPO radical groups create steric hindrance.

The conjugation length distribution can be reflected not only in the UV-vis spectra but also in Raman spectroscopy. With a more planar structure, the conjugated polymers have extended conjugation length relative to a more twisted structure, which can provide further information of the effect of TEMPO radical on the backbone planarization. In **Fig. 3.4 (c)**, the Raman spectra (λ_{exc} = 785 nm) of regioregular P3HT and P3HT-TEMPO-X are presented. The Raman results show that when the TEMPO radical loading is lower than 50%, the band corresponding to symmetric C_α-C_β stretching deformations slowly increases from 1446.5 cm^{-1} to 1447.8 cm^{-1}.[36] This indicates that the introduction of TEMPO radicals at a low level mainly affects the interchain packing rather the chain planarization. However, as the TEMPO loading exceeds 50%, the band shifts to a higher wavenumber, which is 1461.8 cm^{-1} for P3HT-TEMPO-75 and 1465.1 cm^{-1} for P3HT-TEMPO-100, signifying a decrease in the planarity or degree of conjugation along the

backbone.[37] As a result, intrachain electron transport is impeded and the overall electron conductivity further decreases. This observation is consistent with the disappearance of vibronic features for large TEMPO content, and it is also consistent with the previous reports.[38] Thus we conclude that the main cause of the dramatic decrease in the electrical conductivity with increasing TEMPO percentage is a decrease in the P3HT crystallinity due to steric hindrance.

It should be noted that in a prior study it was found that loss in conductivity in another TEMPO-containing conjugated polymer was due to dedoping of the polythiophene backbone. To avoid confusion we remind the reader that the polymer in this current study was examined in the solid state with no electrochemical bias while the prior study of electropolymerized TEMPO containing polythiophene was measured in an electrochemical cell under bias and as a result the two cases are difficult to compare.

In order to further elucidate the aggregation of P3HT-TEMPO-X in the solid state, we investigated solvent-annealed thin films of these polymers by atomic force microscopy (AFM). P3HT is a semi-crystalline polymer and fibers composed of well-packed conjugated segments can be obtained by annealing the film with the presence of organic solvent vapor or by thermal treatment. We first prepared a series of thin film of P3HT and P3HT-TEMPO-X by spin-coating, then the films were annealed in THF vapor overnight prior to the AFM measurements. In **Fig. 3.5 (a)**, we observe that short fibers of P3HT formed after solvent vapor annealing, indicating interchain packing between the conjugated polymer backbones. As TEMPO loading increase to 25%, we note that domains with higher crystallinity are observable in P3HT-TEMPO-25 film, but the domains are disordered with

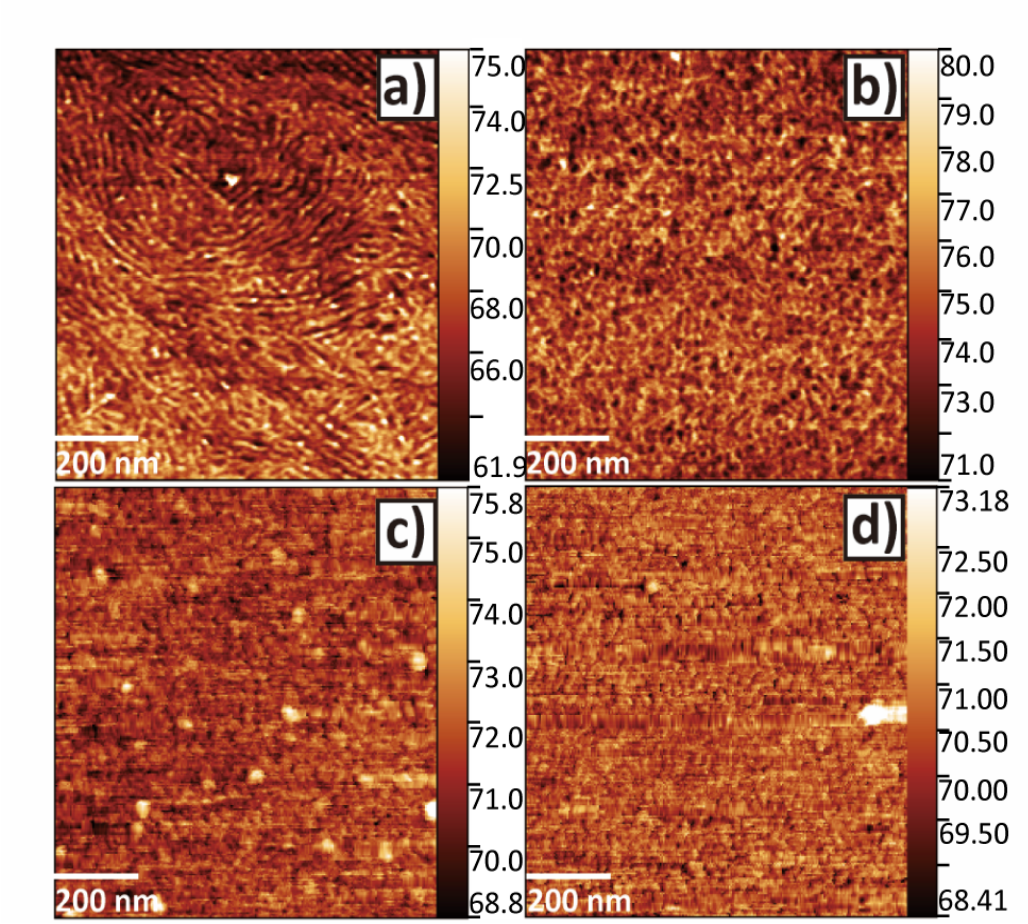

Figure 3.5. Atomic force microscopy phase images of (a) P3HT, (b) P3HT-TEMPO-25, (c) P3HT-TEMPO-50, (d) P3HT-TEMPO-75 after spin-coating from solutions in chlorobenzene and annealing in THF.

negligible or only small grain size (**Fig. 3.5 (b)**). Upon introduction of more TEMPO radical substituents, fiber-like aggregation disappears and polymer chains start to form large amorphous aggregates (**Fig. 3.5 (c)**), which became smaller at a higher TEMPO loading (**Fig. 3.5 (d)**). This indicates that the π-π interactions between the conjugated backbones have been impeded by large steric hindrance of TEMPO groups. As the result, the efficient electron transport pathway cannot be achieved in the conjugated homopolymers with high TEMPO contents because the twisted backbone and amorphous nature of films, which explains why in earlier attempts of such polymer no obvious increase in conductivity has been achieved.

To understand this effect more quantitatively, we consider a charge hopping model. As charge moves through pristine P3HT there are relatively low potential barriers between sites along the same polymer chain (intrachain hopping) compared to the potential barriers between chains (interchain hopping), due to the nature of the conducting backbone. This results in a preference for backbone conduction along the length of the polymer until it terminates. After traveling along the length of the polymer, the charge hops to another nearby chain. Since the interchain hops are unavoidable and correspond to the largest barriers, they dominate the conductance. In the case of pure, regioregular P3HT, the chains are able to stack into ordered, crystalline domains that facilitate interchain hopping. As discussed above, the addition of pendent TEMPO side-chains distort the stacking and thus adds to the disorder in chain-chain orientation, which increases the interchain hopping barrier.

In this treatment, we model charge conduction in P3HT as tunneling through interchain barriers, which are arranged in a random three-dimensional network.[39]

The average number of sites per volume, *N*, can be written as the product of the density of states *g(μ)* and the bandwidth ε_0,

$$N = 2\mathrm{g}(\mu)\varepsilon_0 N$$

where the factor of 2 accounts for sites in the range $\mu \pm \varepsilon_0$. The addition of TEMPO side-chains acts to reduce the number of available sites by pushing them further away in position or energy. This suggests the volumetric density of states is reduced by an amount that is proportional to the TEMPO percentage, *f*. In the simplest model, each TEMPO has a probability *p* for pushing one site out of reach of the transport states. This allows one to write the density of states as a function of *f*,

$$g(\mu) = \frac{3(1-pf)}{8\pi l^3 \varepsilon_0}$$

where *l* is the average inter-site distance. Applying Eq.(2) to the expression for the resistance of a unit segment of a Miller-Abrahams type network[40] yields an expression for the conductivity,

$$\sigma = \sigma_0 \exp\left[\frac{-2l}{a(1-pf)^{\frac{1}{3}}}\right]$$

where *a* represents the carrier wave function localization and σ_0 is a material and temperature dependent term that describes the conductivity due to carrier-phonon interactions. To recover an exponential dependence of conductivity on TEMPO concentration we consider the perturbative limit where *fp* is $\ll 1$. This permits the expansion of Eq.(3) about *fp* = 0,

$$\sigma \approx \sigma_0 \exp\left[\frac{-2l\left(1+\frac{pf}{3}\right)}{a}\right]$$

If we take $p = 1$, the slope of the fit line in Fig. 3 near $f = 0$ gives an estimate for $l/a \sim 30$. Although this simple model cannot simultaneously account for both the low-f and high-f behavior of σ, it qualitatively captures the trend in the data. For larger values of f, we expect that one would need to explicitly account for the dependence of l on f, and there could be contributions from disorder that further decrease the intrachain hopping transport, which would also decrease the conductivity exponentially. We do not make these extensions because five data points cannot constrain a more complex model. Taking a ~ 0.7 Å, corresponding roughly to the covalent radius of carbon,[41] we estimate that the average interchain hopping distance is around 2 nm, which is comparable to but smaller than the average chain length. This result suggests that the crystalline domains have a sizable average separation, and that increasing the TEMPO percentage reduces the average number of accessible crystalline regions available for conductivity, thus exponentially suppressing the conductivity.

Because TEMPO is a radical spin, there is a localized site, typically filled, at some energy below the chemical potential and a localized site, typically empty, above the chemical potential. We see no evidence of transport through such TEMPO-associated sites for carrier hopping, and thus suggest that these sites are not within the range of energies accessible for transport within the materials as we have fabricated them.

3.6 Conclusions

In conclusion, we have synthesized and studied regioregular polythiophene polymers with pendent TEMPO groups on a systematic range of 0 – 80% of the repeating units. This material remains soluble even for the highest TEMPO fraction, has controlled molecular weight, and low dispersity. We found that as we increase the percentage of pendent TEMPO, the conductivity of the film decreases exponentially, which we understand in the context of a disordered network hopping theory. This result based on both experiment and a simple but appropriate model is also consistent with UV-vis absorption measurements of the solid films that show decreasing crystallinity with increasing TEMPO percentage. In light of energy storage applications of stable radical polymers in which one would ideally combine high conductivity from the polythiophene backbone with the redox activity of a stable radical group, our results demonstrate that for this direct approach to increasing radical polymer conductivity, a compromise will be necessary. We point out that for a very large TEMPO fraction, the conductivity is similar to the conductivity that we recently reported in non-conjugated PTMA.[14,42] However, we have shown that by reducing the fraction of radical groups linearly, one can increase conductivity exponentially – by orders of magnitude. Therefore, the insights from this work can guide the engineering of future energy storage materials, and they can motivate the investigation of new copolymers for both combining stable radical groups and conjugated conducting units in a single polymer.

3.7 Acknowledgements

This work was supported the Department of Energy Office of Basic Energy Science (Grant DE-SC0014336). We acknowledge use of the facilities of the Cornell NanoScale Facility, a member of the National Nanotechnology Coordinated Infrastructure (NNCI), supported by the National Science Foundation (NSF) (Grant ECCS-1542081). We also acknowledge the use of shared facilities of the Cornell Center for Materials Research which is supported through the NSF MRSEC program (Grant DMR-1719875) and the shared facilities of the National Biomedical Center for Advanced Electron Spin Resonance Technology, which is supported by the National Institute of General Medical Sciences, a part of the National Institutes of Health (Grant P41GM103521).

3.8 References

1 T. Janoschka, M. D. Hager and U. S. Schubert, *Advanced Materials*, 2012, **24**, 6397–6409.

2 K. Oyaizu and H. Nishide, *Advanced Materials*, 2009, **21**, 2339–2344.

3 K. Nakahara, K. Oyaizu and H. Nishide, *Chemistry Letters*, 2011, **40**, 222–227.

4 K. Zhang, Y. Hu, L. Wang, J. Fan, M. J. Monteiro and Z. Jia, *Polymer Chemistry*, 2017, **8**, 1815–1823.

5 K. Nakahara, S. Iwasa, M. Satoh, Y. Morioka, J. Iriyama, M. Suguro and E. Hasegawa, *Chemical Physics Letters*, 2002, **359**, 351–354.

6 H. Nishide, S. Iwasa, Y.-J. Pu, T. Suga, K. Nakahara and M. Satoh, *Electrochimica Acta*, 2004, **50**, 827–831.

7 Y. Yonekuta, K. Susuki, K. Oyaizu and K. Honda, *Journal of the American Chemical Society*, 2007, **129**, 14128–14129.

8 T. Suga, H. Ohshiro, S. Sugita, K. Oyaizu and H. Nishide, *Advanced Materials*, 2009, **21**, 1627–1630.

9 K. Sato, R. Ichinoi, R. Mizukami, T. Serikawa, Y. Sasaki, J. Lutkenhaus, H. Nishide and K. Oyaizu, *Journal of the American Chemical Society*, 2018, **140**, 1049–1056.

10 X. Yu, A. Mailman, K. Lekin, A. Assoud, C. M. Robertson, B. C. Noll, C. F. Campana, J. A. K. Howard, P. A. Dube and R. T. Oakley, *Journal of the American Chemical Society*, 2012, **134**, 2264–2275.

11 J. Kim, G. Cheruvally, J. Choi, J. Ahn, S. Lee, D. Choi and C. Song, *Solid State Ionics*, 2007, **178**, 1546–1551.

12 J.-K. Kim, Y. Kim, S. Park, H. Ko and Y. Kim, *Energy & Environmental*

Science, 2016, **9**, 1264–1269.

13 J.-K. Kim, J. Scheers, J.-H. Ahn, P. Johansson, A. Matic and P. Jacobsson, *J. Mater. Chem. A*, 2013, **1**, 2426–2430.

14 Y. Zhang, A. Park, A. Cintora, S. R. McMillan, N. J. Harmon, A. Moehle, M. E. Flatté, G. D. Fuchs and C. K. Ober, *Journal of Materials Chemistry C*, 2018, **6**, 111–118.

15 K. Oyaizu, Y. Ando, H. Konishi and H. Nishide, *Journal of the American Chemical Society*, 2008, **130**, 14459–14461.

16 L. Rostro, A. G. Baradwaj and B. W. Boudouris, *ACS Applied Materials & Interfaces*, 2013, **5**, 9896–9901.

17 Y. Joo, V. Agarkar, S. H. Sung, B. M. Savoie and B. W. Boudouris, *Science*, 2018, **359**, 1391–1395.

18 K. Nakahara, J. Iriyama, S. Iwasa, M. Suguro, M. Satoh and E. J. Cairns, *Journal of Power Sources*, 2007, **165**, 870–873.

19 M. Suguro, S. Iwasa and K. Nakahara, *Macromolecular Rapid Communications*, 2008, **29**, 1635–1639.

20 A. Iragi, J. A. Crayston, J. C. Walton and A. Harrison, *Journal of Materials Chemistry*, 1995, **5**, 1291.

21 M. Aydın, B. Esat, Ç. Kılıç, M. E. Köse, A. Ata and F. Yılmaz, *European Polymer Journal*, 2011, **47**, 2283–2294.

22 N. Casado, G. Hernández, A. Veloso, S. Devaraj, D. Mecerreyes and M. Armand, *ACS Macro Letters*, 2016, **5**, 59–64.

23 F. Li, Y. Zhang, S. R. Kwon and J. L. Lutkenhaus, *ACS Macro Letters*, 2016, **5**, 337–341.

24 L. Xu, F. Yang, C. Su, L. Ji and C. Zhang, *Electrochimica Acta*, 2014, **130**,

148–155.

25 F. Li, D. N. Gore, S. Wang and J. L. Lutkenhaus, *Angewandte Chemie International Edition*, 2017, **56**, 9856–9859.

26 Y. Kim, S. Cook, S. M. Tuladhar, S. A. Choulis, J. Nelson, J. R. Durrant, D. D. C. Bradley, M. Giles, I. McCulloch, C.-S. Ha and M. Ree, *Nature Materials*, 2006, **5**, 197–203.

27 X. Shen, W. Hu and T. P. Russell, *Macromolecules*, 2016, **49**, 4501–4509.

28 A. Yokoyama, R. Miyakoshi and T. Yokozawa, *Macromolecules*, 2004, **37**, 1169–1171.

29 R. S. Loewe, P. C. Ewbank, J. Liu, L. Zhai and R. D. McCullough, *Macromolecules*, 2001, **34**, 4324–4333.

30 R. Tkachov, V. Senkovskyy, H. Komber, J.-U. Sommer and A. Kiriy, *J. Am. Chem. Soc.*, 2010, **132**, 7803–7810.

31 M. S. Maji, T. Pfeifer and A. Studer, *Angewandte Chemie International Edition*, 2008, **47**, 9547–9550.

32 E. Kaul, V. Senkovskyy, R. Tkachov, V. Bocharova, H. Komber, M. Stamm and A. Kiriy, *Macromolecules*, 2010, **43**, 77–81.

33 T. K. Kunz and M. O. Wolf, *Polymer Chemistry*, 2011, **2**, 640–644.

34 D. C. Bobela, B. K. Hughes, W. A. Braunecker, T. W. Kemper, R. E. Larsen and T. Gennett, *J. Phys. Chem. Lett.*, 2015, **6**, 1414–1419.

35 H. Sirringhaus, P. J. Brown, R. H. Friend, M. M. Nielsen, K. Bechgaard, B. M. W. Langeveld-Voss, A. J. H. Spiering, R. a. J. Janssen, E. W. Meijer, P. Herwig and D. M. de Leeuw, *Nature*, 1999, **401**, 685.

36 G. Louarn, M. Trznadel, J. P. Buisson, J. Laska, A. Pron, M. Lapkowski and S. Lefrant, *J. Phys. Chem.*, 1996, **100**, 12532–12539.

37 J. Kim, K.-J. Baeg, D. Khim, D. T. James, J.-S. Kim, B. Lim, J.-M. Yun, H.-G. Jeong, P. S. K. Amegadze, Y.-Y. Noh and D.-Y. Kim, *Chem. Mater.*, 2013, **25**, 1572–1583.

38 B. Burkhart, P. P. Khlyabich and B. C. Thompson, *Macromolecules*, 2012, **45**, 3740–3748.

39 B. I. Shklovskii and A. L. Ėfros, *Electronic properties of doped semiconductors*, Springer-Verlag Berlin Heidelberg GmbH, Berlin Heidelberg, Softcover reprint of the original 1st edition 1984., 2013.

40 A. Miller and E. Abrahams, *Physical Review*, 1960, **120**, 745–755.

41 F. A. Carey and R. J. Sundberg, *Advanced Organic Chemistry: Part A: Structure and Mechanisms*, Springer Science & Business Media, 2007.

42 T. Suga, S. Takeuchi, T. Ozaki, M. Sakata, K. Oyaizu and H. Nishide, *Chemistry Letters*, 2009, **38**, 1160–1161.

3.9 Supporting Information

Materials Synthesis and Characterization.

General considerations

All manipulation of air or moisture sensitive compounds were carried out under nitrogen atmosphere using standard Schlenk line techniques. Flash column chromatography was performed using silica gel with particle size 230-400 mesh. ^{1}H spectra were recorded on Varian INOVA 400 (^{1}H, 400 MHz) spectrometers. ^{1}H NMR spectra were referenced with residual non-deuterated solvent shifts ($CHCl_3$=7.26 ppm). Thermal gravimetric analysis (TGA) of polymer samples was performed on a TA Instruments Q500 Thermogravimetric Analyzer with a 16 chamber autosampling platform.

Synthesis of Monomers

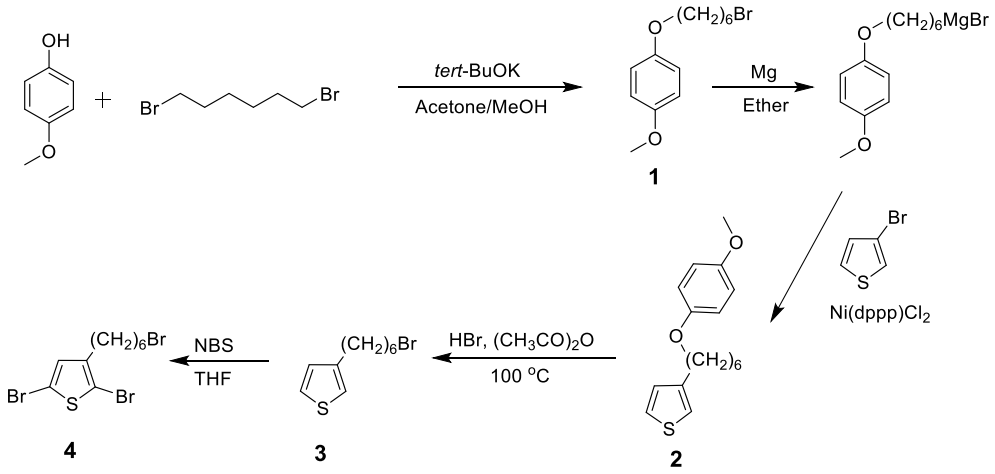

Scheme 3.2. Synthesis route of 2,5-Dibromo-3-(6-bromohexyl)thiophene.

1-(6-Bromohexyloxy)-4-methoxybenzene (1). 4-Methoxyphenol (20.0 g, 161 mmol, 1.0 equiv.) and potassium *tert*-butoxide (21.7 g, 193 mmol, 1.2 equiv.) was

dissolved in a mixture of methanol (80 mL) and acetone (80 mL) and stirred for 30 min at room temperature. The reaction mixture was then added dropwise to a solution of 1,6-dibromohexane (77.9 g, 322 mmol, 2 equiv.) in acetone (80 mL) at reflux temperature, and the reaction mixture was further heated at a reflux temperature until completion (monitored by TLC). The mixture was cooled down to room temperature and DI water was added to dissolve the salt. The product was extracted with diethyl ether and the organic layer was washed with brine and DI water. The organic layer was dried with anhydrous $MgSO_4$, filtered and solvent was under vacuum. Excess amount of 1,6-dibromohexane was removed by vacuum distillation, and the crude product was then purified by repeated recrystallized from methanol. The resulting white crystals were dried under vacuum overnight (32.6 g, 71%).

^{1}H NMR (400 MHz, $CDCl_3$): δ = 6.83 (s, 4H), 3.91 (t, J = 6.4 Hz, 2H), 3.77 (s, 3H), 3.43 (t, J = 6.7Hz, 2H), 1.89 (q, J = 7.0 Hz, 2H), 1.77 (q, J = 6.7 Hz, 2H), 1.54-1.46 (m, 4H) ppm.

3-[6-(4-Methoxyphenoxy)hexyl]thiophene (2). 1-(6-bromohexyloxy)-4-methoxybenzene (10.57 g, 36.8 mmol, 1 equiv.), dissolved in a minimum amount of anhydrous ether (50 mL) was added under inert atmosphere to a suspension of Mg turnings (0.97 g, 40 mmol, 1.3 equiv.) in anhydrous ether (10 mL). The mixture was refluxed for 6 h. The Grignard solution was cooled down to room temperature and then transferred dropwise to an ice-cooled mixture of $Ni(dppp)Cl_2$ (4 mol%) and 3-bromothiophene (5.0 g, 30.7 mmol) in dry ether (15 mL). The reaction mixture was refluxed for 15 h. After completion, the reaction mixture was hydrolyzed with a mixture of HCl (10 mL of a 1 N solution) and ice-water (20

mL), followed by extraction with several portions of ether. Drying of the combined organic phases with anhydrous $MgSO_4$, filtration and removal of the solvent under reduced pressure afforded an orange oil. The crude product was purified via recrystallization from cold hexane, and resultant off-white crystal was further purified via column using a CH_2Cl_2: hexane = 1:4 eluent mixture. Removal of the solvent gave the product as a white solid (yield 6.04 g, 67.9%).

^{1}H NMR (400 MHz, $CDCl_3$): δ = 7.23 (dd, J = 4.9 Hz and 3.0 Hz, 1H), 6.93-6.89 (m, 2H), 6.82 (s, 4H), 3.89 (t, J = 6.5 Hz, 2H), 3.75 (s, 3H), 2.63 (t, J = 7.6 Hz, 2H), 1.82-1.30 (m, 8H) ppm.

3-(6-Bromohexyl)thiophene (3). Under nitrogen atmosphere, a mixture of HBr (48%, 20.2 g, 0.12 mol) and acetic anhydride (20.2 g, 0.198 mol) was added portionwise to 3-[6-(4-Methoxyphenoxy)hexyl]thiophene (0.02 mol) and the reaction mixture was heated at 100 °C for 24 h. After dilution with DI water, the mixture was extracted several times with ether and the combined organic phases were washed with saturated $NaHCO_3$ solution. Drying of the organic phase and removal of the solvent afforded a yellow-brown oil, from which hydroquinone was precipitated by addition of hexane. The solution was then filtered and solvent was removed under reduced pressure. The product was purified via column with a CH_2Cl_2: hexane = 1:4 eluent mixture. Removal of the solvent gave the product as a colorless oil.

^{1}H NMR (400 MHz, $CDCl_3$): δ = 7.22 (dd, J = 4.8 and 2.9 Hz, 1H), 6.93-6.88 (m, 2H), 3.39 (t, J = 6.7 Hz, 2H), 2.62 (t, J = 7.7 Hz, 2H), 1.84 (q, J = 7.0 Hz, 2H), 1.62 (q, J = 7.6 Hz, 2H), 1.52-1.21 (m, 4H) ppm.

2,5-Dibromo-3-(6-bromohexyl)thiophene (4). 3-(6-Bromohexyl)thiophene (2.62 g, 10.6 mmol) was dissolved in anhydrous THF (100 mL), cooled to 0 °C and protected from light. N-Bromosuccinimide (NBS) (4.34 g, 24.4 mmol, 2.3 equiv) was added portionwise and the mixture was stirred at room temperature overnight in the absence of light. The reaction mixture was quenched by pouring it into an ice-cold solution of 1 M NaOH and the mixture was extracted several times with ether. The organic phase was dried over anhydrous $MgSO_4$ and the solvent was evaporated under reduced pressure. The residue was purified via column with a CH_2Cl_2: hexane = 1:4 eluent mixture. The pure fractions were collected and the solvent was removed under reduced pressure affording a colorless oil (3.9 g, 91%). ^1H NMR (400 MHz, $CDCl_3$): δ = 6.75 (s, 1H), 3.38 (t, J = 6.9 Hz, 2H), 2.49 (t, J = 7.7 Hz, 2H), 1.84 (q, J = 7.2 Hz, 2H), 1.54 (q, J = 7.7 Hz, 2H), 1.48-1.38 (m, 2H), 1.38-1.25 (m, 2H) ppm.

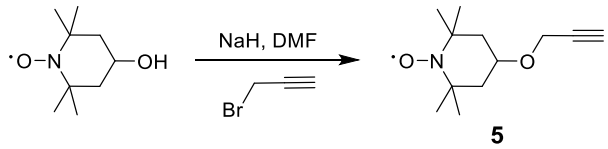

5

Scheme 3.3. Synthesis route of propargyl ether TEMPO.

Propargyl ether TEMPO (5). To a stirring suspension of NaH (60% in mineral oil, 850 mg, 22.0 mmol) in dry DMF (100 mL) 4 hydroxy-TEMPO (3.0 g, 17.44 mmol) was added portionwise at 0 °C and stirred at room temperature for 30 min. Propargyl bromide (2.0 mL, 20.0 mmol) was added dropwise at 0 °C. The resulting mixture was stirred for 3 h at room temperature Water (100 mL) was added and the solution was extracted with ethyl acetate (5 × 50 mL). The combine

organic phase was washed with water (10 × 50 mL) and dried over MgSO4, filtered, evaporated under reduced pressure and purified by column chromatography (silica gel, 10% ethyl acetate in hexane) to give the title compound as an orange solid.

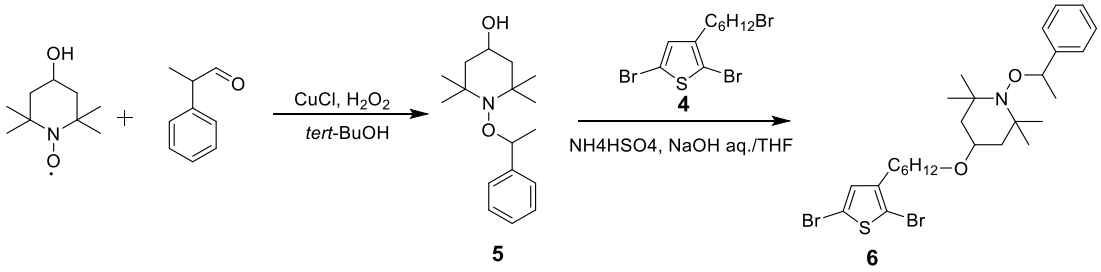

Scheme 3.4. Synthesis route of 4-(6-(2,5-dibromothiophen-3-yl)-hexyl)oxy)-TEMPO-OEtB. 4-OH-TEMPO-OEtB (6).

1-(1-Phenyl-ethoxy)-2,2,6,6-tetramethylpiperidin-4-ol (PEOT) (5). To a solution of 10.0 g (58 mmol) 4-hydroxy-TEMPO in 40 mL *tert*-butanol was added CuCl (200 mg, 3.5 mol%) and 2-phenylpropionaldehyde (16.0 g, 116 mmol). 13.0 g (116 mmol) 30% H_2O_2 was added slowly over a period of 2 h (using a water bath if necessary), after which time the mixture was stirred at room temperature overnight. After completion, the mixture was extracted with methyl *tert*-butyl ether (MTBE) three times. The combined organic layer was washed with 10% ascorbic acid solution, 1 N NaOH solution, DI water and brine. After drying with anhydrous $MgSO_4$, the excess 2-phenylpropionaldehyde was removed under vacuum to give viscous liquid. The crude product was purified by subsequent recrystallization from hexane as a white solid. The crystals were separated by filtration, dried under vacuum to give the target product.

^{1}H-NMR (400 MHz, $CDCl_3$): δ = 7.45-7.24 (*m*, 5H, Ph-H), 4.80 (*q*, 1H, C*H*ON),

3.81 (*m*, 1H); 1.88-1.50 (*m*, 4H, CH_2); 1.48 (*d*, 3H, CH_3CHON); 1.33 (*s*, 3H, CH_3); 1.27 (*s*, 3H, CH_3); 1.13 (*s*, 3H, CH_3); 0.66 (*s*, 3H, CH_3) ppm.

4-(6-(2,5-dibromothiophen-3-yl)-hexyl)oxy)-TEMPO-OEtB. 4-OH-TEMPO-OEtB (6). (1.00 g, 3.6 mmol, 1.0 equiv.), DB3BHT (2.19 g, 5.41 mmol, 1.5 equiv.), tetra-butylammonium bisulfate (0.83 mmol, 0.23 equiv.), 50% NaOH aq solution (2.88 g, 10 equiv.), THF (1 mL) was added into a Schlenk tube. The reaction mixture was stirred at 65 °C overnight. After completion, the mixture was extracted with ethyl acetate three times. The combined organic layer was washed with DI water, and was dried with anhydrous $MgSO_4$. The solvent was removed under vacuum, and the residue was purified by column chromatography (silica gel, 10% ethyl acetate in hexane) to give the title compound as an colorless viscous liquid.

EPR lineshape of the small molecule TEMPO and precursor polymer in solution state.

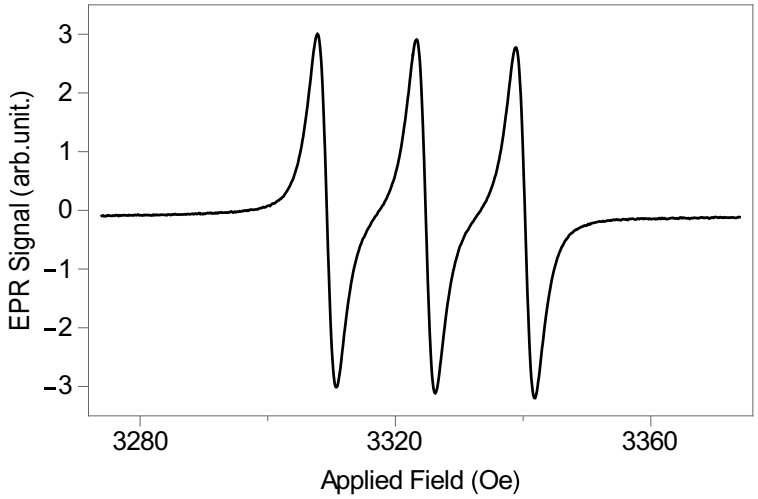

Figure 3.6. Triplet signal observed from EPR of small molecule TEMPO

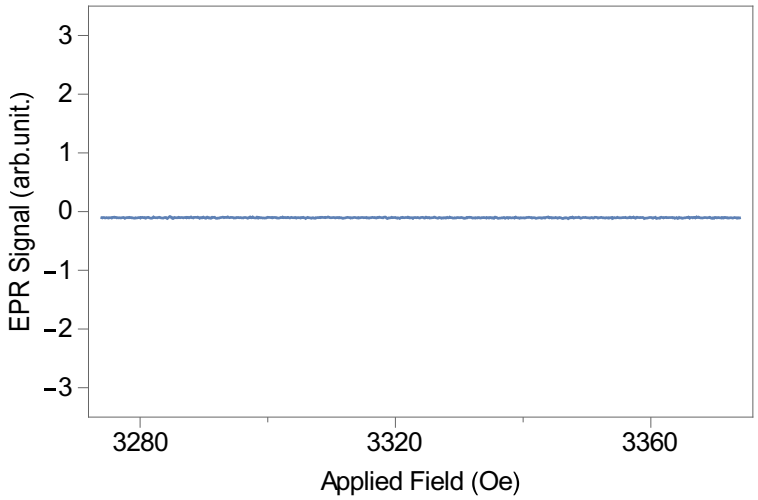

Figure 3.7. No paramagnetic resonance detected from precursor polymer

NMR spectra of precursor polymers

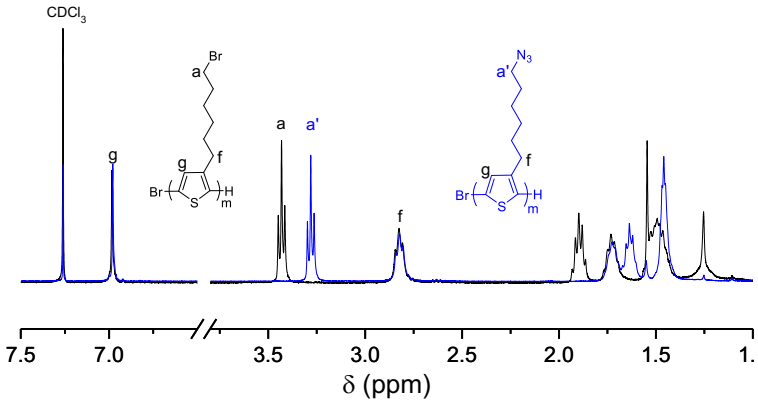

Figure 3.8. ^{1}H NMR spectra of precursor homopolymer P3BrHT and P3HT-azide. The complete conversion is indicated by the disappearance of the triplet at 3.44 ppm (Br-C$\boldsymbol{H}_2$).

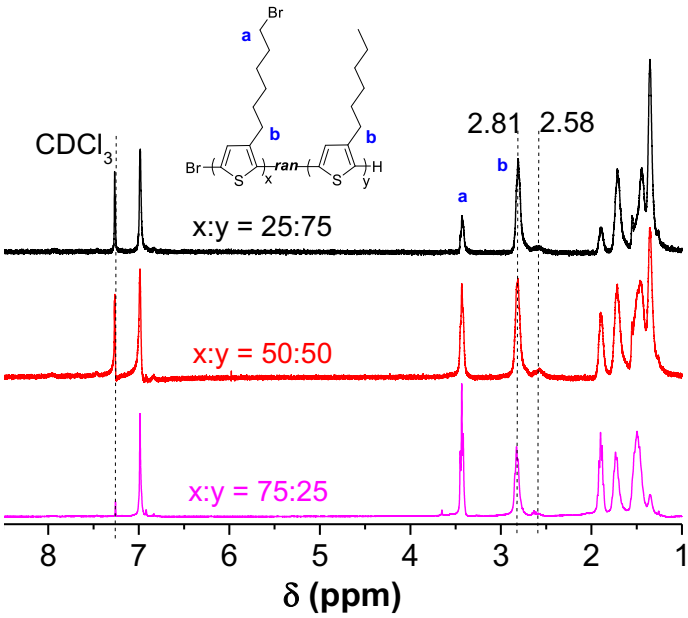

Figure 3.9. The ^{1}H NMR spectra of precursor copolymers P3HT-*ran*-P3BrHT with starting monomer ratio (3HT: 3BrHT = 25:75, 50:50, 75:25). The compositions of the precursor copolymers are determined by calculation with signal integration: 3.44 pm (Br-C$\boldsymbol{H}_2$) and 2.58, 2.81 ppm (Th-C$\boldsymbol{H}_2$). The regioregularity was determined by the ratio between 2.58 and 2.81 ppm.

Analysis of polymer thermal stability

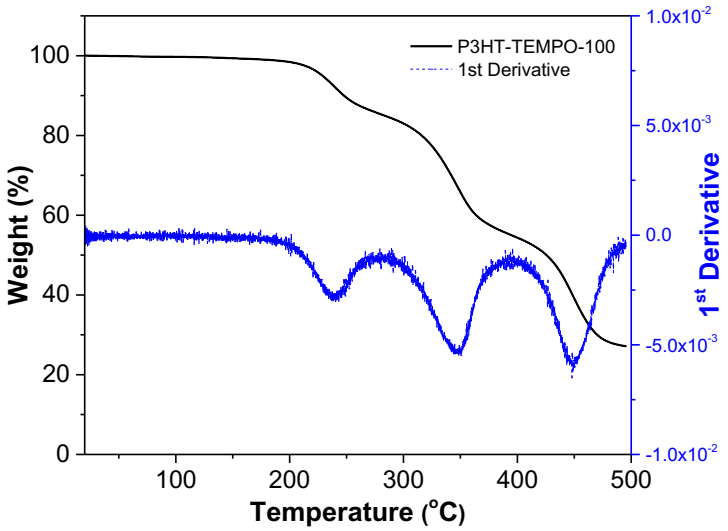

Figure 3.10. Thermal degradation of P3HT-TEMPO-100. The three weight loss stages can be assigned to the decomposition of TEMPO radical groups, triazole rings and side chains on the polythiophene backbones.

CHAPTER 4: DOPING EFFECT ON THE CONJUGATED STABLE RADICAL POLYMERS

4.1 Contributors

This chapter of work was the collaboration between the Ober group, the Fuchs group in Applied Engineering Physics at Cornell and the Lutkenhaus group at Teas A&M University (TAMU). Yiren Zhang (author) prepared all the conjugated radical polymer samples and did the doping experiments. Albert Park (a graduate student in the Fuchs group) carried out the electrical measurements on the polymer films. Shaoyang Wang (a graduate student in the Lutkenhaus group) did the electrochemical measurements of the P3HT homopolymer and P3HT-TEMPO samples.

4.2 Overview

The aim of this work is to describe both the chemical and electrochemical doping process of well-defined conjugated stable radical polymers with a regioregular polythiophene backbone and pendent TEMPO radical groups. Cyclic votammetry (CV) shows a two-step doping mechanism, in which the nitroxide radicals are oxidized to oxoammonium cations before the doping of the polythiophene backbone. In addition, chemical doping of the neutral polymer films with two dopants, iodine and 2,3,5,6-tetrafluoro-7,7,8,8-tetracyanoquinodimethane (F4-TCNQ), has been carried out and the conductivity of doped films increased by 5 orders of magnitude compared with their undoped counterparts. From the results, we can conclude that incorporation of nitroxide radicals in the conjugated polythiophene decreases their capacity compared with that of poly(3-

hexylthiophene) (P3HT), and the nitroxide radicals contribute to ~90% of their final transport capacity. The conductivity of the solid-state polymer film can be efficiently improved with iodine doping by 5 orders of magnitude. However, the sterically hindered TEMPO radicals still impede the charge transport in the doped samples, which causes an overall conductivity decreases as TEMPO content increases.

4.3 Introduction

Stable radical polymers have attracted a great deal of attention in the last two decades because of their promising application as energy storage materials for pure organic batteries and capacitors.[1] One of the most prominent aliphatic stable radical polymers is PTMA, whose electrochemical properties and cathode performance have been studied extensively. Most of the intriguing properties of PTMA come from the pendent stable nitroxide radical group on the side chains, which can undergo fast single-electron oxidation to become an oxoammonium cation or single-electron reduction to become an aminoxyl anion.[2] Since these redox reactions do not include any structural rearrangements, the electron transfer rates are usually fast and the potentials are constant through the whole process. From the perspective of electrode fabrication, this has advantages over their conjugated counterparts, which suffer from low doping capacity (less than 10% for polyacetylene) and floating oxidation potential that strongly depends on the doping level.[3] However, the great advantage of a conjugated backbone is that it has an extended π-conjugated system, which stores energy as delocalized charge carriers and facilitates the charge transport in films due to formation of conductive

pathways.[4]

Although aliphatic stable radical polymers are thought of as promising electrode materials, they still suffer from the low electrical conductivity and carbon additives must be incorporated for practical fabrication of organic batteries. Subsequently, attention has shifted to more promising materials, as conjugated polymers can provide enough electron transport as well as extra redox capability compared with inert carbon additives. In **Chapter 3**, by studying a conjugated stable radical polymer with P3HT backbone and pendent TEMPO radicals in its neutral state, we showed that steric hindrance induced by bulky TEMPO radicals can alter the crystallinity of the solid-state thin film, thus inhibiting the efficient electron transport in the neutral polymer films.[5] However, in practical energy storage systems, polymer films will experience reversible oxidation and reduction, which can potentially transform an insulating neutral radical polymer into a semi-conducting or even conducting one by p-type or n-type doping.[6] Due to the presence of two distinct oxidative potentials of the conjugated backbone and pendent radical sites, a detailed study of the charge storage and transport mechanism represents a demanding task.

An essential strategy to achieving high electrical conductivity in conjugated polymers is doping, and many methods have been developed in past decades, including electrochemical doping, chemical doping, *in-situ* doping, radiation doping and charge injection doping.[3] For conjugated polymers, the addition of dopants can efficiently generate polarons and bipolarons as charge transfer species, which provides more efficient electron transport compared with the solitons in the undoped counterparts. Numerous cases have been reported in prior literature,

including polythiophene[7–9], polypyrrole[10,11], polyaniline[12,13], polyacetylene[14,15] and poly(p-phenylene)[16]. A commonly used dopant is 2,3,5,6-tetrafluoro-7,7,8,8-tetracyanoquinodimethane (F4-TCNQ), which shows better stability in the corresponding charge transfer complex[17,18] and has been introduced to a π-conjugated oligothiophene-based liquid crystal for conductivity enhancement[19].

On the other hand, the doping concept also applies to the non-conjugated stable radical species, where a neutral stable radical can be oxidized by an electrochemical cell or an electron acceptor to become an oxoammonium cation. Few cases have been reported to date. Nishide *et al.* oxidized the PTMA homopolymer with sodium hypochlorite and found the presence of the oxoammonium can improve the macroscopic electric conductivity by two orders of magnitude.[20] Boudouris *et al.* have also reported that the conductivity of PTMA homopolymer can be improved by varying the oxidation time or addition of external small molecule oxoammonium cation as a p-type dopant.[21] Another doping strategy for nitroxide radicals is the formation of a charge transfer complex with an appropriate molecular acceptor, such as F4-TCNQ or 2,3-dichloro-5,6-dicyanobenzo-1,4-quinone (DDQ).[22] However, this approach has not yet been applied to the radical polymers.

The conjugated stable radical polymers have attracted a great deal of attention in the recent decade because the presence of two redox species and the potential application in optoelectronics and organic batteries. Traditionally, these polymers are prepared *via* either oxidative or electrochemical polymerization, which causes poor control over the polymer structure and leaves inherent doping in the final product. However, both electrical and electrochemical properties of these polymers

are sensitive to the polymer structure, aggregation state and doping state. Therefore, it is extremely important from the basic research point of view to study the effect of structure and doping state in the conjugated stable radical polymers to assure complete reproducibility of physical properties. Some early attempts were made on the doping of conjugated stable radical polymers for both solid-state conductivity and electrode performance.[23–26] However, due to the lack of structure control and processability, we cannot definitely ascribe the increase of conductivity to a specific redox component, and the doping mechanism is still unclear. Recently, the electrochemical behavior of conjugated polymers with pendent nitroxide radicals have been explored *via* well-controlled electrochemical doping as an alternative to the traditional chemical counterpart. Lutkenhaus *et al.* have synthesized polythiophenes with TEMPO radical pendent groups and varied the alkyl spacers between the radical and backbone. By careful electrochemical measurement, they found the low capacity might be ascribed to the unusual internal charge transfer between the radical and polythiophene backbone.[27,28] Jia *et al.* cyclopolymerized a TEMPO-containing 1,6-heptadiyne monomer using a Grubbs 3rd generation catalyst and studied the electrochemical properties of the resultant polymer. They found that a slow scan within a broad potential window and/or small current flow can cause continuous irreversible electrochemical oxidation of polyene backbone and intramolecular charge transfer resulting in a low Coulombic efficiency (57-80%).[29] Therefore, improving electrode performance and solid-state conductivity both require precise manipulation of doping level and detailed understanding of the correlation between the different charge transport mechanism in the conjugated stable radical polymers.

As a further step in the analysis of the effect of doping on all-conjugated stable

radical polymers, P3HT-TEMPO-X, we have conducted several electrochemical measurements on the regioregular P3HT homopolymer and P3HT-TEMPO-100 sample. Then, two dopants, iodine and F4-TCNQ, were used to oxidize the neutral polymer films. The former is an oxidizer that can oxidize both the polythiophene backbone and TEMPO radical, while the latter is a "charge-transfer dopant" that undergoes intermolecular electron transfer with the polythiophene backbone. Finally, the electrical conductivity of the doped polymer films was measured with a four-point probe technique. The effect of both electrochemical and chemical doping will be discussed based on change of capacity and conductivity.

4.4 Experimental section

4.4.1 Materials

All chemicals were purchased from Sigma-Aldrich and used as received unless otherwise noted. Anhydrous tetrahydrofuran (THF) was distilled over sodium/benzophenone mixture under nitrogen atmosphere and dried under vacuum before use. The dopant, 2,3,5,6-tetrafluoro-7,7,8,8-tetracyanoquinodimethane (F4-TCNQ), was synthesized according to literature procedures[30] and recrystallized in anhydrous dichloromethane before use.

4.4.2 Solution and solid-state doping

For solution doping, a neutral P3HT-TEMPO-X solution was prepared by dissolving the polymer in chlorobenzene, THF or dioxane to give 20 mg/mL polymer stock solutions. Then a specific amount of dopant was added into the solution and dissolved completely. The homogeneous mixture was then placed in

dark overnight and mixed thoroughly before testing.

For solid-state doping, the neutral P3HT-TEMPO-X films were prepared by drop-casting 20 mg/mL polymer solutions onto silicon substrates. For iodine doping, the P3HT-TEMPO-X films were placed in a flask with iodine chips and the polymers were doped with iodine vapor under vacuum at room temperature for 20 h. For F4-TCNQ doping, a F4-TCNQ solution (10 mg in acetonitrile) was drop-casted onto the neutral polymer films. The solvent was then slowly evaporated under ambient condition to give the doped samples.

4.4.3 Solution-state spin characterization

Solutions for EPR were prepared in THF such that they contain the equivalent of 1mM concentration of the clicked TEMPO group and the corresponding equivalent of dopant molecules. Measurements were repeated three times for each of the clicked species using independently prepared solutions. The EPR data were normalized with respect to a reference solution with the same nominal concentration of TEMPO spins. We report the average and standard error of the three measurements, which primarily originates from the inhomogeneous solution after doping and uncertainty in solution preparation. All measurements were made using a Bruker X-band EPR spectrometer at room temperature.

4.4.4 Solid-state conductivity measurements

In the case of doped P3HT-TEMPO-X, we measured the conductivity laterally using the four-wire device and setup used for the undoped samples, which is described in **Chapter 3**. Microfabricated 4-wire lateral templates with 2.5 mm length and 10 or 20 μm separation were patterned using photolithography. 100 nm

thick, gold contact electrodes were prepared by sputtering and lift-off on a thermally oxidized silicon substrate. To obtain the conductivity without contribution from parasitic contact resistance, all four electrodes were used for measurement, applying current to the outer electrodes with a Keithley 6610 precision current sourcemeter and reading voltages from the inner electrodes with a Keithley 6514 electrometer. Film thickness measured using a Tencor Alphastep profilometer. As a control sample, films of P3HT homopolymers was prepared in chlorobenzene and measured in a similar fashion using the 4-wire template. All measurements were done in a dark, vacuum-sealed and continuously pumped chamber to exclude the effect of moisture and air.

4.4.5 Electrochemical measurements of P3HT-TEMPO-X

All the electrochemical measurements were performed in a three-electrode electrochemical cell using a Gamry Interface 1000 electrochemical analyzer inside an argon-filled glovebox. A solution of 0.5 M $LiCF_3SO_3$ in ethylene carbonate (EC)/diethyl carbonate (DEC) (v:v = 3:7) was used as electrolyte. The P3HT-TEMPO-X polymers were drop-casted onto ITO substrate with a mass loading of ~0.34 mg/cm^2 to give the working electrode. Cyclic voltammetry was conducted in a voltage range of 3.0 - 4.2 V. Galvanostatic cycling experiments at different charging currents were conducted from 3.0 to 4.2 V. The charging currents were calculated based on the area of the electrodes. Open circuit potential was monitored over the course of 6 h where the electrodes were first treated by charging the electrodes using linear sweep voltammetry at 10 mV/s. The theoretical charge capacity of polymer is calculated using the following formula:

$$Theoretical\ Charge\ Capacity\ \left(\frac{mAh}{g}\right) = \frac{96500\ (n)}{3600(MWt/1000)}$$

4.5 Discussion

4.5.1 Electrochemical doping of P3HT-TEMPO-X

To have a more thorough *in-situ* study of the doping mechanism, we first carried out the cyclic votammetry (CV) of the P3HT homopolymer and P3HT-TEMPO-100 sample. The representative CV of the neutral regioregular P3HT and P3HT-TEMPO-100 at scan rate of 1 mV/s are shown in **Fig. 4.1**. The CV of regioregular P3HT recorded in 0.5 M $LiCF_3SO_3$ (in EC/DEC, v:v = 3:7) solution showed two distinct successive components at 3.3 V and 3.75 V vs. Li/Li^+, which indicates a two-step redox process occurred upon doping of P3HT.[31] First, the neutral polythiophene backbone is oxidized to generate polarons (radical cations), after which the polarons recombined to bipolarons (dications).[32] On the other hand, the CV of P3HT-TEMPO at a scan rate of 1 mV/s differs remarkably from those of the P3HT. It exhibited only one pair of redox peaks, though both regioregular P3HT backbone and TEMPO radical pendent groups can undergo redox reactions. The peak separation between the anodic and cathodic peaks for the P3HT-TEMPO indicates the irreversible reaction of doping and dedoping. The cathodic peak observed at ~ 3.5 V (vs. Li/Li^+ reference electrode, scan rate 1 mV) are owing to the nitroxide radical's faster redox kinetics and the lower redox potential compared with the polythiophene backbone.

The electrochemical cell was then subjected to galvanostatic charge/discharge testing between 3.0 and 4.2 V at charge and discharge densities of 2, 5, 10 and 20 $\mu Ah/cm^2$ (**Fig. 4.2**). The lowest potential was set to 3.0 V since it has been

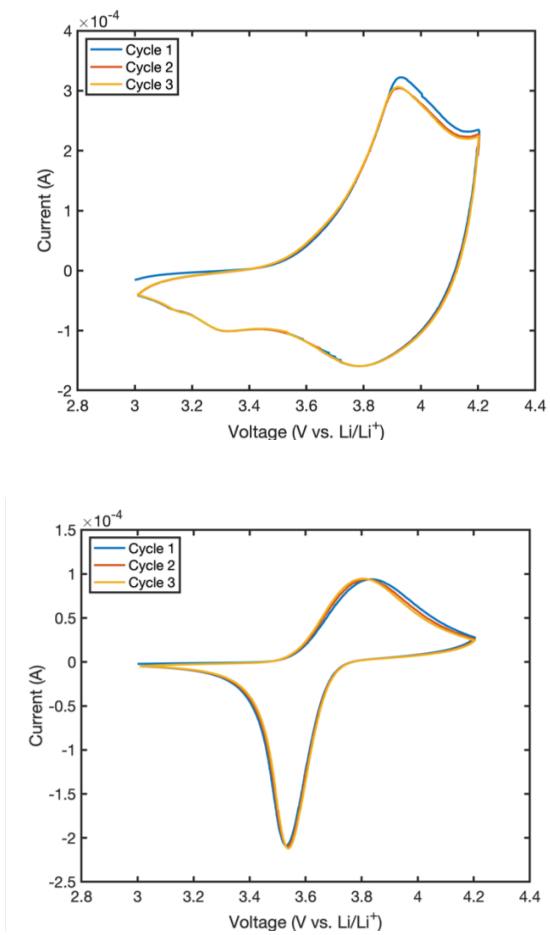

Figure 4.1. CV study of P3HT homopolymer (above) and P3HT-TEMPO-100 (below). Scan rate = 1 mV/s, A solution of 0.5 M $LiCF_3SO_3$ in ethylene carbonate (EC)/diethyl carbonate (DEC) (v:v = 3:7) as electrolyte, Li/Li^+ reference electrode.

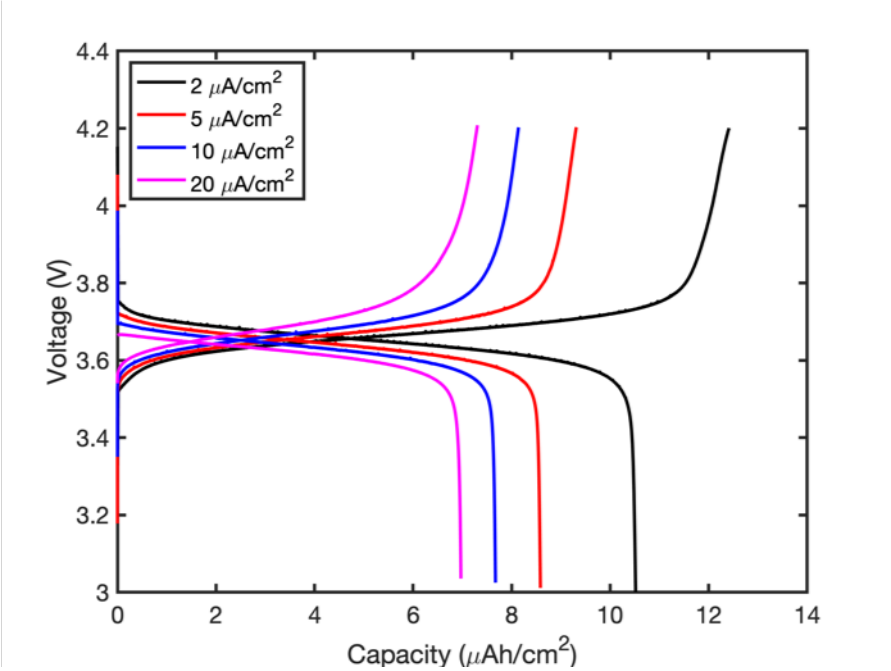

Figure 4.2. Galvanostatic charge/discharge profiles of P3HT-TEMPO-100 at different current densities from 3.0 V to 4.2 V. Three cycles at each current density.

proposed in previous report that an irreversible reduction of nitroxide radical to aminoxyl anion (N-O$^-$) can happen below 3.0 V, which can cause an unrecoverable discharge capacity.[24] At the lowest rate of 2 μA/cm^2, the areal capacity for P3HT-TEMPO-100 was calculated to be 36.5 mAh/g, which is 55.3% of the corresponding theoretical capacities (calculated to be 66.0 mAh/g assuming the redox reaction only happen on the nitroxide groups). The discharge capacity of P3HT-TEMPO-100 dropped gradually from 36.5 mAh/g to 24.3 mAh/g as current density increased from 2 to 20 μA/cm^2 (**Table 4.1**). Upon charging, a flat plateau at ~ 3.6 V appeared due to the oxidation of TEMPO radical (N-O•) to oxoammonium ($^+$N=O), which is consistent with the previous reports.[24,27] As charging proceeded, the potential increased and again plateaued at ~ 4.2 V, which can be ascribed to the oxidation of the polythiophene backbone. During the discharge process, the TEMPO radical was regenerated by reduction of oxoammonium cation. These results suggest that the incorporation of TEMPO radicals in polythiophene affect the electrochemical doping process.

In electrochemical doping, the amount of charge reversibly exchanged during redox cycles can give insights to the doping mechanism. To know the contributions of the polythiophene backbone and TEMPO radical groups to the capacity, we then carried out the galvanostatic charging to various potential cut-offs at a current density of 5 μA/cm^2. In **Fig. 4.3**, P3HT-TEMPO-100 showed a much lower capacity compared with regioregular P3HT. In P3HT-TEMPO-100, the TEMPO moiety contributed over 90% to the total capacity. This lower discharge capacity compared to the full theoretical capacity may be due to the inability for simultaneous electrochemical oxidation of the nitroxide groups

Table 4.1. Galvanostatic charge/discharge summary of P3HT-TEMPO-100 at different current densities.

Current density (μA/cm^2)	Charge (μA/cm^2)	Discharge (μA/cm^2)	Coulombic efficiency
2	12.4	10.5	84.7%
5	9.3	8.6	92.2%
10	8.1	7.7	94.2%
20	7.3	7.0	95.4%

proposed in previous report that an irreversible reduction of nitroxide radical to aminoxyl anion (N-O$^-$) can happen below 3.0 V, which can cause an unrecoverable discharge capacity.[24] At the lowest rate of 2 μA/cm^2, the areal capacity for P3HT-TEMPO-100 was calculated to be 36.5 mAh/g, which is 55.3% of the corresponding theoretical capacities (calculated to be 66.0 mAh/g assuming the redox reaction only happen on the nitroxide groups). The discharge capacity of P3HT-TEMPO-100 dropped gradually from 36.5 mAh/g to 24.3 mAh/g as current density increased from 2 to 20 μA/cm^2 (**Table 4.1**). Upon charging, a flat plateau at ~ 3.6 V appeared due to the oxidation of TEMPO radical (N-O•) to oxoammonium ($^+$N=O), which is consistent with the previous reports.[24,27] As charging proceeded, the potential increased and again plateaued at ~ 4.2 V, which can be ascribed to the oxidation of the polythiophene backbone. During the discharge process, the TEMPO radical was regenerated by reduction of oxoammonium cation. These results suggest that the incorporation of TEMPO radicals in polythiophene affect the electrochemical doping process.

In electrochemical doping, the amount of charge reversibly exchanged during redox cycles can give insights to the doping mechanism. To know the contributions of the polythiophene backbone and TEMPO radical groups to the capacity, we then carried out the galvanostatic charging to various potential cut-offs at a current density of 5 μA/cm^2. In **Fig. 4.3**, P3HT-TEMPO-100 showed a much lower capacity compared with regioregular P3HT. In P3HT-TEMPO-100, the TEMPO moiety contributed over 90% to the total capacity. This lower discharge capacity compared to the full theoretical capacity may be due to the inability for simultaneous electrochemical oxidation of the nitroxide groups

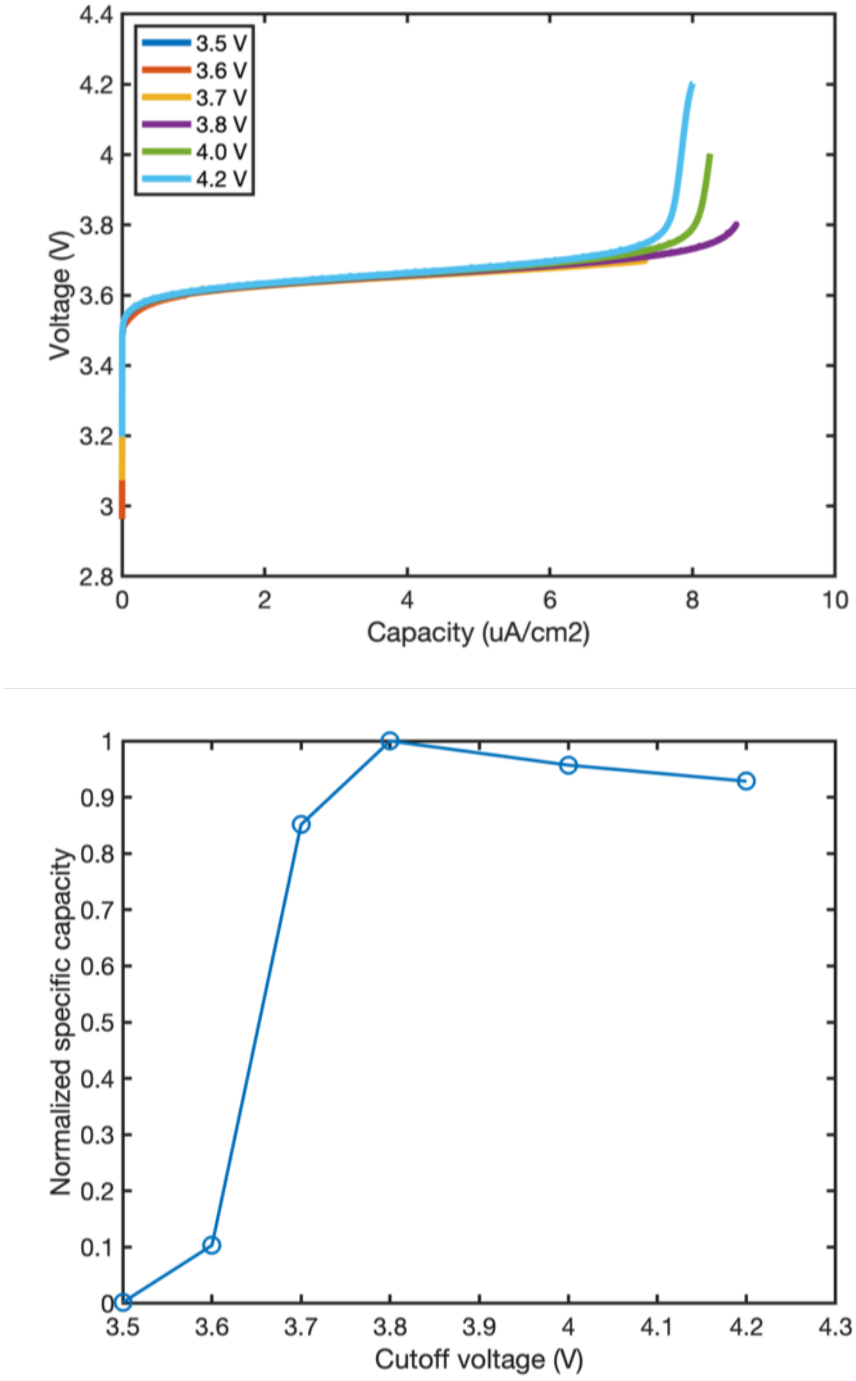

Figure 4.3. P3HT-TEMPO-100 charged to different cutoff voltages (upper) and Normalized specific capacity of the P3HT-TEMPO-100 vs. cut-off voltages (lower).

and slow counterion diffusion into the composite or combination of these.[26] It has been proposed that internal charge transfer between the conjugated polythiophene backbone and TEMPO radicals can happen during the redox process, which decrease the overall capacity of the P3HT-TEMPO.

To examine the possibility of internal charge transfer, the open circuit potential (OCP) relaxation monitoring was carried out on P3HT and P3HT-TEMPO-100 (**Fig. 4.4**). The polymers were charged to 4.2 V and then held there for 50 s. Then, the bias was removed, and the OCP was monitored over the course of 6.0 h, which provides enough time for the redox active species to interact and equilibrate. The value at which the potential equilibrates and the rate at which it arrives there indicate the nature of the internal charge transfer. The OCP relation of polymer P3HT-TEMPO showed a two-step transition consisting of a rapid voltage decay from 4.02 to 3.72 V within the first 1 h, then a gradual voltage dropped to around 3.69 V in the next 2 h, and finally a stabilization at around 3.67 V at the end of 6 h. To compare, the P3HT homopolymer only showed a gradual voltage drop starting from 4.2 V, and finally stabilized at around 3.93 V at the end of 6 h. The different OCP results suggest that the internal electron transfer exists in the doping and dedoping of nitroxide radical-containing polythiophenes.

4.5.2 Chemical doping of PTMA

Knowing that there exist two redox sites in the neutral P3HT-TEMPO-X polymer, it would be a necessity to know if a specific chemical dopant will react on only one or both the polythiophene backbone and the TEMPO radical pendent groups. First, we tested if the iodine can oxidize the TEMPO stable radicals on an inert polymer backbone in solution. While many studies have used these dopants

for the conjugated polythiophenes and postulated the structure-property relationships, few attempts have been made on the chemical doping of aliphatic radical polymers. To this end, PTMA was used as a model polymer since the poly(methacrylate) backbone cannot be oxidized by iodine. PTMA was first dissolved in THF to give 1 mM of stable radical species in solution, then an excess amount (5.0 equiv.) of iodine and F4-TCNQ was added, respectively. Solution EPR showed that the PTMA/iodine mixture had radical yield of 31%, which is much lower than the original radical yield of 80% in the parent PTMA. On the other hand, the TEMPO radicals in PTMA were not oxidized by F4-TCNQ, as indicated by the similar high radical yield in the mixture (88%). The different behaviors of PTMA towards iodine and F4-TCNQ can be explained by the charge transfer mechanism of the single electron to the different donors. Iodine simply acts as an oxidizer, which oxidizes the TEMPO radical to the corresponding oxoammonium cation, thus decreasing the total yield in the doped PTMA. However, the charge transfer between F4-TCNQ and TEMPO radical requires the close proximity between each other, such as in 1:1 cocrystals. In the solution state, a low concentration and larger distance exclude the possibility of efficient charge transfer, thus preventing the PTMA from being doped.

4.5.3 Conductivity of the doped P3HT-TEMPO-X

To know the effect of the doping in the conjugated stable radical polymers, we doped the P3HT-TEMPO-X films with iodine and F4-TCNQ, respectively. For iodine, the polymer films were prepared by drop-casting, followed by doping with iodine vapor under vacuum for 20 hours. For F4-TCNQ, a solution doping method was used by drop-casting F4-TCNQ solution onto the neutral P3HT-TEMPO-X

for the conjugated polythiophenes and postulated the structure-property relationships, few attempts have been made on the chemical doping of aliphatic radical polymers. To this end, PTMA was used as a model polymer since the poly(methacrylate) backbone cannot be oxidized by iodine. PTMA was first dissolved in THF to give 1 mM of stable radical species in solution, then excess amount (5.0 equiv.) of iodine and F4-TCNQ was added, respectively. Solution EPR showed that the PTMA/iodine mixture had radical yield of 31%, which is much lower than the original radical yield of 80% in the parent PTMA. On the other hand, the TEMPO radicals in PTMA were not oxidized by F4-TCNQ, as indicated by the similar high radical yield in the mixture (88%). The different behaviors of PTMA towards iodine and F4-TCNQ can be explained by the charge transfer mechanism of the single electron to the different donors. Iodine simply acts as an oxidizer, which oxidizes the TEMPO radical to the corresponding oxoammonium cation, thus decreasing the total yield in the doped PTMA. However, the charge transfer between F4-TCNQ and TEMPO radical requires the close proximity between each other, such as in 1:1 cocrystals. In the solution state, a low concentration and larger distance exclude the possibility of efficient charge transfer, thus preventing the PTMA from being doped.

4.5.3 Conductivity of the doped P3HT-TEMPO-X

To know the effect of the doping in the conjugated stable radical polymers, we doped the P3HT-TEMPO-X films with iodine and F4-TCNQ, respectively. For iodine, the polymer films were prepared by drop-casting, followed by doping with iodine vapor under vacuum for 20 hours. For F4-TCNQ, a solution doping method was used by drop-casting F4-TCNQ solution onto the neutral P3HT-TEMPO-X

films. The conductivity of the doped and undoped sample are shown in **Fig 4.5**. Iodine vapor acts as an efficient chemical dopant for polythiophene, since the conductivity of all the doped samples are enhanced by 3-5 orders of magnitude. The conductivity of doped P3HT homopolymer control sample show conductivity of ~20 S/cm, which is consistent with the previous reports. However, the existence of bulky TEMPO radical groups still decreases the overall conductivity in doped films, as indicated by the values of P3HT-TEMPO-X (X = 0, 25, 50%) This means the major contribution of electron transport in doped films comes from the oxidation-generated polarons or bipolarons, while the TEMPO redox couple remains silent. For F4-TCNQ, conductivity was slightly improved upon doping, while the value is much lower compared to its iodine-doped counterparts. We speculate the reason is because the doping using F4-TCNQ requires the insertion of molecular dopants between the polythiophene chains to form charge-transfer complex. While in the solution doping process, the diffusion of dopant through thick drop-casted polymer film and structural rearrangements are more difficult compared with the iodine doping. To improve the results, vapor-phase F4-TCNQ doping using spin-coated thin film polymer sample might be a potential method.

4.6 Conclusions

In this work, both chemical and electrochemical doping have been carried out on the conjugated stable radical polymers, P3HT-TEMPO-X. The electrochemical properties of P3HT and P3HT-TEMPO-100 have been investigated by cyclic voltammetry, and the results suggest that the doping of the redox process of P3HT-TEMPO-X is dominated by the nitroxide radicals due to their faster redox kinetics and lower oxidative potential compared with the polythiophene backbone.

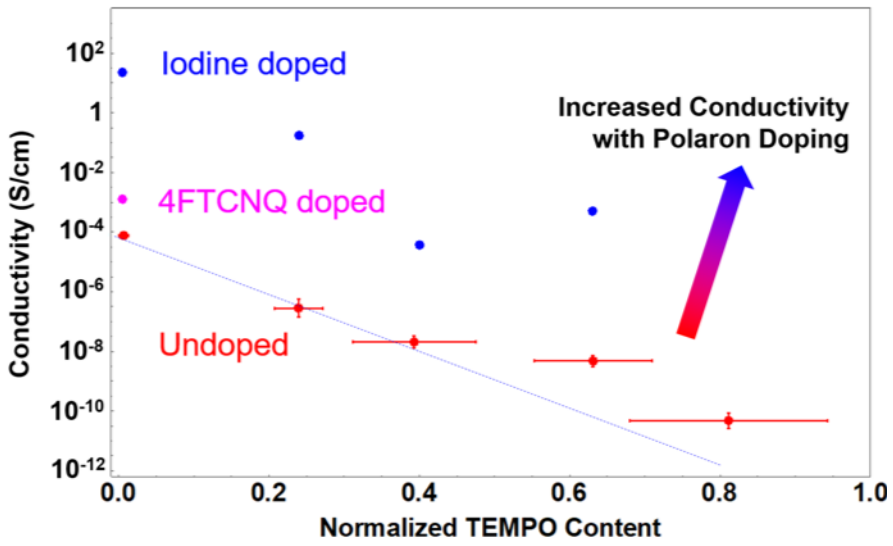

Figure 4.5. Electrical conductivity of undoped P3HT-TEMPO-X films, films doped with iodine and films doped with F4-TCNQ.

However, the P3HT-TEMPO-100 sample showed much lower capacity compared with the unsubstituted P3HT, which can be ascribed to the potential internal charge transfer between the nitroxide radical group and the polythiophene backbone. We have also tried chemical doping with iodine and F4-TCNQ and observed an increase of electrical conductivity up to 5 orders of magnitude in the iodine-vapor doped P3HT and P3HT-TEMPO-X films. However, the presence of more bulky TEMPO radical groups did not contribute to the overall conductivity upon doping, since the conductivity still decrease with the TEMPO radical after deep doping. At this time, we have insufficient information about the *in-situ* interactions between dopants and neutral polymer films, and the current improvement we are working on is using *in-situ* doping together with conductivity measurements to study the doping process more carefully. Also, W-band measurements will be used to distinguish the different charge carriers in the doped P3HT-TEMPO-X.

4.7 Acknowledgements

This work was supported the Department of Energy Office of Basic Energy Science (Grant DE-SC0014336). We acknowledge use of the facilities of the Cornell NanoScale Facility, a member of the National Nanotechnology Coordinated Infrastructure (NNCI), supported by the National Science Foundation (NSF) (Grant ECCS-1542081). We also acknowledge the use of shared facilities of the Cornell Center for Materials Research which is supported through the NSF MRSEC program (Grant DMR-1719875) and the shared facilities of the National Biomedical Center for Advanced Electron Spin Resonance Technology, which is supported by the National Institute of General Medical Sciences, a part of the National Institutes of Health (Grant P41GM103521).

4.8 References

1 T. Janoschka, A. Teichler, A. Krieg, M. D. Hager and U. S. Schubert, *Journal of Polymer Science Part A: Polymer Chemistry*, 2012, **50**, 1394–1407.

2 E. P. Tomlinson, M. E. Hay and B. W. Boudouris, *Macromolecules*, 2014, **47**, 6145–6158.

3 P. Kar, *Doping in Conjugated Polymers: Kar/Doping*, John Wiley & Sons, Inc., Hoboken, NJ, USA, 2013.

4 L. W. Shacklette, M. Maxfield, S. Gould, J. F. Wolf, T. R. Jow and R. H. Baughman, *Synthetic Metals*, 1987, **18**, 611–618.

5 Y. Zhang, A. M. Park, S. R. McMillan, N. J. Harmon, M. E. Flatté, G. D. Fuchs and C. K. Ober, *Chemistry of Materials*, 2018, **30**, 4799–4807.

6 H. Shirakawa, E. J. Louis, A. G. MacDiarmid, C. K. Chiang and A. J. Heeger, *Journal of the Chemical Society, Chemical Communications*, 1977, 578.

7 K. Kaneto, S. Hayashi, S. Ura and K. Yoshino, *Journal of the Physical Society of Japan*, 1985, **54**, 1146–1153.

8 T. Johansson, W. Mammo, M. Svensson, M. R. Andersson and O. Inganäs, *J. Mater. Chem.*, 2003, **13**, 1316–1323.

9 A. M. Glaudell, J. E. Cochran, S. N. Patel and M. L. Chabinyc, *Advanced Energy Materials*, 2015, **5**, 1401072.

10 R. S. Hutchins and L. G. Bachas, *Analytical Chemistry*, 1995, **67**, 1654–1660.

11 A. M. Waller and R. G. Compton, *Journal of the Chemical Society, Faraday Transactions 1: Physical Chemistry in Condensed Phases*, 1989, **85**, 977.

12 D. W. Hatchett, M. Josowicz and J. Janata, *The Journal of Physical Chemistry B*, 1999, **103**, 10992–10998.

13 O. P. Dimitriev, *Macromolecules*, 2004, **37**, 3388–3395.

14 C. K. Chiang, C. R. Fincher, Y. W. Park, A. J. Heeger, H. Shirakawa, E. J. Louis, S. C. Gau and A. G. MacDiarmid, *Physical Review Letters*, 1977, **39**, 1098–1101.

15 D. MacInnes, M. A. Druy, P. J. Nigrey, D. P. Nairns, A. G. MacDiarmid and A. J. Heeger, *Journal of the Chemical Society, Chemical Communications*, 1981, 317.

16 D. M. Ivory, G. G. Miller, J. M. Sowa, L. W. Shacklette, R. R. Chance and R. H. Baughman, *The Journal of Chemical Physics*, 1979, **71**, 1506–1507.

17 J. Hynynen, D. Kiefer, L. Yu, R. Kroon, R. Munir, A. Amassian, M. Kemerink and C. Müller, *Macromolecules*, 2017, **50**, 8140–8148.

18 K. E. Watts, B. Neelamraju, E. L. Ratcliff and J. E. Pemberton, *Chemistry of Materials*, , DOI:10.1021/acs.chemmater.9b01549.

19 B. X. Dong, Z. Liu, M. Misra, J. Strzalka, J. Niklas, O. G. Poluektov, F. A. Escobedo, C. K. Ober, P. F. Nealey and S. N. Patel, *ACS Nano*, 2019, **13**, 7665–7675.

20 T. Suga, S. Takeuchi, T. Ozaki, M. Sakata, K. Oyaizu and H. Nishide, *Chemistry Letters*, 2009, **38**, 1160–1161.

21 L. Rostro, S. H. Wong and B. W. Boudouris, *Macromolecules*, 2014, **47**, 3713–3719.

22 S. Nakatsuji, A. Takai, K. Nishikawa, Y. Morimoto, N. Yasuoka, K. Suzuki, T. Enoki and H. Anzai, *Journal of Materials Chemistry*, 1999, **9**, 1747–1754.

23 M. Tanaka, K. Hatta, T. Edura, K. Tsutsui, Y. Wada and H. Nishide, *Polymers for Advanced Technologies*, 2007, **18**, 925–931.

24 M. Aydın, B. Esat, Ç. Kılıç, M. E. Köse, A. Ata and F. Yılmaz, *European*

Polymer Journal, 2011, **47**, 2283–2294.

25 T. K. Kunz and M. O. Wolf, *Polymer Chemistry*, 2011, **2**, 640–644.

26 M. Aydin and B. Esat, *Journal of Solid State Electrochemistry*, 2015, **19**, 2275–2281.

27 F. Li, D. N. Gore, S. Wang and J. L. Lutkenhaus, *Angewandte Chemie International Edition*, 2017, **56**, 9856–9859.

28 F. Li, Y. Zhang, S. R. Kwon and J. L. Lutkenhaus, *ACS Macro Letters*, 2016, **5**, 337–341.

29 Y. Xie, K. Zhang, M. J. Monteiro and Z. Jia, *ACS Applied Materials & Interfaces*, 2019, **11**, 7096–7103.

30 R. C. Wheland and E. L. Martin, *The Journal of Organic Chemistry*, 1975, **40**, 3101–3109.

31 M. Trznadel, M. Zagórska, M. Lapkowski, G. Louarn, S. Lefrant and A. Pron, *J. Chem. Soc., Faraday Trans.*, 1996, **92**, 1387–1393.

32 M. Trznadel, A. Pron and M. Zagorska, *Synthetic Metals*, 1999, **101**, 118–119.

CHAPTER 5: SYNTHESIS AND CHARACTERIZATION OF DIBLOCK ROD-COIL STABLE RADICAL POLYMERS

5.1 Contributors

In this chapter, Yiren Zhang (author) synthesized and characterized all the polymer samples, including poly(3-hexylthiophene) (P3HT) macroinitiators, polymer segments for click reactions and the final diblock rod-coil copolymers. Zhubing Han (a former graduate student in Ober group) and Carson Britt (REU student in 2016 summer) contributed tremendously in the synthesis and purification of P3HT-BiBB macroinitiators.

5.2 Overview

The purpose of this work is to provide well-defined P3HT-*b*-PTMA rod-coil block copolymer systems that can form self-assembled structures, which can be used for the study of cathode performance and solid-state electronic transport. To have a more accurate quantification of their electronic and electrochemical properties, it is necessary to obtain reproducible block copolymers with predictable molecular weights and narrow molecular weight distributions. To this end, two different synthesis methods, "grafting from" and "grafting to", have been developed for the preparation of P3HT-*b*-PTMA samples. The "grafting from" method uses a P3HT-BiBB macroinitiator, and the PTMA block was attached *via* ATRP of precursor monomer and subsequent chemical oxidation. However, further characterization of the synthesized copolymers revealed the uncontrolled growth of coil block from the macroinitiator as well as the inevitable oxidation of

with pendent stable radicals, as many electrochemists expected. However, the simple introduction of TEMPO nitroxide radicals onto the side chains of polythiophene (P3HT-TEMPO) does not result in a straightforward improvement in performance. In **Chapter 3**, we have observed that the introduction of sterically hindered TEMPO radical groups in P3HT will affect the π-π interactions between the semicrystalline chains, thus impeding both intramolecular and intermolecular electron transport process and decrease the macroscopic conductivity.[10] Also, due to the poor solubility of the neutral P3HT-TEMPO polymers, the molecular weight needs to be low for electrode fabrication, which caused the solubilization of the oxidized samples to the electrolyte during cycling. Very recently, unusual internal charge transfer between the conjugated backbone and TEMPO radicals have been observed in the single-component conjugated radical polymers (P3HT-TEMPO), which can impair the overall capacity of the polymer electrodes.[11] In this situation, we need to rethink if there is a better architecture we can adopt for the P3HT and TEMPO system to address the abovementioned drawbacks in P3HT-TEMPO.

Although polythiophene and TEMPO nitroxide radical both have redox capability, their behaviors in electrode films differ. Considering electron transport, the major conductive characteristics of polythiophenes are dominated by interchain hopping between π-conjugated backbones, whereas the electron hopping between adjacent TEMPO radicals is negligible.[10] Considering charge storage, the TEMPO radical has lower oxidative potential and faster redox capability, and it is responsible for ~ 90% of the charge storage when covalently attached to the polythiophene backbones.[11] In this context, a rod-coil block copolymer architecture with self-assembly capability consisting of a conjugated polymer block and a stable radical polymer block with the aim to self-organize them into a

with pendent stable radicals, as many electrochemists expected. However, the simple introduction of TEMPO nitroxide radicals onto the side chains of polythiophene (P3HT-TEMPO) does not result in a straightforward improvement in performance. In **Chapter 3**, we have observed that the introduction of sterically hindered TEMPO radical groups in P3HT will affect the π-π interactions between the semicrystalline chains, thus impeding both intramolecular and intermolecular electron transport process and decrease the macroscopic conductivity.[10] Also, due to the poor solubility of the neutral P3HT-TEMPO polymers, the molecular weight needs to be low for electrode fabrication, which caused the solubilization of the oxidized samples to the electrolyte during cycling. Very recently, unusual internal charge transfer between the conjugated backbone and TEMPO radicals have been observed in the single-component conjugated radical polymers (P3HT-TEMPO), which can impair the overall capacity of the polymer electrodes.[11] In this situation, we need to rethink if there is a better architecture we can adopt for the P3HT and TEMPO system to address the abovementioned drawbacks in P3HT-TEMPO.

Although polythiophene and TEMPO nitroxide radical both have the redox capability, their behaviors in electrode films differ. Considering electron transport, the major conductive characteristics of polythiophenes are dominated by interchain hopping between π-conjugated backbones, whereas the electron hopping between adjacent TEMPO radicals is negligible.[10] Considering charge storage, the TEMPO radicals has lower oxidative potential and faster redox capability, and they are responsible for ~ 90% of the charge storage when covalently attached to the polythiophene backbones.[11] In this context, a rod-coil block copolymer architecture with self-assembly capability consisting of a conjugated polymer block and a stable radical polymer block with the aim to self-organize them into a

lamellar structures may be a possible solution for the disadvantages such as low conductivity due to low crystallinity of all-conjugated radical polymer, and low capacity due to the unwanted internal charge transfer. At the molecular scale, macroscopic electron transport is favored by the electron hopping through the well-packed conjugated phase, while the hopping between the adjacent TEMPO radical, the charge storage sites, is negligible. One advantage of the P3HT-containing copolymers is the ability to form lamellar structure with length about 10-20 nm, which is close to the typical exciton diffusion length.[12,13] In a highly ordered nanostructure from the block copolymers, charges may cross the boundaries between highly conductive crystalline conjugated phase and poorly conductive amorphous phase of stable radicals.[14] By rational control of the two-phase system, we can also explore the effect of microstructure and orientation on the electronic and electrochemical behavior of these block copolymers.

Among a variety of conjugated polymers, regioregular head-to-tail (HT) coupled P3HT is one of the most important representative π-conjugated polymers owing to its excellent characteristics including high charge carrier mobility, solution processability, and synthetic versatility. The synthetic approach can be divided into two categories: i) polymerization using P3HT macroinitiator (the "grafting from" method), and ii) coupling of two separate rod and coil blocks (the "grafting to" method).[15] So far, many P3HT-containing block copolymers have been synthesized based on Grignard metathesis (GRIM) polymerization incorporated with anionic polymerization,[16–18] living radical polymerization[19–23], ring-opening polymerization[24,25], and click reaction[26–29]. Although these conjugated rod-coil block copolymers have been extensively investigated, it is still

challenging to find the appropriate synthetic approach for copolymers with well-defined structures, as well as to understand their self-assembly behaviors in both solution and solid-state films.[15] Because of the additional structural control factor and functionality provided by the π-π interaction between the conjugated segments, the microphase separation of rod-coil block copolymers can give interesting morphologies, such as lamellar, spherical, cylindrical, vesicular structures, which differ from the phase separation of the well-studied conventional coil-coil block copolymers.[30–35]

In this study, we demonstrate the facile synthesis of the diblock copolymers containing a regioregular P3HT segment and a stable radical polymer, PTMA. The regioregular polythiophene segments are prepared by the nickel-catalyzed GRIM polymerization reported by McCullough, followed by quenching using various conditions to give different end-capping groups. These P3HT blocks were then functionalized with various moieties and employed in synthesizing well-defined P3HT-*b*-PTMA using both "grafting from" and "grafting to" methods.

5.4 Experimental Section

5.4.1 Materials

2,5-dibromo-3-hexylthiophene (DB3HT) was purchased from Ark Pharm. Ethynylmagnesium chloride solution (0.5 M in THF), *t*-butylmagnesium chloride solution (1.0 M in THF), 1,3-bis(diphenylphosphino)propane nickel(II) chloride [Ni(dppp)Cl_2], CuI were purchased from Sigma Aldrich. Tris(2-dimethylaminoethyl)amine (Me_6TREN, 99+%) was purchased from Alfa Aesar.

2,5-Dibromo-3-hexylthiophene was purchased from Ark. Pharm. Inc. Bare copper wire (gauge #26, diameter = 0.4050 mm) was purchase from Arcor Electronics and used without any chemical treatment. Anhydrous THF was distilled from sodium/benzophenone mixture prior to synthesis of monomer and polymerizations. The synthesis of PMPEOT and oxidation of PTMPM-azide using $Na_2WO_4/Na_2EDTA/H_2O_2$ have been described in **Chapter 2**. Preparation of the P3HT-BiBB macroinitiator followed the four-step procedure reported in McCullough's report.[21] The azide-substituted initiator for ATRP and SET-LRP, 3-azidopropyl 2-bromoisobutyrate, was synthesized following the reported procedures.[36]

5.4.2 Characterization

^{1}H-NMR studies of the synthesized monomers and polymers were performed in $CDCl_3$ using a Varian INOVA 400 (^{1}H, 400 MHz) spectrometer. Molecular weights (M_n) and dispersities (Đ) of the polymers were determined by gel permeation chromatography (GPC). The GPC was performed on Waters Ambient Temperature GPC equipped with a Waters 410 differential refractive index detector. GPC columns were eluted at 1.0 mL/min with tetrahydrofuran (THF) at 40 °C. Polymer thin films were characterized by Asylum MFP-3D atomic force microscope (AFM) using the tapping mode (AC mode) and silicon cantilevers (model: ACCESS-NC).

5.4.3 Synthesis of P3HT-alkyne

The P3HT-alkyne was synthesized following a modified procedure. In a 100 mL round-bottom flask purged with nitrogen, 2,5-dibromo-3-hexylthiophene (3.03

g, 9.3 mmol, 1.0 equiv.) was dissolved in 20 mL of anhydrous THF. Then 9.3 mL of *t*-butylmagnesium chloride solution (1.0 M in THF, 1.0 equiv.) was added to the solution, and the mixture was stirred at 25 °C for 20 h. Then 78.6 mg of Ni(dppp)Cl_2 ([M]:[Ni] = 56:1, 166 μmol) was added in one portion to start the polymerization. After stirring for 20 min, the ethynylmagnesium chloride (1.33 mmol, 8 equiv. to Ni, 2.66 mL) was added, and mixture was further stirred at room temperature for 30 min. The P3HT-alkyne was recovered by precipitation in cold methanol, and repeated washing with methanol and hexane. The purified polymer was dried overnight under vacuum at room temperature and stored at -20 °C under nitrogen to avoid homocoupling.

5.4.4 Synthesis of PTMPM-azide via ATRP

TMPM (7.89 g, 35.00 mmol, 70.0 equiv.) was placed in a 100 mL Schlenk flask with a magnetic stir bar. Then 3-azidopropyl 2-bromoisobutyrate (0.5 mmol, 1.0 equiv.) and PMDETA (208.8 μL, 1.00 mmol, 2.0 equiv.) in 16 mL of anhydrous toluene was added. The flask was subjected to three freeze-pump-thaw cycles, and the mixture was transferred to a Schlenk flask with CuBr (35.86 mg, 0.25 mmol, 0.5 equiv.) using cannula transfer under nitrogen. The mixture was stirred thoroughly to dissolve the CuBr and reacted at 70 °C for 4 h. The polymerization was terminated by cooling to room temperature and exposure to air. The mixture was diluted with a small portion of DCM and filtered through a short neutral Al_2O_3 column to remove the copper catalyst. The filtrate was concentrated under vacuum, and PTMPM-azide was recovered by precipitation in cold hexane. The polymer was collected by filtration and dried overnight under vacuum at 40 °C.

5.4.5 Oxidation of P3HT-*b*-PTMPM by *m*CPBA

P3HT-*b*-PTMPM (200 mg) was dissolved in 10 mL of DCM in a 50 mL round bottom flask, and the mixture was cooled to 0 °C. Then, *m*CPBA (2 equiv. to the amine group) in 5 mL DCM was added dropwise into the polymer solution upon vigorous stirring at 0 °C. After complete addition, the mixture was warmed up to room temperature and further stirred for 3 hours. The crude polymer was recovered by precipitation in cold methanol, filtration and repeated washing by methanol and hexane. The resultant polymer was dried overnight under vacuum at room temperature.

5.4.6 Typical procedure for the synthesis of PTMPM-azide via SET-LRP

A 25 mL Schlenk tube was charged with 1.00 g (4.44 mmol) of TMPM and purged under nitrogen for 30 min. Then 2 mg (8.96 μmol) $CuBr_2$ and 42.5 μL of Me_6TREN were dissolved together in isopropanol (2.5 mL) and purged under nitrogen for 20 min before being added to the monomer. Finally, 26.3 μL (0.1776 mmol) EBiB was added to the mixture via a syringe, and a magnetic stir bar wrapped with copper wire (5 cm) was anchored next to the side arm using a magnet. The mixture was further purged through three freeze-pump-thaw cycles, and then warmed to room temperature. The magnetic stir bar wrapped with copper wire was then dropped in to start the polymerization. The mixture was then stirred at 25 °C for 70 min, then cooled with liquid nitrogen and exposed to air to terminate the reaction. The solvent was removed under vacuum, and the crude PTMPM was used directly for analysis and subsequent oxidation.

well-characterized, and two critical questions arose based on the documented experimental results: i) How can we carry out controlled ATRP reaction from P3HT-BiBB macroinitiator using TMPM as the precursor monomer? Although GPC traces of the copolymers showed an increasing trend in total M_n compared with the P3HT macroinitiator, the Đ values are mostly between 1.7 - 1.9, indicating the poor homogeneity of the block copolymers.[37] Also, the secondary amine group of the monomer, TMPM, can interfere with the chelation process of ATRP catalyst, which makes the polymerization inefficient. Due to the lower initiation efficiency of P3HT macroinitiator, these abovementioned factors make the "grafting from" a challenging method. ii) Will the oxidative generation of TEMPO radicals interfere with the conjugated P3HT segment, considering its capability of being p-doped by some oxidizers? In Fan's thesis, quantitative EPR analysis results of the P3HT-*b*-PTMA, which are the essential criteria for confirmation of the stable radical contents in the final diblock polymers, are missing.[37] As a result, it is necessary to have a more thorough study of this synthesis route.

We prepared the diblock copolymer by first synthesizing P3HT-BiBB macroinitiator, following the method described previously by McCullough *et al.* (**Scheme 5.1**).[19,21] Vinyl terminated regioregular P3HT was prepared by GRIM polymerization and subsequent *in situ* end group functionalization with vinylmagnesium bromide. A mixture of hydrochloric acid/methanol mixture was used to quench the reaction to avoid the disproportionation and resultant homocoupling of P3HT blocks. Then, the vinyl end group was converted to the hydroxy group *via* hydroboration-oxidation, which was first reacted with BiBB to

well-characterized, and two critical questions arose based on the documented experimental results: i) How can we carry out controlled ATRP reaction from P3HT-BiBB macroinitiator using TMPM as the precursor monomer? Although GPC traces of the copolymers showed an increasing trend in total M_n compared with the P3HT macroinitiator, the Đ values are mostly between 1.7 - 1.9, indicating the poor homogeneity of the block copolymers.[37] Also, the secondary amine group of the monomer, TMPM, can interfere with the chelation process of ATRP catalyst, which makes the polymerization inefficient. Due to the lower initiation efficiency of P3HT macroinitiator, these abovementioned factors make the "grafting from" a challenging method. ii) Will the oxidative generation of TEMPO radicals interfere with the conjugated P3HT segment, considering its capability of being p-doped by some oxidizers? In Fan's thesis, quantitative EPR analysis results of the P3HT-*b*-PTMA, which are the essential criteria for confirmation of the stable radical contents in the final diblock polymers, are missing.[37] As a result, it is necessary to have a more thorough study of this synthesis route.

We synthesize the diblock copolymer by first synthesizing P3HT-BiBB macroinitiator, following the method described previously by McCullough *et al.* (**Scheme 5.1**).[19,21] Vinyl terminated regioregular P3HT was prepared by GRIM polymerization and subsequent *in situ* end group functionalization with vinylmagnesium bromide. A mixture of hydrochloric acid/methanol mixture was used to quench the reaction to avoid the disproportionation and resultant homocoupling of P3HT blocks. Then, the vinyl end group was converted to the hydroxy group *via* hydroboration-oxidation, which was first reacted with BiBB to

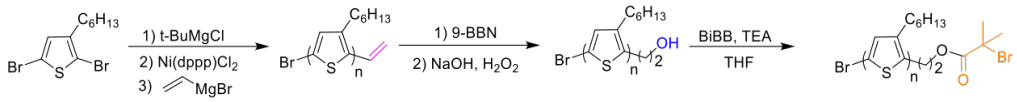

Scheme 5.1. Synthesis route of bromoester terminated macroinitiator P3HT-BiBB.

have the bromoester terminated P3HT macroinitiator. The NMR of the precursor chain-end functionalized P3HT provided evidence of the successful conversion of the end groups.

With the P3HT-BiBB macroinitiator, we attempted to grow the second block of PTMPM and PMPEOT using ATRP. **(Scheme 5.2)** According to the reported recipe, 100 equivalents of monomer were added due to the inefficient initiation from P3HT macroinitiator. GPC trace (**Fig. 5.1**) shows evidence of a chain growth of PTMPM second block initiated by P3HT macroinitiator. However, a major peak with an average elution time appears at the same location as for the P3HT macroinitiator, suggesting the inefficient initiation from P3HT chain end. This unreacted P3HT peak in GPC traces appeared in all our synthesized copolymer samples and have also been reported in many previous reports of P3HT-containing copolymer synthesis using the "grafting from" method. Although the unreacted P3HT can be removed by the solvent extraction method, the "grafting from" method still suffers from the low yield and poor control over the coil ratio due to the necessary long reaction time.

5.5.2 Compatibility of P3HT block with the oxidizing conditions

In an ideal case, we hope the oxidative treatment of our diblock precursor copolymer, P3HT-*b*-PTMPM, can work exclusively on the PTMPM block, while the P3HT block can be inert towards the oxidizers. For P3HT-*b*-PTMPM, only *m*CPBA in dichloromethane can be used since the other condition, Na_2WO_4/H_2O_2 oxidation, needs methanol as solvent, while the diblock precursor polymer is barely soluble in methanol. Some previous attempts have been made on the *m*CPBA-mediated oxidation of polythiophenes grafted with PTMPM on the side

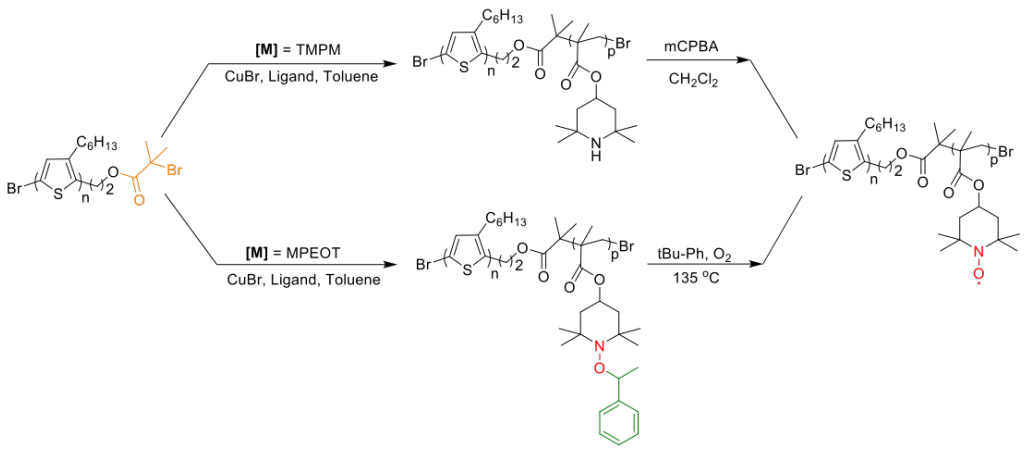

Scheme 5.2. Synthesis route of P3HT-*b*-PTMA diblock copolymer through ATRP of precursor monomers TMPM and MPEOT and subsequent oxidation to generate TEMPO radicals.

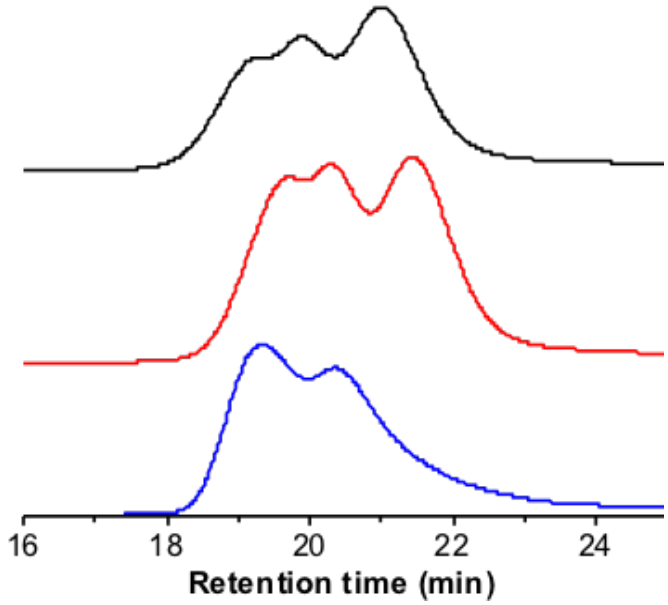

Figure 5.1. Representative GPC traces of crude P3HT-*b*-PTMPM (black and red line) and P3HT-*b*-PMPEOT (blue line).

because of the aggregation. ^{1}H NMR spectrum of the recovered polymer showed shifted and broadened proton peaks on the thiophene rings beyond 7.26 ppm (**Fig. 5.2**), which is consistent with the reports from Campos *et al.*.[39] These findings suggested that the *m*CPBA oxidation is incompatible with the P3HT block, and the oxidation of PTMPM using peracid needs to be carried out before the introduction of the P3HT block.

We also tested the compatibility of P3HT with the thermolysis condition of PMPEOT. The diblock copolymer P3HT-*b*-PMPEOT was dissolved in *tert*-butylbenzene and heated to 135 °C with oxygen bubbling. No obvious color change of the polymer solution was observed, while the conversion of PTMA was not high due to the slow reaction rate.

5.5.3 Synthesis of P3HT-*b*-PTMA via "Grafting to" method

Because of the poor control of ATRP from P3HT-BiBB macroinitiators and inevitable oxidation of P3HT block by *m*CPBA, the "grafting from" has been proved to be an unsuccessful method. As a result, the "grafting to" method, using highly efficient coupling reactions between two separate polymer segments, has been proposed. Considering the ease of synthesis and compatibility with TEMPO (which has been proved in **Chapter 3**), we decided to prepare one regioregular P3HT block with an alkyne end group and another PTMA block with azide end group. After that, these two blocks can be covalently linked *via* copper-catalyzed azide click reaction. The detailed synthesis route is shown in **Scheme 5.3**. The alkyne-terminated P3HT block (M_n = 7.9 kDa, Đ = 1.11) was prepared by GRIM polymerization and subsequent *in situ* end group functionalization with ethynylmagnesium bromide. To avoid the homocoupling between the alkyne

because of the aggregation. ^{1}H NMR spectrum of the recovered polymer showed shifted and broadened proton peaks on the thiophene rings beyond 7.26 ppm (**Fig. 5.2**), which is consistent with the reports from Campos *et al.*.[39] These findings suggested that the *m*CPBA oxidation is incompatible with P3HT block, and the oxidation of PTMPM using peracid needs to be carried out before the introduction of the P3HT block.

We also tested the compatibility of P3HT with the thermolysis condition of PMPEOT. The diblock copolymer P3HT-*b*-PMPEOT was dissolved in *tert*-butylbenzene and heated to 135 °C with oxygen bubbling. No obvious color change of the polymer solution was observed, while the conversion of PTMA was not high due to the slow reaction rate.

5.5.3 Synthesis of P3HT-*b*-PTMA via "Grafting to" method

Because of the poor control of ATRP from P3HT-BiBB macroinitiators and inevitable oxidation of P3HT block by *m*CPBA, the "grafting from" has been proved to be an unsuccessful method. As a result, the "grafting to" method, using highly efficient coupling reactions between two separate polymer segments, has been proposed. Considering the ease of synthesis and compatibility with TEMPO (which has been proved in **Chapter 3**), we decided to prepare one regioregular P3HT block with an alkyne end group and another PTMA block with azide end group. After that, these two blocks can be covalently linked *via* copper-catalyzed azide click reaction. The detailed synthesis route is shown in **Scheme 5.3**. The alkyne-terminated P3HT block (M_n = 7.9 kDa, Đ = 1.11) was prepared by GRIM polymerization and subsequent *in situ* end group functionalization with ethynylmagnesium bromide. To avoid the homocoupling between the alkyne

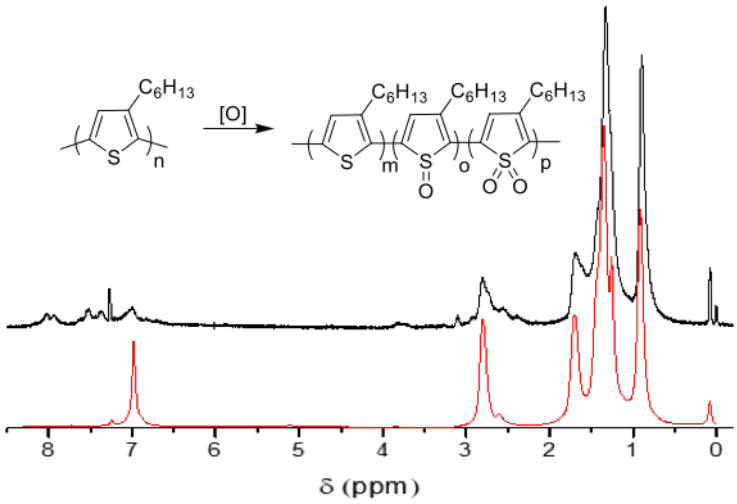

Figure 5.2. Oxidation of P3HT homopolymer in chloroform using *m*CPBA as the oxidant.

groups, the crude polymer was purified by thorough washing with an excess amount of methanol instead of the commonly used Soxhlet extraction. Meanwhile, the azide terminated PTMA (M_n = 35.8 kDa, Đ = 1.11) was prepared from oxidation of azide-terminated PTMPM precursor polymer, which was prepared by ATRP of TMPM from an azide-substituted initiator. (**Scheme 5.3**) Again, the *m*CPBA oxidation was strong enough to oxidize the azide group, which makes $H_2O_2/Na_2EDTA/Na_2WO_4$ the only alternative.[5] The azide click reaction between the P3HT-alkyne and PTMA-azide is very efficient, as shown in the GPC trail of the crude P3HT-*b*-PTMA after precipitation. (**Fig. 5.3**) This indicates that the complete coupling reaction between P3HT-alkyne and P3HT-azide was successfully carried out. Because there are fewer steps of end group functionalization on the P3HT block, the was less unfunctionalized P3HT block remaining, which shows a better efficiency regarding the cumbersome synthesis of the P3HT-containing ATRP macroinitiators. Earlier this year, there is one report on the synthesis of a similar P3HT-*b*-PTMA diblock copolymer. Instead of using Grignard metathesis, the P3HT-alkyne was synthesized using turbo-Grignard mediated deprotonation of thiophene monomer. Compared with their reported Đ values of the copolymers (1.33 - 1.34), our synthesis method appears to be a more controlled method considering its easier synthesis and lower Đ.[40]

The synthesized P3HT-*b*-PTMA is very soluble in dichloromethane due to the introduction of the PTMA block and exhibited the characteristic orange color of P3HT in solution. However, the P3HT-*b*-PTMA in the solid state shows a dark purple color, suggesting that the interchain packing of P3HT segments was maintained even the PTMA block ration is close to 80% in the block copolymer.

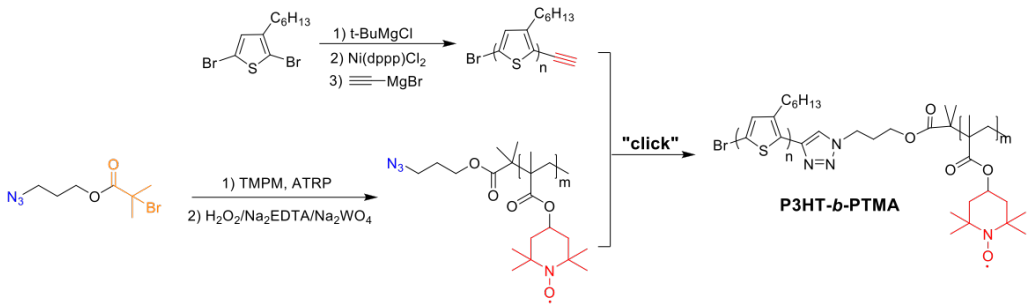

Scheme 5.3. Synthesis route of P3HT-*b*-PTMA block copolymer though azide-click reaction between P3HT-alkyne segment and PTMA-azide segment.

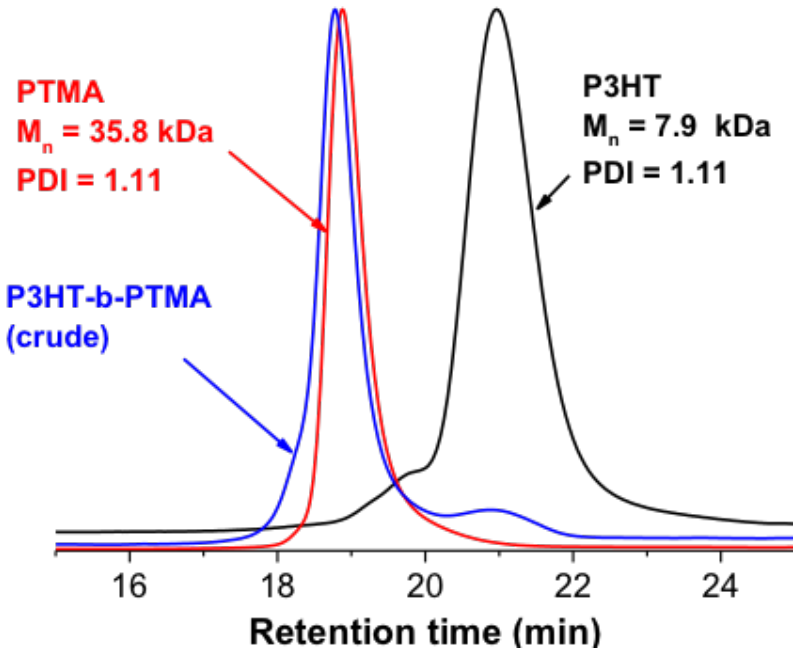

Figure 5.3. GPC traces of P3HT-alkyne (black line), PTMA-azide (red line) and crude P3HT-*b*-PTMA block polymers (blue line).

Since UV-vis absorption spectra only give the packing state of individual P3HT chains rather than the long-range order of the crystalline P3HT fibers, we also took the phase contrast AFM images of the annealed P3HT-*b*-PTMA films. As shown in **Figure 5.4**, the annealed P3HT thin film has short crystalline fibers dispersed in the amorphous matrix, and short-range order can be observed. For the P3HT-*b*-PTMA diblock copolymer film, although the phase image demonstrated the capability to form the P3HT crystalline fibers, no long-range order can be observed in the film due to the excess amount of the PTMA coil block. To have a well-controlled lamellar phase in the P3HT-containing diblock copolymer system, we need to have a better ratio control of the two blocks.

5.5.4 Better block ratio control using SET-LRP

Although the P3HT-*b*-PTMA diblock copolymer can be readily prepared using the azide-click reaction mediated "grafting to" method, the molecular control of PTMA remains a big problem for the better tune of the block ratio. The preferred molecular weight for the P3HT block for self-assembly study is always around 10 kDa, while the most available PTMA synthesis recipes usually give polymers with a molecular weight above 30 kDa to avoid possible dissolution of the polymer into the electrolyte. However, for the diblock copolymer study, such mismatch in block ratio does not give us a phase separation with long-range order. To achieve better long-range order in self-assembly study, we need to either decrease the length of the PTMA block or increase the length of the P3HT block to have a block ratio closer to 1 to 1.

In the previous attempts of ATRP synthesis of PTMPM precursor polymer, it has been recognized that the growth of the chain was too fast, while the initiation

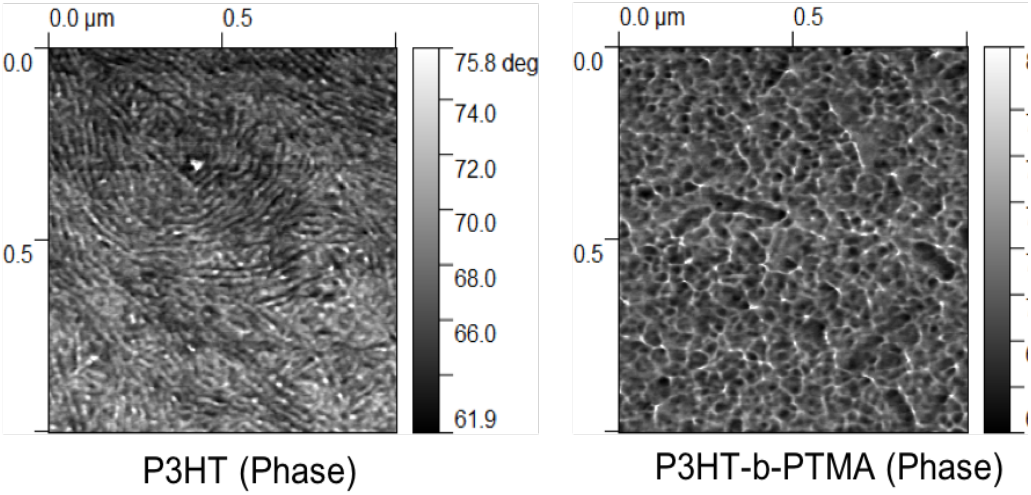

Figure 5.4. Phase images of P3HT and P3HT-*b*-PTMA diblock copolymer. The polymer films are spin-coated from THF solution and annealed in THF at room temperature overnight.

was not simultaneous at the first stage. This makes quenching the polymerization after a short period of time an unfavorable method because it gives us fewer PTMPM chains with much higher molecular weight than expected. A similar phenomenon has been described in detail for the synthesis of PMPEOT precursor polymers.[41] To synthesize shorter PTMPM block with low Đ, we need to have faster initiation and faster deactivation of the living radical intermediate compared to the common ATRP process. We also want to achieve a high monomer conversion because the low-M_n PTMPM has excellent solubility, which excludes the possibility of polymer purification by simple precipitation. In this context, we chose SET-LRP as an alternative for the PTMPM block synthesis because of its linear first-order kinetics in Cu(0) wire/PMDETA-mediated polymerization of TMPM (**Scheme 5.4**).[42] For a higher activation and monomer conversion, we used Me_6TREN as the ligand and carried out the reaction in isopropanol at 25 °C, using [TMPM]/[I]/Cu(II)Br_2/Me_6TREN = 50/1/0.05/0.8 as the molar ratio.[43] As expected, the polymerization of TMPM proceeded straightforwardly, and the monomer consumption was almost complete after 70 minutes, as indicated by the disappearance of TMPM monomer peak and appearance of PTMPM peak at 4.78 ppm (**Fig. 5.5**). Due to the high monomer conversion, the resulting PTMPM-azide after solvent removal can be used directly for the subsequent oxidation treatment with H_2O_2/Na_2EDTA/Na_2WO_4, which avoids the difficult precipitation process of low molecular PTMPM segment in cold hexane.

We also investigated the controlled character of the SET-LRP of TMPM by analyzing the MW of the PTMPM segment as a function of [TMPM]/[I], and the results are presented in **Fig. 5.6**. While most of the available recipes in

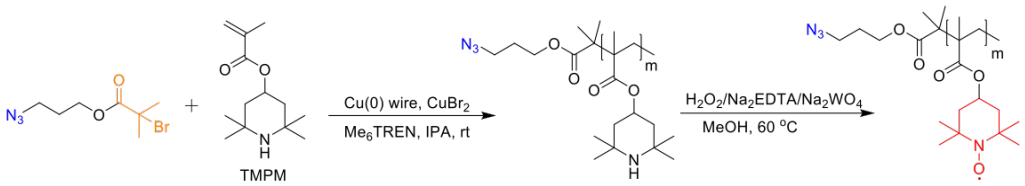

Scheme 5.4. Synthesis route of PTMA-azide segment using SET-LRP of TMPM and subsequent TEMPO generation via Na_2WO_4/H_2O_2 oxidation.

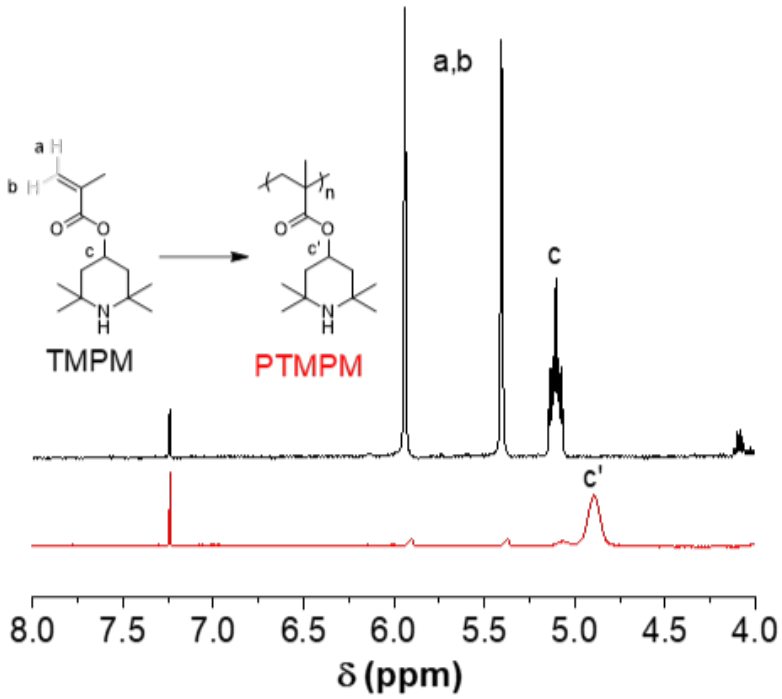

Figure 5.5. NMR spectra of TMPM monomer and PTMPM synthesized *via* SET-LRP. The molar ratio of [TMPM]/[I]/Cu(II)Br_2/Me_6TREN was 50/1/0.05/0.8, and the reaction was carried out in isopropanol at 25 °C.

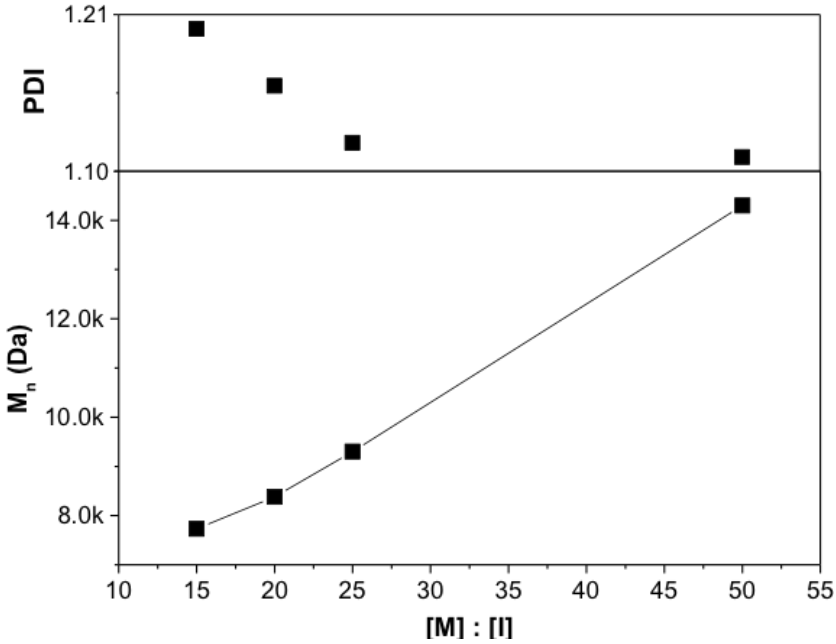

Figure 5.6. M_n and dispersity (Đ) of PTMA oxidized from the corresponding PTMPM precursor polymers versus [TMPM]/[I].

published articles focused on the preparation of long PTMPM segment, the MW control for low MW PTMPM is rarely reported. We carried out the SET-LRP of TMPM for [TMPM]/[I] of 50, 25, 20, 15, and the resultant PTMPM samples were oxidized to PTMA to measure their M_n and Đ. We can see the MW increased as an approximately linear manner with the [PTMPM]/[I], while Đ gradually increase to 1.20 when M_n decreased to 8.0 kDa. Considering the controlled MW and Đ of the PTMPM block, the click reaction with P3HT-alkyne are expected to give us a more predictable control over the MW and block ratio of the resulting P3HT-*b*-PTMA, which can make the resultant diblock polymers more suitable candidates for the future self-assembly study and conductivity measurements.

5.6 Conclusion

In summary, we have shown that the preparation of diblock rod-coil diblock copolymers consisting of conjugated poly(3-hexylthiophene) segment and insulating PTMA segment using both "grafting from" and "grafting to" methods. We find that the sequential addition of TMPM onto a P3HT-containing macroinitiator *via* ATRP is not efficient, and the oxidation with peracid inevitably oxidizes the P3HT block. However, the end-end coupling reaction between P3HT-alkyne and PTMA-azide has higher efficiency and also provides block copolymers with precisely controlled molecular weight and low Đ. The block ratio of rod and coil segments can be further tuned by the synthesis of short PTMA-azide block using SET-LRP. The synthesized P3HT-*b*-PTMA could be used for various applications, such as functional polymer electrodes with tunable electrochemical properties. Also, the self-assembly of rod-coil diblock copolymers can be achieved

by tuning block ratio or various annealing conditions, which gives many possible morphologies and resultant electronic properties. These morphologies provide continuous conjugated P3HT phases, which can facilitate the electron transport process in the stable radical polymer films and improve the overall conductivity of the thick stable radical films. With the carefully tailored block copolymer architectures, the orientation and confinement of the radical groups within the stable radical domains can also be tuned.

5.7 Acknowledgements

This work was supported the Department of Energy Office of Basic Energy Science (Grant DE-SC0014336). We acknowledge the use of shared facilities of the Cornell Center for Materials Research which is supported through the NSF MRSEC program (Grant DMR-1719875) and the shared facilities of the National Biomedical Center for Advanced Electron Spin Resonance Technology, which is supported by the National Institute of General Medical Sciences, a part of the National Institutes of Health (Grant P41GM103521).

5.8 Reference

1 K. Nakahara, K. Oyaizu and H. Nishide, Chemistry Letters, 2011, 40, 222–227.

2 J.-K. Kim, J.-H. Ahn, G. Cheruvally, G. S. Chauhan, J.-W. Choi, D.-S. Kim, H.-J. Ahn, S. H. Lee and C. E. Song, *Metals and Materials International*, 2009, **15**, 77–82.

3 K. Nakahara, J. Iriyama, S. Iwasa, M. Suguro, M. Satoh and E. J. Cairns, *Journal*

of Power Sources, 2007, **165**, 398–402.

4 C.-H. Lin, J.-T. Lee, D.-R. Yang, H.-W. Chen and S.-T. Wu, *RSC Advances*, 2015, **5**, 33044–33048.

5 B. Ernould, O. Bertrand, A. Minoia, R. Lazzaroni, A. Vlad and J.-F. Gohy, *RSC Advances*, 2017, **7**, 17301–17310.

6 W. Guo, Y.-X. Yin, S. Xin, Y.-G. Guo and L.-J. Wan, *Energy Environ. Sci.*, 2012, **5**, 5221–5225.

7 Y. Li, Z. Jian, M. Lang, C. Zhang and X. Huang, *ACS Applied Materials & Interfaces*, 2016, **8**, 17352–17359.

8 J. Kim, G. Cheruvally, J. Choi, J. Ahn, S. Lee, D. Choi and C. Song, *Solid State Ionics*, 2007, **178**, 1546–1551.

9 J.-K. Kim, G. Cheruvally, J.-H. Ahn, Y.-G. Seo, D. S. Choi, S.-H. Lee and C. E. Song, *Journal of Industrial and Engineering Chemistry*, 2008, **14**, 371–376.

10 Y. Zhang, A. M. Park, S. R. McMillan, N. J. Harmon, M. E. Flatté, G. D. Fuchs and C. K. Ober, *Chemistry of Materials*, 2018, **30**, 4799–4807.

11 F. Li, D. N. Gore, S. Wang and J. L. Lutkenhaus, *Angewandte Chemie International Edition*, 2017, **56**, 9856–9859.

12 J. E. Kroeze, T. J. Savenije, M. J. W. Vermeulen and J. M. Warman, *The Journal of Physical Chemistry B*, 2003, **107**, 7696–7705.

13 U. Scherf, A. Gutacker and N. Koenen, *Accounts of Chemical Research*, 2008, **41**, 1086–1097.

14 P. Pingel, A. Zen, R. D. Abellón, F. C. Grozema, L. D. A. Siebbeles and D. Neher, *Advanced Functional Materials*, 2010, **20**, 2286–2295.

15 C.-L. Liu, C.-H. Lin, C.-C. Kuo, S.-T. Lin and W.-C. Chen, *Progress in Polymer Science*, 2011, **36**, 603–637.

16 C.-A. Dai, W.-C. Yen, Y.-H. Lee, C.-C. Ho and W.-F. Su, *Journal of the American Chemical Society*, 2007, **129**, 11036–11038.

17 T. Higashihara, K. Ohshimizu, A. Hirao and M. Ueda, *Macromolecules*, 2008, **41**, 9505–9507.

18 T. Higashihara and M. Ueda, *Macromolecules*, 2009, **42**, 8794–8800.

19 M. C. Iovu, M. Jeffries-EL, E. E. Sheina, J. R. Cooper and R. D. McCullough, *Polymer*, 2005, **46**, 8582–8586.

20 M. C. Iovu, C. R. Craley, M. Jeffries-EL, A. B. Krankowski, R. Zhang, T. Kowalewski and R. D. McCullough, *Macromolecules*, 2007, **40**, 4733–4735.

21 C. R. Craley, R. Zhang, T. Kowalewski, R. D. McCullough and M. C. Stefan, *Macromolecular Rapid Communications*, 2009, **30**, 11–16.

22 Y. Lee, K.-I. Fukukawa, J. Bang, C. J. Hawker and J. K. Kim, *Journal of Polymer Science Part A: Polymer Chemistry*, 2008, **46**, 8200–8205.

23 T. M. S. K. Pathiranage, M. Kim, H. Q. Nguyen, K. E. Washington, M. C. Biewer and M. C. Stefan, *Macromolecules*, 2016, **49**, 6846–6857.

24 B. W. Boudouris, C. D. Frisbie and M. A. Hillmyer, *Macromolecules*, 2010, **43**, 3566–3569.

25 C. P. Radano, O. A. Scherman, N. Stingelin-Stutzmann, C. Müller, D. W. Breiby, P. Smith, R. A. J. Janssen and E. W. Meijer, *Journal of the American Chemical Society*, 2005, **127**, 12502–12503.

26 M. Urien, H. Erothu, E. Cloutet, R. C. Hiorns, L. Vignau and H. Cramail, *Macromolecules*, 2008, **41**, 7033–7040.

27 Y. Sakai-Otsuka, S. Zaioncz, I. Otsuka, S. Halila, P. Rannou and R. Borsali, *Macromolecules*, 2017, **50**, 3365–3376.

28 E. Ji, V. Pellerin, L. Rubatat, E. Grelet, A. Bousquet and L. Billon,

Macromolecules, 2017, **50**, 235–243.

29 L. Pessoni, J. De Winter, M. Surin, N. Hergué, N. Delbosc, R. Lazzaroni, P. Dubois, P. Gerbaux and O. Coulembier, *Macromolecules*, 2016, **49**, 3001–3008.

30 M. Lee, B.-K. Cho and W.-C. Zin, *Chemical Reviews*, 2001, **101**, 3869–3892.

31 N. Sary, R. Mezzenga, C. Brochon, G. Hadziioannou and J. Ruokolainen, *Macromolecules*, 2007, **40**, 3277–3286.

32 L. Rubatat, X. Kong, S. A. Jenekhe, J. Ruokolainen, M. Hojeij and R. Mezzenga, *Macromolecules*, 2008, **41**, 1846–1852.

33 Y. Li, S. Lin, X. He, J. Lin and T. Jiang, *The Journal of Chemical Physics*, 2011, **135**, 014102.

34 N. Sary, C. Brochon, G. Hadziioannou and R. Mezzenga, *The European Physical Journal E*, 2007, **24**, 379–384.

35 Y.-K. Fang, C.-L. Liu, C. Li, C.-J. Lin, R. Mezzenga and W.-C. Chen, *Advanced Functional Materials*, 2010, **20**, 3012–3024.

36 Z. Tian, X. Liu, C. Chen and H. R. Allcock, *Macromolecules*, 2012, **45**, 2502–2508.

37 F. Fan, *Cornell University Library*, , DOI:10.7298/x4f769jw.

38 C.-H. Lin, C.-M. Chau and J.-T. Lee, *Polymer Chemistry*, 2012, **3**, 1467.

39 S. Wei, J. Xia, E. J. Dell, Y. Jiang, R. Song, H. Lee, P. Rodenbough, A. L. Briseno and L. M. Campos, *Angewandte Chemie International Edition*, 2014, **53**, 1832–1836.

40 N. Hergué, B. Ernould, A. Minoia, J. De Winter, P. Gerbaux, R. Lazzaroni, J.-F. Gohy, P. Dubois and O. Coulembier, *Polymer Chemistry*, 2019, **10**, 2570–2578.

41 F. Behrends, H. Wagner, A. Studer, O. Niehaus, R. Pöttgen and H. Eckert, *Macromolecules*, 2013, **46**, 2553–2561.

42 O. Bertrand, B. Ernould, F. Boujioui, A. Vlad and J.-F. Gohy, *Polymer Chemistry*, 2015, **6**, 6067–6072.

43 K. Zhang, Y. Hu, L. Wang, J. Fan, M. J. Monteiro and Z. Jia, *Polymer Chemistry*, 2017, **8**, 1815–1823.

CHAPTER 6: CONCLUSIONS AND PERSPECTIVES

Conductivity in aliphatic stable radical polymers:

The main focus of the work presented in this dissertation has been to synthesize a series of stable radical polymers and carry out a detailed investigation into their electron transport processes. The non-conjugated polymers with pendent nitroxide stable radical groups have seen substantial progress and development in the past two decades mainly as promising electrode materials for energy storage applications. However, their inherent electrical conductivity has not been a heated topic until recently. In **Chapter 2**, we illustrated different methods of synthesis of PTMA, the model aliphatic nitroxide radical polymer, and characterized their spin and oxoammonium cation content for each type. By careful conductivity measurements with a four-wire lateral device, we proved that a neat PTMA thin film is highly insulating regardless of the presence of oxoammounium cations, which is consistent with a number of previous reports.

At this point, there are three directions which can be explored for non-conjugated stable radical polymers. First, novel stable radical moieties can be synthesized and incorporated into the polymer structure as alternatives to the commonly used nitroxide radicals. Despite their convenient preparation, the nitroxide radicals have their spins too localized on the nitrogen and oxygen, which makes the single electrons more unlikely to delocalize to adjacent sites. This is also consistent with many earlier studies from the early organic chemists who have explored numerous kinds of radical structures in order to achieve high conductivity in neutral molecular solids. It has been shown previously that π-conjugation and heteroatoms can efficiently improve the conductivity in molecular stable radicals. Thus, introduction

of such radicals may retain the electron transport capability in the molecular state with appropriate treatment and make the polymeric form a more promising candidate for conducting radical polymers.

Another point of interest and new direction is the effect of the polymer backbone mobility on the macroscopic electrical conductivity in stable radical polymer films. According to Boudouris's recent report on high electrical conductivity in poly(4-glycidyloxy-2,2,6,6-tetramethylpiperidine-1-oxyl), a relatively low glass transition temperature (T_g) can facilitate charge transfer activities between nitroxide radical sites, which results in higher macroscopic conductivity in thin films. However, we cannot definitively state that the low T_g of a PEO backbone is a critical factor, since other low T_g polymers, such as PDMS, have been used and no enhancement of conductivity has been observed. To carry out a systematic study, one possibility might be to use a copolymer system as backbones in which the T_g can be tuned by its compositional variation, while the stable radical content remains the same to similar numbers of hopping sites. One possible candidate is the copolymer of *o*-phthalaldehyde and ethyl glyoxylate (**Scheme 6.1**), which can be easily prepared by cationic polymerization and shows tunable Tg from -20 °C to ~ 130 °C.

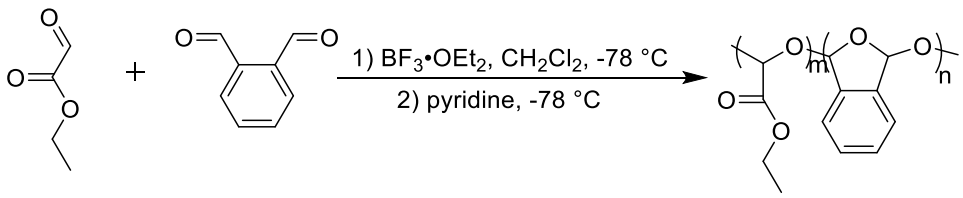

Scheme 6.1. Copolymerization of ethyl glyoxylate and *o*-phthalaldehyde using cationic polymerization.

Finally, measurement condition has also been an extremely important aspect for the electron transport study in stable radical polymers. The four-probe technique is

known as the most reliable method for electrical conductivity measurement of polymer films because it can eliminate the influence of contact resistance between the sample and electrodes. However, it is difficult to measure the conductivity of highly insulating polymer since the measured current is too low due to a wider electrode spacing and smaller cross-sectional area for the contact between sample and electrodes. This usually requires better commercial equipment and more accurate calibration. For Boudouris' group, only the early conductivity values in PTMA reported were based on the lateral devices, while the later higher conductivities are mostly based on sandwich devices with various extra layers.

Since the conductivity of nitroxide radical polymers is sensitive to film thickness, device fabrication and measurement condition, it would be necessary to have a reliable set-up and careful measurement protocols for accurate results. So far there is still no further experimental proof from other research groups that can observe results similar to Boudouris', and battery research groups still have not benefited from the reported high conductivity values. Perhaps a more interesting study would be to reinvestigate how the different setups and measurement conditions can affect the macroscopic electron transport in the non-conjugated stable radical polymers.

Conductivity in conjugated stable radical polymers:

In **Chapter 3**, we have demonstrated the ability to prepare conjugated stable radical polymers with regioregular polythiophene backbones and tunable pendent stable radical content. By combining Grignard metathesis (GRIM) polymerization and azide-click chemistry, we are able to synthesize P3HT-TEMPO samples with controllable MW, low PDI and tunable radical content. Also, our P3HT-TEMPO

samples exhibit good solubility, which enables better solution characterization than previously and cannot be done for the sample prepared by traditional oxidative and electrochemical polymerizations. By systematically varying the radical content in the copolymers, we found that introduction of bulky nitroxide radical pendant groups impedes both intrachain and interchain charge transfer, which results in lower conductivity in the samples with higher TEMPO incorporation.

Despite the cumbersome synthesis of the conjugated stable radical polymers, a more interesting design will be an all-conjugated design with conjugated backbone, conjugated spacer and conjugated pendent radicals in a single polymer structure. In our current design, the long alkyl spacer and six-member ring of TEMPO radical are all saturated, which increases the space between the backbone and the radical spins. As the incorporation of extended π-conjugated spacers and conjugated radicals can efficiently delocalize the spins, the all-conjugated samples might exhibit more interesting magnetic, optical or electrical properties. One possible synthesis route is to prepare thiophene monomers with fused nitroxide stable radicals and use oxidative coupling reactions to produce the final conjugated radical polymers (**Scheme 6.2 (a)**). Another possible route is based on a polythiophene precursor with functional pendent groups at 3- position of the thiophene monomers. The radicals can be attached by highly efficient coupling reactions that can generate conjugated spacers, such as Suzuki coupling or Honer-Wadsworth-Emmons reaction (**Scheme 6.2 (b)**).

Doping of all-conjugated stable radical polymers:

In addition to investigating the charge transport in the neutral P3HT-TEMPO sample, **Chapter 4** also described both the chemical and electrochemical doping of

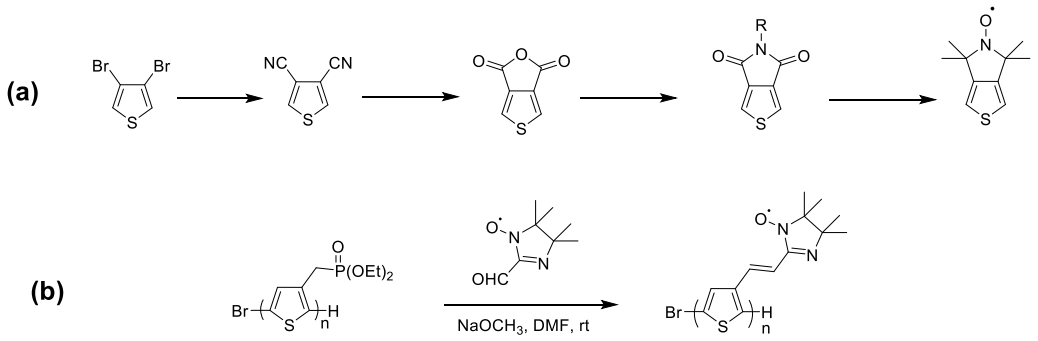

Scheme 6.2. (a) Proposed synthesis route of thiophene monomer containing fused nitroxide stable radicals. (b) Synthesis of all-conjugated polythiophene with Honer-Wadsworth-Emmons reaction.

conjugated stable radical polymers. While the synthesis and electrochemical properties have been well documented in the previous literature, significantly less effort has been directed toward understanding the doping mechanism and structure-property relationships of the all-conjugated radical polymers. In this work, we have revealed that both iodine and F4-TCNQ can oxidize the polythiophene and TEMPO radical, which results in enhanced electrical conductivity in the chemically doped P3HT-TEMPO-X films. Our collaborators also carried out electrochemical doping of the neutral polymer on ITO electrodes, which shows a two-step redox process upon charging. First, the nitroxide radicals were oxidized to oxoammonium at ~ 3.5 V (vs. Li^+/Li), while the polythiophene backbones were not oxidized until the potential reached ~ 4.2 V. The P3HT-TEMPO-100 showed much lower capacity compared with the regioregular P3HT, which can be mainly ascribed to the unusual internal charge transfer between the backbone and pendent radicals.

While the two-step doping process in P3HT-TEMPO-100 has been revealed, perhaps a more interesting study would be to identify the contribution from polarons and radical spins to the overall conductivity by using *in-situ* measurements. The ratio

of dopant to redox sites, the oxidation potential of different components and the conformation of doped films are all factors that could potentially affect charge transfer, and each should be investigated. To address these factors, our collaborators have designed a setup for vapor-phase doping with *in-situ* electrical measurements, which could give more quantitative information regarding the doping effect on the macroscopic conductivity (**Fig. 6.1 (a-b)**). A similar doping setup has been used in the doping of an oligothiophene-based conjugated liquid crystal in our group. Combined with the solid-state *in-operando* EPR (**Fig. 6.1 (c)**), we can also do W-band measurement to precisely sort out the sources of EPR signals from the polarons from polythiophene, spins from nitroxide radicals or radical anions from the dopants.

With the detailed electrochemical characterization of the P3HT-TEMPO-X copolymers, a more in depth understanding of their charge storage and charge transport in the electrodes can be established. Recently, the Lutkenhaus group has systematically synthesized conjugated radical polymers with polythiophene and polydithienopyrrole backbones, with bears a redox potential higher and lower than that of the TEMPO radical, respectively. The discharge performance of the radical-containing polymers was found to be lower compared with their radical-free counterpart, which was ascribed to the internal charge transfer that occurs between the two redox components. In order to design a conjugated radical polymer with both high electrical conductivity and high capacity, it would be a necessary step for the polymer chemists to find appropriate combinations of conjugated backbone and radicals. So, a potential direction to go is to explore the library of conjugated polymers and stable radicals, and this work can be expanded to the general areas of

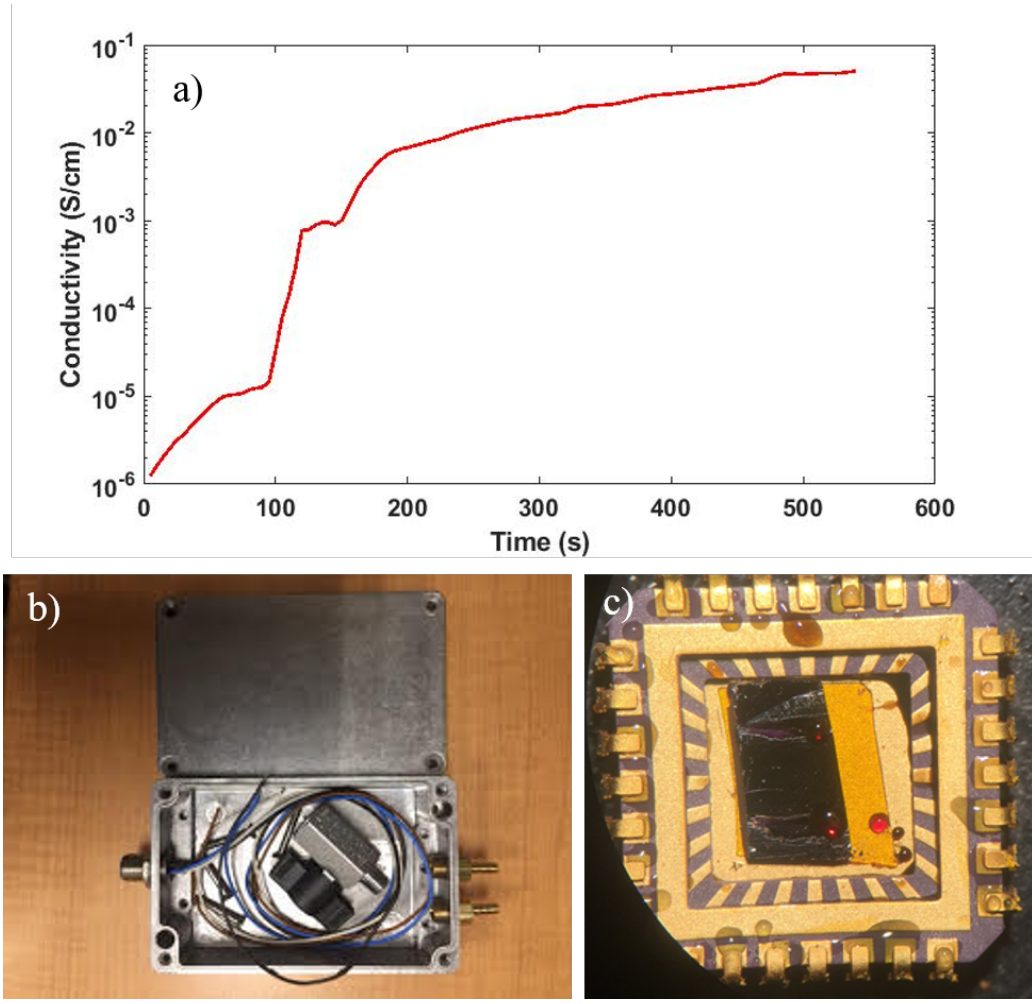

Figure 6. 1. (a) Conductivity of P3HT homopolymer using in-situ doping of iodine vapor. (b) Setup for in-situ doping and conductivity measurements, including the vacuum chamber. (c) *In-operando* EPR chip with doped P3HT film on silicon substrate. Liquid formed due to the possible reaction of iodine with metal followed by hydrolysis.

better electrode materials.

Rod-coil diblock copolymer with stable radical pendent groups:

The advantage of the block copolymer is that they can have microphase separation can form long-range ordered structure by appropriate treatment. Also presented in **Chapter 5** is a facile method to prepare rod-coil diblock copolymers containing a regioregular P3HT segment and a PTMA segment that has been developed using GRIM polymerization. Two methods, "grafting from" and "grafting to", were demonstrated in this thesis to provide the final rod-coil block copolymer. We found the "grafting from" method, which relies on ATRP of a precursor monomer from a P3HT-BiBB macroinitiator and subsequent oxidation to recover the radicals. However, this method suffers from poor control over the chain growth as well as the inevitable oxidation of the polythiophene block during the radical generation. As an alternative, the "grafting to" method involving the end-end coupling between P3HT-alkyne and PTMA-azide can efficiently produce final rod-coil copolymers with precisely controlled molecular weight and low Đ. This method can be expanded to the synthesis of more rod-coil stable radical block copolymers that can have potential application in a wide range of areas.

Once a well-defined polymer structure and tunable copolymer composition have been achieved, the next step would be to investigate how phase separation can be achieved through appropriate annealing conditions, and how charge storage and transport can benefit from ordered domains. The phase separation can be observed with AFM, TEM and small angle x-ray scattering (SAXS). With the improved characterization of block copolymers, a more in depth understanding of a stable radical polymer sample can be achieved and more reproducible phase diagram of

these samples could be developed. Alignment and selection of a microphase will be useful for the future studies of charge transport in solid-state films or charge storage on an electrode surface, since it is possible to position specific microstructures in such a way that a conducing polymer phase can be well aligned with respect to electrical contact points.